THE UNIVERSITY
of EDINBURGH

A Study Towards the Quantitative Definition of the Kynurenine Pathway

AUTHOR: TOBY MURRAY

MScR Surgery

SUPERVISOR: MR DAMIAN MOLE

AUGUST 2016

WORD COUNT: 18,429

Table of Contents

Declaration

I, Toby Benjamin James Murray, declare that the work detailed and described in this dissertation is written by myself and represents the work that is my own. Any contributions from the published or unpublished work of others have been fully acknowledged in the proper manner. This work has not been submitted for any other degree or professional qualification.

Signed

Toby Benjamin James Murray BSc (Hons) MSc

Acknowledgments

I would like to personally thank my supervisor, Mr. Damian Mole, for the opportunity to carry out this research and degree. His help and support has been phenomenal.

I would also like to show my gratitude to everybody else who has helped me throughout the year. To Dr. Xiaozhong Zheng, for his superb training in the cannulation and infusion experiments, and also his unwavering support and organisation throughout the year. To Mr. George Just, for his incredible support in the development of the mass spectrometry and plasma extraction assay, whilst also being the hero when problems arose (very frequently I might add) with the LC-MS/MS system! To Dr. Natalie Homer, for her guidance and undivided attention when I needed help in the mass spectrometry lab. To Dr. Scott Webster, for his wisdom in the chemical, statistical and pharmacokinetic aspects to the project. To Dr. Iain Uings, for his support in helping me understand the principles of pharmacokinetics, and the interpretation of the data.

I would also like to thank Mrs. Margaret Binnie and Dr. Karen Sooy who took me under their wing when I first started in the mass spectrometry lab. To Mr. Alastair Hayes who has been a brilliant source of wisdom, support and ideas throughout the year.

My gratitude must also go to the Royal College of Surgeons of England, for their financial award that helped with the costs of the degree.

Lastly, I would like to thank my parents Dr Jim Murray and Mrs Susan Murray. Without their unwavering support, none of this would have been possible. They have been true rocks throughout my entire university career.

Abstract

The kynurenine pathway is the prime pathway for the metabolism of the essential amino acid, tryptophan (TRP), and also the de novo pathway for nicotinamide adenine dinucleotide (NAD^+) production. The kynurenine pathway is important in the pathogenesis of multi-organ dysfunction syndrome following severe acute pancreatitis (AP-MODS) due to the metabolism of kynurenine (KYN) into cytotoxic 3-hydroxykynurenine (3HK) by the enzyme kynurenine 3-monooxygenase (KMO). Mice with absent Kmo gene expression (KMO^{null}) have marked reductions in extrapancreatic organ injury post AP.

This dissertation describes the pharmacokinetics (PK) of the kynurenine pathway after intravenous infusion of deuterated or heavy carbon stable isotopes (tracers) of four kynurenine pathway compounds (D_5-TRP, $^{13}C_6$-KYN, D_5-kynurenic acid (KYNA) and $^{13}C_6$-3HK) into rats (n=13).

Liquid chromatography-electrospray ionisation tandem mass spectrometry (LC-MS/MS) is the most frequently used method to monitor kynurenine pathway compound levels in plasma. This dissertation reports a new method of extraction of plasma samples, using solid phase extraction (SPE), alongside improvement and optimisation of existing LC-MS/MS protocols using a reverse phase ultra-high performance C18-pentafluorophenyl column. This has enabled the analysis of each main metabolite in the kynurenine pathway in a single assay. Mass spectra of compounds were detected using electrospray ionisation (ESI) in both positive and negative polarity employing multiple reaction monitoring (MRM) modes over a 9 min total run time with an injection volume of 10 µL and flow rate of 0.4 mL/min. The method for each compound was shown to be reproducible and accurate (RSD < 25%) and each corresponding standard curve demonstrated linearity (R^2 >0.99).

Single compartment temporal PK analysis of tracers in rat plasma, during the elimination phase, reveals short mean half-lives for each compound, suggesting that metabolism through the kynurenine pathway is rapid ($t_{1/2}$ 12.14 – 29.12 mins). There was a marked difference in the volume of distribution of each analyte (D_5 KYNA 0.12; $^{13}C_6$-3HK 0.21; $^{13}C_6$-KYN 0.96 and D_5-TRP 0.92 (µg/kg)/(µg/L)). Enzyme rates of formation of each analyte were also identified (KYN 20.73; KYNA 2.21; 3HK 3.68 (µg/L)/min)

In conclusion, a new accurate and reliable LC-MS/MS method for the analysis of kynurenine pathway metabolites has been developed. PK analysis has identified important and significant differences in the apparent volumes of distribution of each metabolite. Thus, it can be suggested that TRP and KYN are readily distributed to tissue whilst KYNA and 3HK are largely confined to the plasma compartment.

Lay Summary

The chemical, tryptophan, is essential for the healthy functioning of cells in the body. It is present in the diet. However, it is known that some breakdown products of tryptophan, formed in the body, can be toxic to cells and be related to several severe disease conditions. Blocking these breakdown products could be a means to treating these severe diseases. This study measured the levels of tryptophan breakdown products and their length of life in blood in the healthy animal. To accurately and reliably measure these breakdown products, it was also necessary to develop a new, sophisticated assay method. Thus, this study adds to the understanding of these compounds and will contribute to the background knowledge required to aid the potential production of new treatments.

Abbreviations

$^{13}C_6$ 3HK	Heavy Carbon 3-Hydroxykynurenine	**k_{el}**	Elimination Constant
$^{13}C_6$ KYN	Heavy Carbon Kynurenine	**K_M**	Michaelis Constant
3HAA	3-Hydroxyanthranilic Acid	**KMO**	Kynurenine 3-monooxygenase
3HAO	3-Hydroxyanthranilate 3,4-dioxygenase	**KMO^{null}**	KMO Knockout
3HK	3-Hydroxykynurenine	**KYN**	Kynurenine
AA	Anthranilic Acid	**KYNA**	Kynurenic Acid
ADME	Absorption, Distribution, Metabolism, Elimination	**KYNU**	Kynureninase
AKI	Acute Kidney Injury	**LC-MS/MS**	Liquid Chromatography tandem Mass Spectrometry
AMPA	α-Amino-3-hydroxi-5-Metylisoxazol-4-Propansyra	**LipE**	Lipophilic Efficiency
AP	Acute Pancreatitis	**LPS**	Lipopolysaccharide
AP-MODS	Acute Pancreatitis Multiple Organ Dysfunction Syndrome	**Log*P***	1-octanol-water Partitioning Coefficient
ATP	Adenosine Triphosphate	**LOQ**	Limit of Quantification
AUC	Area Under Curve	**MRM**	Multiple Reaction Monitoring
BSA	Bovine Serum Albumin	**MTBE**	Methyl Tert-Butyl Ether
Ca^{2+}	Calcium	***m/z***	Parent/Product Transition
CH_3OH	Methanol	**nACHR**	Nicotinic Acetylecholine Receptor
C_i	Initial Concentration	**NAD^+**	Nicotinamide Adenine Dinucleotide
CL	Clearance	**NADPH**	Nicotinamide Adenine Dinucleotide Phosphate
CL_{met}	Hepatic Clearance	**NEFA**	Non-esterified Fatty Acid
CL_{ren}	Renal Clearance	**NH_4OH**	Ammonium Hydroxide
CL_{tot}	Total Clearance	**NMDA**	*N*-methyl-*D*-aspartate
CNS	Central Nervous System	**nNOS**	Neuronal Nitric Oxide Synthase
COX-2	Cyclooxygenase-2	**NO**	Nitric Oxide
C_p	Concentration in Plasma	**O^{2-}**	Superoxide
Cu^{2+}	Copper	**$ONOO^-$**	Peroxynitrite
D_5-KYNA	Deuterated Kynurenic Acid	**PD**	Pharmacodynamics
D_5-TRP	Deuterated Tryptophan	**PK**	Pharmacokinetics
DCM	Dichloromethane	**PFP**	Pentafluorophenyl
DNA	Deoxyribonucleic Acid	**PPT**	Protein Precipitation

EDTA	Ethylenediaminetetraacetic Acid	**PRPP**	Phosphoribopyrophosphate
ESI	Electron Spray Ionisation	**QPRT**	Quinolinic Acid Phosphoribosyltransferase
FAD	Flavin Adenine Dinucleotide	**QUIN**	Quinolinic Acid
FDA	Food and Drug Administration	**R^2**	Linear Regression Correlation Coefficient
Fe^{3+}	Iron	**ROS**	Reactive Oxygen Species
GIT	Gastrointestinal Tract	**RQ**	Relative Quantity
GPR	G Protein-coupled Receptor	**RSD**	Relative Standard Deviation
H_2O	Water	**SLE**	Supported Liquid Extraction
H_2O_2	Hydrogen Peroxide	**SPE**	Solid Phase Extraction
H_3PO_4	Phosphoric Acid	**$t_{1/2}$**	Half Life
HD	Huntington's Disease	**TCA**	Trichloroacetic Acid
HLB	Hydrophilic Lipophilic Balanced	**TDO**	Tryptophan 2,3-dioxygenase
HPLC	High Performance Liquid Chromatography	**TNF-α**	Tumour Necrosis Factor Alpha
IDO	Indoleamine 2,3-dioxygenase	**TRP**	Tryptophan
IFN-γ	Interferon Gamma	**UV**	Ultraviolet
IL-1β	Interleukin 1-Beta	**V_d**	Volume of Distribution
IV	Intravenous	***v/v***	Volume to Volume
KAT	Kynurenine aminotransferase	**XA**	Xanthurenic Acid
		UHPLC	Ultra-High Performance Liquid Chromatography

Section 1: The Kynurenine Pathway

Tryptophan metabolism *via* the kynurenine pathway is a fundamental biological process that has generated increasing levels of attention in recent years. The pathway is likely to be involved in a range of diseases, including tumour immune resistance, neurodegeneration and multiple organ failure secondary to acute pancreatitis (Chen & Guillemin, 2009; Mole *et al*., 2008; Mole *et al*., 2016; Uyttenhove *et al*., 2003).

1.1 Introduction to Tryptophan

Tryptophan (TRP) is one of the nine essential amino acids that cannot be synthesised by mammals, therefore all TRP is acquired through the diet. TRP accounts for just one per cent of the recommended daily intake of essential amino acids (WHO/FAO/UNU, 2007), yet it serves as a precursor in the manufacture of several important biologically active metabolites including melatonin, serotonin and kynurenines (de Jong *et al.,* 2009). TRP is the end product of a biosynthesis pathway involving the common precursor chorismate (Figure 1.1), a biochemical important in the formulation of many alkaloids, indoles, vitamin K, folate and amino acids, including phenylalanine and tyrosine. These, together with TRP, are important precursors to the production of neurotransmitters. The shikimate pathway that provides chorismate is not present in animals, thus chorismate has to be obtained from the diet. The synthesis of TRP consumes a vast amount of energy, requiring products of other pathways to provide essential carbons and nitrogens, these products include L-glutamine, the universal donor of amines, adenosine triphosphate (ATP), erythrose-4-phosphate, phosphoribopyrophosphate (PRPP) and L-serine, thus the formation of TRP can be seen as biologically expensive (Yanofsky, 2007). It has been suggested that the ability for mammalian cells to produce TRP was lost because of the biologically costly process of TRP formation. This, together with the abundance of TRP in the diet, led to a lack of evolutionary pressure to preserve the genes needed to produce TRP in animals. Conversely, in prokaryotes and eukaryotes, the genes necessary for TRP biosynthesis have been highly conserved (Xie *et al.,* 2003).

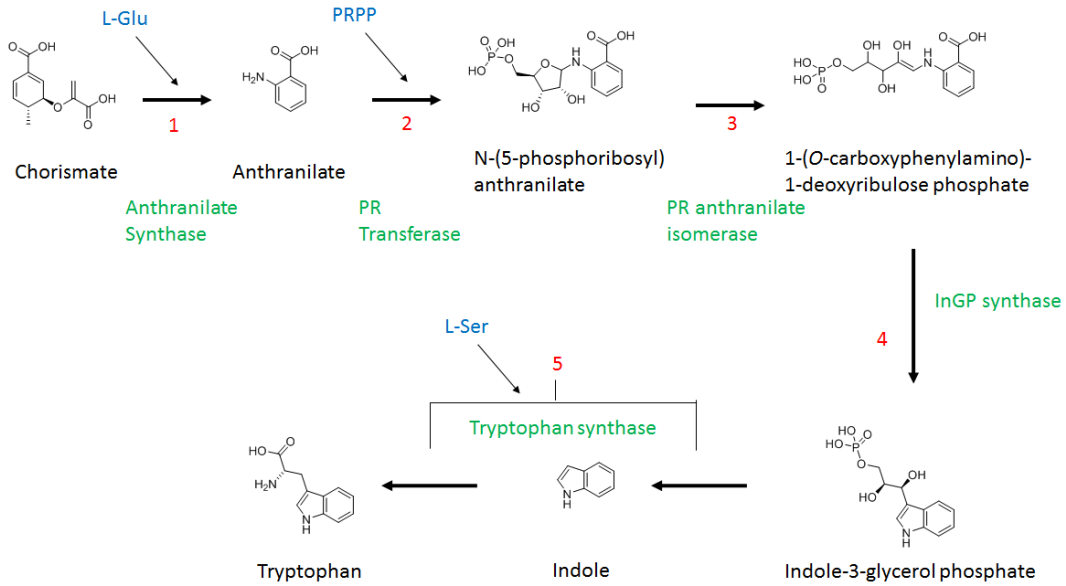

(**Figure 1.1 - The Tryptophan Biosynthetic Pathway.** The pivotal precursor to the production of aromatic amino acids is chorismate, a product of the shikimate pathway which is not present in animals. Chorismate is catalysed by anthranilate synthase using glutamine to produce anthranilate, glutamate and pyruvate. In many eukaryotes, mainly fungi, this enzyme is part of a multifunctional protein complex, divided into two subunits α and β. For instance in *Neurospora Crassa*, subunit β is encoded by the gene for phosphoribosylanthranilate isomerase (TRP1) which provides the active sites for reactions 3 and 4 (in red). The α subunit is encoded by TRP2 (anthranilate synthase) and provides the active site for reaction 1 when combined with subunit β provides the site for glutamine binding to catalyse anthranilate synthesis. The other two enzymes involved in this pathway are independent enzymes that are encoded by separate genes (Hutter *et al.,* 1986).)

Table 1.1 - Genetic profile of enzymes involved in TRP biosynthesis (PUBMED)

Gene	**Enzyme Encoded**	**Function**	**Lineage**
TRP1	Phosphoribosylanthranilate isomerase	Catalyses step 3 in the biosynthesis of TRP	Eukaryota Fungi Dikaryota Ascomycota Saccharomycotina Saccharomycetes Saccharomycetales Saccharomycetaceae Saccharomyces
TRP2	Anthranilate Synthase	Catalyses step 1 of TRP biosynthesis; Forms enzyme complex with indole-3-glycerol-phosphate synthase	
TRP3	Anthranilate synthase/ indole-3-glycerol-phosphate synthase	Contribute to Anthranilate synthase and indole-3-glycerol-phosphate synthase activity Catalyses steps 1 and 4 in biosynthesis of TRP	
TRP4	Anthranilate phosphoribosyltransferase	Catalyses step 2 in biosynthesis of TRP	
TRP5	Tryptophan synthase	Catalyses step 5 in biosynthesis of TRP	
*trp*A	Tryptophan synthase (α subunit)	Involved in step 5 of TRP biosynthesis α subunit catalyses the cleavage of indole-3-glycerol-phosphate to indole and d-glyceraldehyde 3-phosphate. It then channels indole to the β subunit	Bacteria Proteobacteria Gammaproteobacteria Enterobacteriales Enterobacteriaceae Escherichia
*trp*B	Tryptophan synthase (β subunit)	Involved in step 5 of TRP biosynthesis. β subunit catalyses the pyridoxal 5'-phosphate-dependent reaction of indole with L-serine to form L-tryptophan.	
*trp*C	Indole-3-glycerolphosphate synthetase and N-(5-phosphororibosyl_ anthranilate isomerase	Catalyses the conversion of PR anthranilate to CdRP and also the ring closure of CdRP to IGP (reactions 3 and 4)	
*trp*D	Component II of anthranilate synthase/anthranilate phosphoribosyltransferase	Catalyses 2nd step of TRP biosynthesis Component II of anthranilate synthase is a glutamine amidotransferase aiding in step 1 of TRP biosynthesis. In E.coli this component also contains phosphoribosyl-anthranilate transferase – further catalysing step 2 of TRP biosynthetic pathway by adding PRPP to anthranilate.	
*trp*E	Component I of anthranilate synthase	Catalyses 1st step of TRP biosynthesis by catalysing the formation of anthranilate using chorismate and ammonia. Also involved in the TRP negative feedback loop.	
*trp*F	N-(5'-phosphoribosyl)anthranilate isomerase	Catalyses step 4 in TRP biosynthesis	Bacteria Proteobacteria Gammaproteobacteria
*trp*G	Component II of anthranilate synthase	Combines with trpE to catalyse the formation of anthranilate and glutamate from chorismate and glutamine. Provides the activity of glutamine amidotransferase.	Pseudomonadales Pseudomonadaceae Pseudomonas

1.1.1 The Structure of Tryptophan

The structure of TRP consists of an indole ring, a five-membered ring with nitrogen bonded to a benzene ring, an α-carboxylic group and an amino group (Figure 1.2**).**

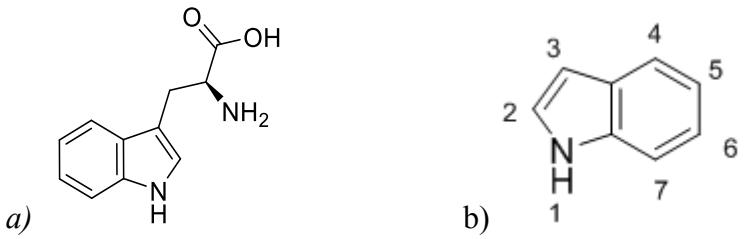

a) b)

(**Figure 1.2** – a) The Structure of Tryptophan b) The Structure of the Indole Ring – the aromatic compound, indole, consists of a six-membered benzene ring fused with a five-membered, nitrogen-containing pyrrole ring at positions 2,3 on the pyrrole ring.)

The presence of the indole ring allows tryptophan to bind to albumin through its indole-benzodiazepine site (Sudlow site II) (Conrad *et al.* 2009) with high affinity at physiological serum pH levels (McMenamy, 1965), therefore enabling TRP to be transported through the circulation bound to albumin (90%). The remainder (10%) is bioavailable in its free form in the resting state. The indole ring provides the basis to animal derivatives such as serotonin and melatonin. Other derivatives of indole have multiple biological actions. For example 2,3-diaryl-subsituted indoles possess anti-inflammatory and analgesic properties mediated by cyclooxygenase-2 (COX-2) inhibition (Kalgutkar *et al.,* 2005; Laube *et al*., 2014).

The TRP-albumin interaction is of major importance to the pharmacokinetic and pharmacodynamic profile of TRP (Yamasaki *et al.,* 2013). This interaction provides a variety of functions, it stops the passive diffusion of the amino acid out of the circulation and through the endothelium of tissues or the blood brain barrier (BBB), prevents metabolism, excretion and action with therapeutic targets (Koch-Weser & Sellers, 1976). At physiological resting state, the ratio of albumin-bound to free TRP is in equilibrium (McMenamy, 1965). Because the binding of TRP to albumin is readily reversible, albumin can act as a reservoir for TRP, enabling the release and replenishment of the TRP pool when biotransformation of the amino acid is upregulated. It has been reported that this ratio can change significantly during different physiological states. For instance, free TRP levels can be affected by the

serum concentration of non-esterified fatty acids (NEFAs) (Fernstrom & Fernstrom, 2006; Ruddick *et al*., 2006), the presence of benzodiazepines (Muller & Wollert, 1975) and the lipid-lowering agent clofibrate (Spano *et al.,* 1974). NEFAs displace TRP from the Sudlow site II binding site, elevating the concentration of free TRP in the circulation. This phenomenon is reportedly seen in multiple physiological states, for instance during intense exercise training (Bassami *et al.,* 2007), activation of the sympathetic nervous system (Dunn & Welch, 1991), and possibly in the obese (Karpe *et al.,* 2011). This elevation in serum TRP subsequently results in elevated tissue levels, upregulating TRP metabolism.

1.1.2 Metabolism of Tryptophan

TRP is metabolised *via* several pathways including bacterial degradation in the gastrointestinal tract, serotonin production and subsequent melatonin production in the pineal gland, protein synthesis and the kynurenine pathway (Keszthelyi *et al.,* 2009). This dissertation will focus on the kynurenine pathway.

1.2 The Kynurenine Pathway

It is estimated that up to 99% of the metabolism of dietary tryptophan is metabolised *via* the kynurenine pathway (Fig 5) (Stone & Darlington, 2002) (Keszthelyi *et al*., 2009), with the remaining 1% being converted into serotonin. This generates a set of biologically active indole-derived metabolites, termed ‘kynurenines’.

1.2.1 The Kynurenines

The kynurenine pathway culminates in the production of NAD^+, which is a fundamental component to metabolic processes occurring in all cells. These processes include the Krebs cycle, glycolysis, transcription and deoxyribonucleic acid (DNA) repair (Lin & Guarente, 2003). The kynurenine pathway metabolite that is the main precursor for NAD^+ production is quinolinic acid (QUIN).

TRP is initially metabolised by indoleamine 2,3-dioxygenase (IDO) and tryptophan 2,3-dioxygenase (TDO). Formylkynurenine is then rapidly, non-enzymatically,

converted into kynurenine (KYN). Although KYN is an intermediate metabolite, there have been suggestions that it also exerts powerful actions itself, with one study identifying a role for KYN in stimulating the expression of nerve growth factor in cholinergic neurons (Dong-Ruyl *et al.,* 1998). KYN is also present in high quantities within human eye lenses acting as a filter of ultraviolet (UV) light (Vazquez *et al.,* 2002), and has been linked to the formation of cataracts *via* UV irradiation (Varma & Hegde, 2010). KYN provides the substrate to three different enzymes producing different metabolites that exert diverse physiological effects. KMO converts KYN into the toxic 3-hydroxykynurenine (3HK); Kynurenine aminotransferase (KAT) converts KYN into KYNA which is neuroprotective, by virtue of being an antagonist at the *N*-methyl-*D*-aspartate (NMDA) receptor and competitive antagonist of QUIN (Boegman, *et al.,* 1985; Guillemin *et al*., 2001) (Figure 1.3). Anthranilic acid is produced from KYN by kynureninase (Mandi & Vecsei, 2012; Vecsei *et al.,* 2013). It is the creation of these toxic and neuroactive metabolites that has generated the present interest in the kynurenine pathway, as these metabolites have fundamental roles in inflammation, immunity and the pathogenesis of neurological disorders (Robert Schwarcz *et al.,* 2012).

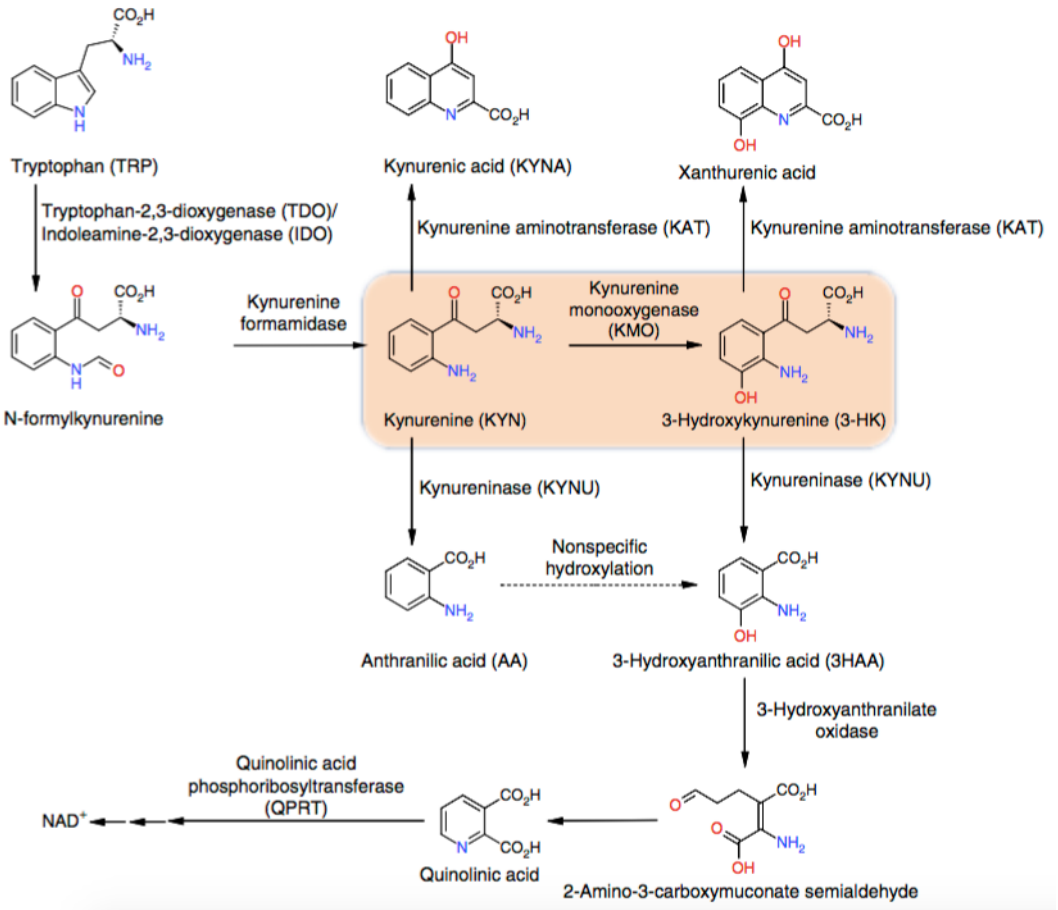

(**Figure 1.3 – Diagram of the Kynurenine Pathway** The main enzyme of interest is KMO (highlighted). This converts KYN into 3HK, a cytotoxic compound, which is then further metabolised into 3-hydroxyanthranilic acid (3HAA) by kynureninase (KYNU) and then into QUIN, a key compound in the de novo synthesis of NAD^+. KYNU also metabolises KYN into anthranilic acid (AA) which then hydroxylates into 3HAA, bypassing 3HK production (Mole *et al*., 2016).)

1.2.1.1 3-Hydroxykynurenine

The production of 3HK by KMO is the predominant route of KYN metabolism (Lugo-Huitron *et al*., 2013). 3HK is further metabolised into 3-hydroxyanthranilic acid (3HAA) by kynureninase and through subsequent reactions to eventually form the coenzyme NAD^+. Alternatively, 3HK can be metabolised by KAT to form XA, a free radical scavenger (Schwarcz *et al*., 2012).

3HK is a cytotoxic metabolite that exerts oxidative damage and induces cell death, thus contributing to the pathogenesis of tissue injury and neurodegenerative conditions (Colin-Gonzalez *et al.,* 2013). The oxidation of 3HK is readily catalyzed by copper (Cu^{2+}) and iron (Fe^{3+}) in physiological conditions to generate the reactive oxygen species (ROS), hydrogen peroxide (H_2O_2) and superoxide (O_2^-). ROS are powerful inducers of oxidative stress and thus contribute to inflammation, endothelial dysfunction, cellular apoptosis and tissue damage (Coyle & Kader, 2007; Goldstein *et al*., 2000). This auto-oxidation process is believed to be the main mechanism behind 3HK-driven neurotoxicity rather than acting on specific receptors (Thevandavakkam *et al.,* 2010). Experimental medical studies have shown that levels of 3HK are increased in neurological pathologies such as Huntington's disease (Thevandavakkam *et al.*, 2010), Parkinson's disease (Colin-Gonzalez *et al.*, 2013; Okuda *et al.,* 1998) and pneumococcal meningitis. However, some studies have identified 3HK to be a scavenger of free radicals and potentially acting as an antioxidant (Christen *et al.,* 1990; Goshima *et al,* 1986; Leipnitz *et al.*, 2007). It has been proposed that these anti-oxidant effects occur at natural physiological concentrations and the oxidative stress properties at high concentrations (Colin-Gonzalez *et al.*, 2013). Alternatively, 3HK may potentiate the effects of another toxic metabolite of the kynurenine pathway, QUIN, and the two together may form the underlying cause of neurotoxicity (Guidetti & Schwarcz, 1999).

More recently, 3HK has been proposed as the driver of systemic inflammation, and subsequent multi organ dysfunction following tissue injury due to trauma, acute pancreatitis, chronic renal failure and sepsis (Mole *et al*., 2016). This gives rise to the concept that KMO is the fundamental gate-keeper enzyme which by determining the fate of the kynurenine pathway metabolism can directly affect the severity of the inflammation.

1.2.1.2 Quinolinic Acid

QUIN is formed *via* the incorporation of O_2 into 3-hydroxyanthranilic acid (3HAA) by 3-hydroxyanthranilate 3,4-dioxygenase (3HAO), this initially produces the unstable 2-amino-3-carboxymuconate semialdehyde which spontaneously converts to QUIN (Foster *et al.,* 1986). This metabolite provides the substrate for NAD^+ production by quinolinic acid phosphoribosyltransferase (QPRT) (Foster *et al.,* 1985). In situations of inflammation, QUIN production in macrophages is very much reliant on the induction of IDO *via* interleukins and cytokines such as interferon-γ (IFN-γ) and tumour necrosis factor-α (TNF-α) (Guillemin, 2012).

QUIN can be metabolised peripherally and in the central nervous system (CNS) (Lugo-Huitron *et al*., 2013). However, studies have established that QUIN cannot cross the BBB, and therefore QUIN metabolism in the periphery and CNS are independent (Foster *et al.,* 1984; Lugo-Huitron *et al*., 2013). Kohler *et al*. identified that the cells with the greatest abundance of QPRT in rat brains are glial cells (Kohler, *et al.,* 1987) and the highest reported activity is located in the olfactory bulb (Foster *et al.*, 1985). However, QPRT is present in considerably lower quantities in comparison with 3HAO. This results in a Michaelis binding constant (K_M), that is 80 times less than that of 3HAO, leading to an accumulation of QUIN in conditions where the kynurenine pathway is upregulated (Foster *et al.,* 1986). As QUIN is a neurotoxin when present in excess, this upsurge may be pathologically important in neurological disease states (Lugo-Huitron *et al*., 2013), for example Alzheimer's disease, Parkinson's disease, Huntington's disease, motor neuron disease, multiple sclerosis, HIV-associated neurocognitive impairment and psychological dysregulation such as severe depression (Najjar *et al.,* 2013).

QUIN is a powerful glutamate agonist and therefore exerts an excitatory effect at the NMDA receptor located on human primary astrocytes (Lugo-Huitron *et al*., 2013), especially on the subgroup that contains the subunits GluN1 and GluN2A (Guillemin, 2012). NMDA over-activation is regarded as a well-established process that elicits neurodegeneration (Vecsei *et al*., 2013). Over stimulation of NMDARs triggers an influx of Ca^{2+}, elevating cytosolic Ca^{2+} concentrations (Akaike *et al.* 1999). This results in the upregulation of neuronal nitric oxide synthase (nNOS) and subsequent production of nitric oxide (NO). NO can react with superoxide to produce

peroxynitrite ($ONOO^-$), a potent inducer of neuronal death (Lafon-Cazal *et al.,* 1993; Santamaria *et al*., 2001). NMDAR-triggered Ca^{2+} influx also initiates iron-catalyzed production of hydroxyl free radicals ($^{\cdot}OH$) and induces lipid peroxidation, thereby provoking DNA fragmentation, altering cell membrane fluidity and ion permeability resulting in neuronal dysfunction (Santamaria *et al.*, 2001). Therefore, QUIN-mediated Ca^{2+} influx can result in astrocyte death (Guillemin, 2012).

Santamaria *et al.* investigated the role of QUIN in oxidative stress by incubating rat synaptosomes with varying concentrations of QUIN. In support of previous findings (Rios & Santamaria, 1991), these experiments exhibited a concentration-dependent rise in lipid peroxidation-related ROS formation, which was dampened by administration of glutamate receptor antagonists (Santamaria *et al.*, 2001). QUIN-mediated neurotoxicity has also been reported to be completely eradicated by the administration of MK-801, an NMDAR antagonist (Frumento *et al.*, 2002). This reversal of lipid peroxidation therefore gives scope to further research that aims to investigate and identify potential enzymes that can be targeted to directly reduce the production and subsequent accumulation of QUIN, including KMO.

1.2.1.3 Kynurenic Acid

Kynurenic Acid (KYNA), is a NMDAR antagonist, and therefore protects against neuronal excitotoxicity by glutamate-derived excitotoxins and QUIN. KYNA also exerts non-competitive inhibition on nicotinic acetylcholine receptors (nAChRs), in particular α7nAChR. α7nAChR inhibition decreases extracellular GABA levels, thus affecting the inhibitory neuronal network (Beggiato *et al*., 2014). As a consequence, compromised α7nAChR activity and KYNA are implicated in multiple neurological disorders, for example schizophrenia and Huntington's, diseases in which GABA dysregulation features prominently in the pathogenesis (Wassef *et al.,* 2003; Yamamura *et al.,* 1980).

Following the reporting by Lapin of a reduction in the severity of QUIN-induced seizures after KYNA administration (Lapin, 1976), KYNA has been the subject of investigations exploring the potential as an anticonvulsant and in neuroprotection (Moroni *et al.,* 2012; Stone, 2000). Foster *et al*. reported that KYNA blocks QUIN-mediated seizures and neurotoxic damage in rats (Foster *et al.,* 1984). In the brain, KYNA is produced mainly in glial cells *via* the catabolism of KYN by KATs (Figure 1.4) and acts on a specific binding site within the NMDAR, namely the strychnine-insensitive glycine-binding site (glycine allosteric site) (Szalardy *et al*., 2012). KYNA also exerts an inhibitory effect on acetylcholine-regulated pathways *via* presynaptic α7nAChRs, exerting anti-glutaminergic properties providing further protection from NMDA-mediated excitotoxicity and neurodegeneration (Vecsei *et al*., 2013). KYNA also effects the α-amino-3-hydroxi-5-metylisoxazol-4-propansyra (AMPA) receptor at high concentrations, and also has an effect on the G protein-coupled receptor 35 (GPR35) (Wennstrom *et al*., 2014).

The exact role of KYNA in neuroprotection is still debated as there are additional studies that can be construed as contradictory, including investigations into KYNA in Alzheimer's disease. It has been reported that peripheral levels of KYNA are significantly reduced in plasma and red blood cells in patients who have Alzheimer's (Hartai *et al.*, 2007). Another group observed decreased levels in cerebrospinal fluid (CSF) (Baran *et al.,* 1999). Together, these studies suggest that downregulation of KYNA may result in a loss of neuroprotection. This uncertainty has prompted recent investigations by Wennstrom *et al*. into the correlation between KYNA levels and

symptomatic Alzheimer's patients, which have been inconclusive (Wennstrom *et al*., 2014). Interestingly, pre-clinical studies, using transgenic mouse models of Alzheimer's and Huntington's disease which have used pharmacological inhibitors of KMO to increase KYNA levels have described a significant protection against neurodegeneration in these models (Zwilling *et al*., 2011). While these preclinical experiments show promise, and have potentiated interest and further research into drug development for KMO inhibition in neurodegenerative diseases (Reinhart & Kelly, 2011), they are complicated by the fact that the pro-drug of KMO used in these experiments, JM6, has been subsequently shown not to be converted to the active KMO inhibitor that was theoretically proposed (Beconi *et al*., 2012).

Peripherally, KYNA plays an important role in the regulation of the immune system and in the oncogenesis of gastric cancer *via* selectively activating the G protein-coupled receptor 35 (GPR35), a receptor present in immune and gastrointestinal cells (Chen & Guillemin, 2009; Wang *et al.*, 2006). Heightened levels of KYNA during inflammation reduce TNFα levels, induced by lipopolysaccharide (LPS), providing an anti-inflammatory mechanism (Wang *et al*., 2006).

1.2.2 Kynurenine 3-Monoxygenase

Kynurenine 3-monoxygenase (KMO), also known as kynurenine 3-hydroxylase, is a flavin adenine dinucleotide (FAD)-dependent, monomeric protein that is part of the external flavoprotein aromatic hydroxylase family (Breton *et al*., 2000). KMO consists of 486 amino acids and has a molecular mass of ≈55.8 kDa when in its dissociated form, located on the outer membrane of mitochondria (Alberati-Giani *et al*., 1997; Crozier & Moran, 2007; Okamoto *et al.,* 1967; Uemura & Hirai, 1998) in macrophages and microglia (Wilson *et al*., 2014). The KMO gene is located on 1q42-q44 (Wonodi *et al*., 2014). KMO has a vital role in the kynurenine pathway. Its function is to catalyse the hydroxylation of KYN into the cytotoxic intermediate 3HK and water, using nicotinamide adenine dinucleotide phosphate (NADPH) as an electron donor, and one atom of oxygen (Figure 1.4) (Breton *et al*., 2000). Initiation of KMO activity is dependent on the abundance of its substrate KYN.

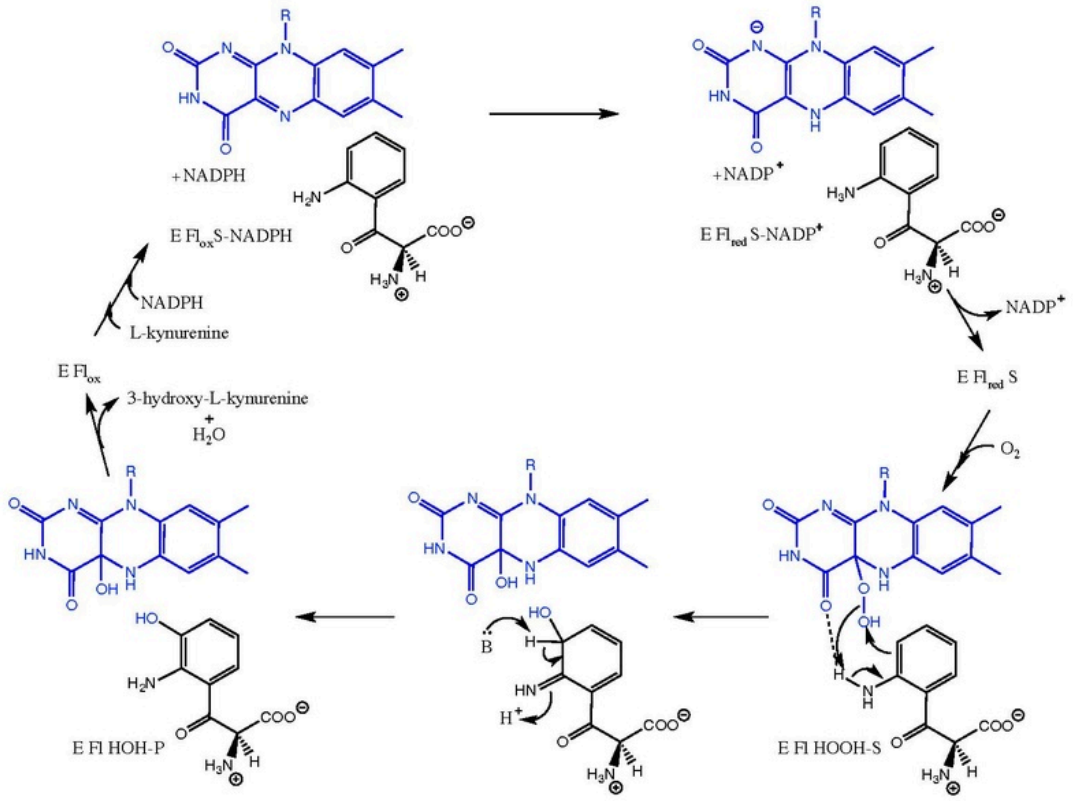

(**Figure 1.4 - The Proposed Hydroxylation of KYN by KMO**. KMO hydroxylates KYN resulting in the irreversible production of the toxic metabolite 3HK. The dotted lines represent theorised binding.)

1.2.2.1 The Structure of KMO

The structure of KMO was identified in *Saccharomyces cerevisiae* in 2013 (Amaral *et al*., 2013) and has a 51% similarity to the human form. Human KMO crystal structure studies have been unsuccessful to date because the presence of a C-terminal transmembrane helix causes difficulties in purification (Wilkinson, 2013). FAD is tightly bound non-covalently and the reduction of FAD by cofactors NADPH or reduced NAD^+ (NADH) is fundamental to the activity of KMO and the catalysis of KYN into 3HK (Breton *et al*., 2000; Smith *et al.,* 2016). The Mole group has used the *Pseudomonas fluorescens* KMO (*pf*KMO) structure for drug design. The residues surrounding the binding pocket of KYN, are structurally conserved in humans. Therefore, with the exemption of HIS320 which is exchanged for phenylalanine in human KMO, the binding pocket of *pf* KMO is hypothesized to be identical to human KMO (Mole *et al*., 2016).

*Pf*KMO consists of three domains (Figure 1.5) all of which encapsulate a split hydrophobic and hydrophilic binding pocket. The first domain (domain 1) binds to FAD *via* a nucleotide protein structural motif, an N-terminal Rossmann-like fold consisting of five parallel β-strands. Two anti-parallel β-strands connect this domain with the second domain (domain 2) which is responsible for interacting with KYN. Domain 3 lines the other side of the binding pocket (Wilkinson, 2013).

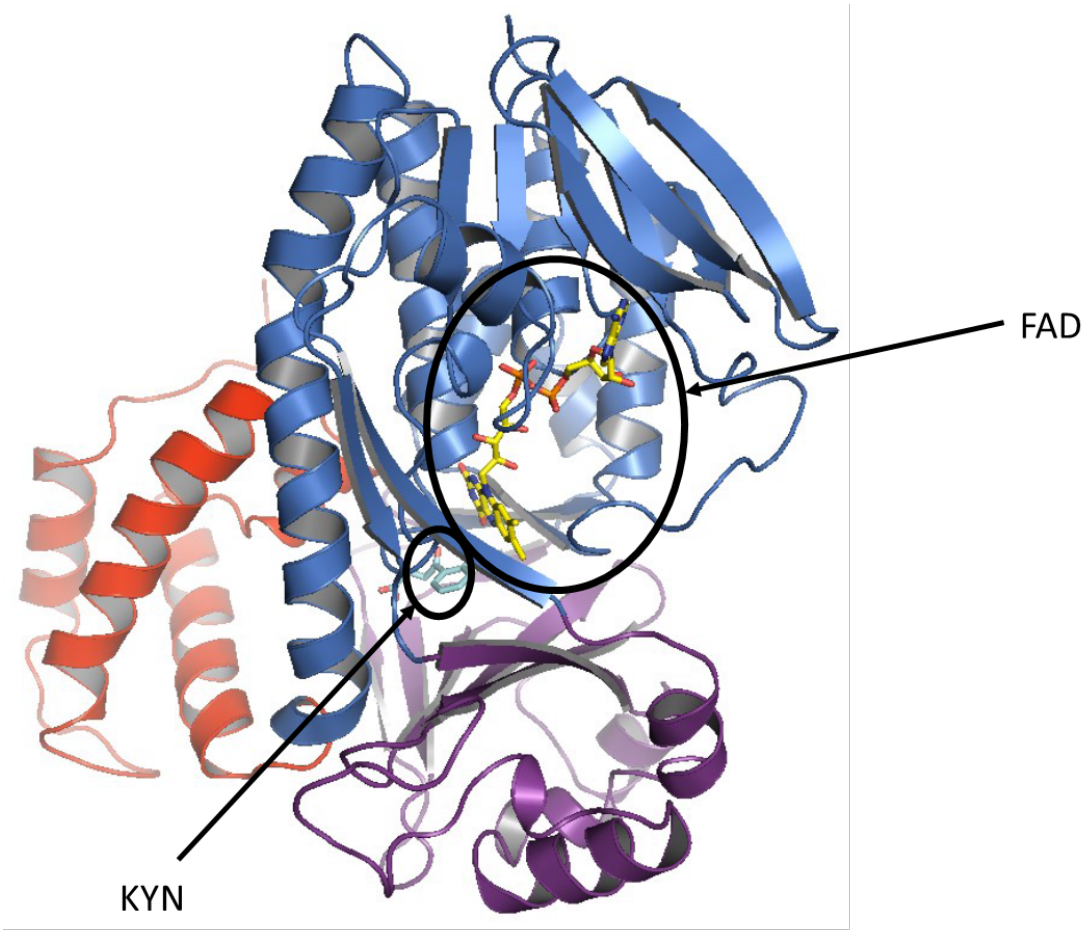

(**Figure 1.5 - The Three Domains of KMO.** An illustration representing the three domains of KMO, blue, red and purple respectively, bound to both FAD and KYN. Figure from (Wilkinson, 2013))

Inhibitors of KMO have been developed previously. Most were analogues of KYN (*o-, m-, and p*-nitrobenzoylalanine) but these were identified to have a role in NADPH oxidation, creating a peroxyflavin species that subsequently decays, generating hydrogen peroxide (Crozier-Reabe *et al.,* 2008). Thus research has diverted from analogues of KYN to benzenesulphonamide scaffolds (Röver *et al.,* 1997), including Ro 61-8048, a potent competitive inhibitor of KMO . The latter has failed to progress due to unspecified toxicology concerns.

1.2.2.2 Distribution of KMO

Distribution studies of KMO activity in rats have revealed that there is a modest, ubiquitous level of activity in the brain, whilst the highest levels of activity are found in the liver and kidney (Erickson *et al.,* 1992). Further studies by the Mole group into *Kmo* mRNA expression in wild-type C57BL6 mouse tissue has shown high *Kmo* expression in liver and kidney, and moderate expression in secondary lymphoid tissue, including spleen, lung, mesenteric and peripheral lymph nodes Mole *et al*., 2016) (Figure 1.6). KMO activity is a key rate determinant of the downstream kynurenine pathway. Decreased KMO activity alters KYN concentrations through a buildup of substrate, increases KYNA through diversion of KYN metabolism, and decreases 3HK, 3HAA and QUIN (Crozier & Moran, 2007). This altered metabolic profile drastically changes the inflammatory and neurodegenerative landscape. KMO activity is upregulated in inflammatory states (Alberati-Giani *et al.*, 1997) *via* IFN-γ, interleukin-1β (IL-1β) and LPS (Campbell *et al.,* 2014).

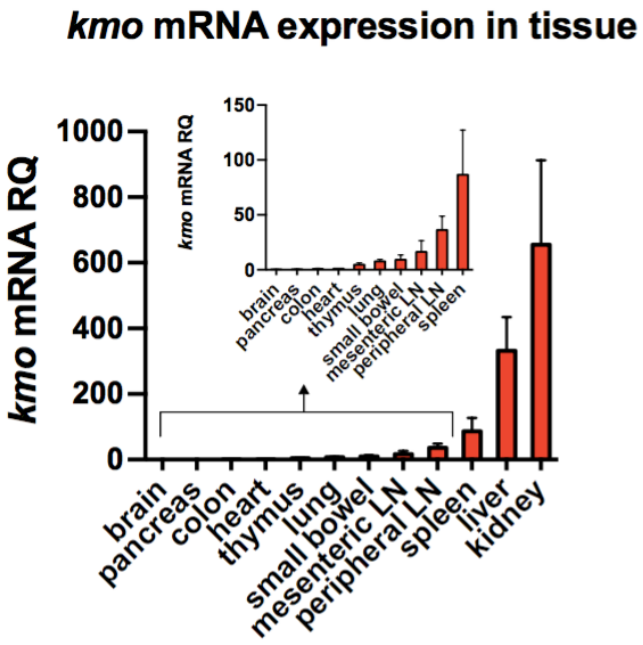

(Figure 1.6 – *Kmo* mRNA Expression in Tissue. KMO expression is predominant in liver and kidney tissue. KMO expression is also present in secondary lymphoid tissues such as mesenteric and peripheral lymph nodes. (Mean ± standard error of the mean; *Kmo* mRNA expression is relative to an 18S RNA internal control from kidney tissue extract from wild-type C57BL6 mice, which was assigned a value of RQ = 1 x 10^3; LN = lymph node) reproduced from (Mole *et al.*, 2016)**)**

1.2.2.3 KMO Interactions with KYN

The mechanism of KMO highlighted in Figure 1.4 is complex and is yet to be fully determined (Smith *et al*., 2016). The Mowat group at the University of Edinburgh has successfully crystalised a *Pf*KMO-KYN co-structure and this can be used to model KYN's interaction with KMO and FAD (Wilkinson, 2013). KYN interacts with the oxygen on the isoalloxazine ring of the noncovalently bound FAD in a hydrophobic pocket. This pocket is lined by residues Leu213, Ile215, Ile224, Leu226, Phe238 and Phe319. The carboxylate group sits in the hydrophilic pocket encapsulated by residues Arg84, Tyr98, His320, Asn369 and Tyr404 whilst interacting *via* hydrogen bonds with Arg84, Tyr98 and Asn369 (Figure 1.7) (Wilkinson, 2013).

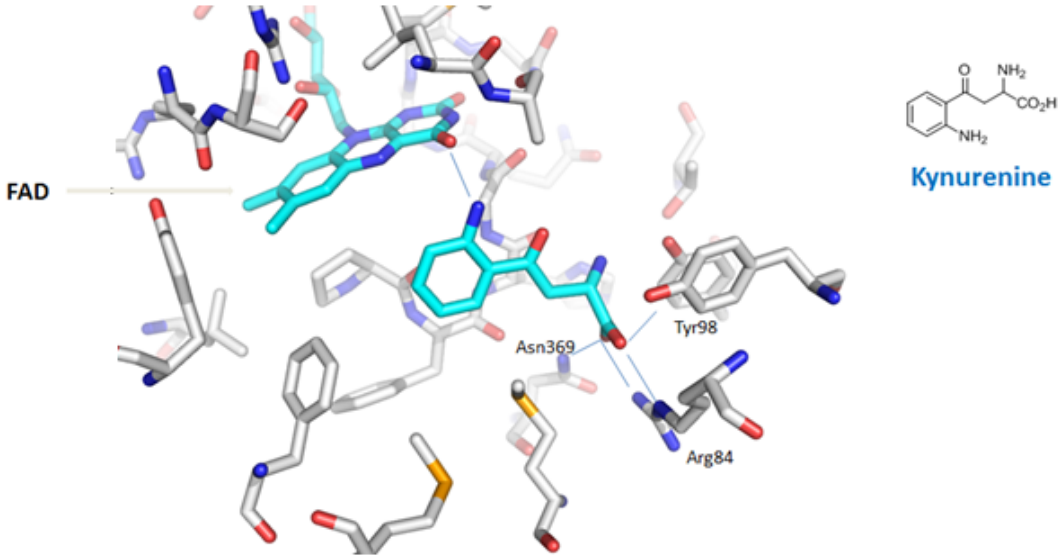

(**Figure 1.7 - The KMO Binding Pocket**. The FAD and KYN binding domains. Proposed bonds are displayed and main KMO residues highlighted. Enzyme residues (grey), KYN and FAD (cyan). Heteroatoms are coloured as: Sulphur (yellow); nitrogen (blue); and oxygen (red).)

1.2.2.4 The Role of KMO in Pathology

1.2.2.4.1 Neurodegeneration

KMO is predominantly expressed in microglial cells in the brain, however general expression in the brain is low (Amaral *et al*., 2013). Inflammatory states induce the infiltration of macrophages into the brain, increasing levels of QUIN propagating toxic effects on neurons (Guillemin *et al.,* 2003). QUIN injected directly into the brain, in particular the nucleus basalis, creates a glutamate receptor excitotoxic environment, reproducing the neurochemical alterations seen in Huntington's Disease (HD) (Boegman *et al*., 1985) (Stoy *et al*., 2005). QUIN injections have therefore been used as a mouse model of HD (R. Schwarcz *et al.,* 1983). QUIN administration has been reported to induce the expression of *huntingtin*, the gene responsible for the development of HD, adding further credence to the hypothesis that QUIN may play a role in the induction of HD (Tatter *et al,*. 1995). In contrast, Stoy *et al.* studied the possible role of the kynurenine pathway in HD patients, comparing peripheral serum samples with healthy volunteers. There were no differences in QUIN levels between patients and healthy volunteers despite an elevated KYN:TRP ratio in HD patients (Stoy *et al.*, 2005). However, these authors acknowledged that peripheral serum concentrations may not be directly representative of the CNS environment. Raised 3HK levels have been observed in Parkinson's disease (Ogawa *et al.*, 1992), mouse models of Huntington's disease (Guidetti et al., 2006), rat models of multiple sclerosis (Chiarugi *et al.*, 2001) and infantile spasms (Yamamoto *et al.,* 1994). Open-approach "bottom up" metabolomics studies, have also identified an increase of 3HK in association with Parkinson's disease (Lewitt *et al.,* 2013).

1.2.2.4.2 KMO in Systemic Inflammation and Acute Pancreatitis.

KMO activity is important in systemic and local inflammation, in particular that resulting from acute pancreatitis (AP).

The incidence of AP in the UK is reported to be between 15 and 42 per 100,000 population. The incidence of AP is increasing, possibly due to increasing alcohol consumption (Ellis *et al.,* 2009; Goldacre & Roberts, 2004; McKay *et al.,* 1999; Phillip *et al.,* 2014). The mortality rate of severe AP cases, despite the advances in intensive medical support and care ranges between 15-30% (Beckingham & Bornman, 2001; Gooszen *et al.,* 2013). The proportion of AP deaths occurring in the first week of admission has remained between forty to sixty per cent. This is due to the high risk of developing multiple organ dysfunction syndrome (MODS) in the early stages of severe AP, which is normally the cause of death in these patients (McKay *et al.*, 1999). Since the 1970's, there has been no progress in treatment with most therapies used to treat the symptoms rather than the disease itself (Phillip *et al*., 2014). Therefore, it is important to understand in more detail the cellular and hormonal mechanisms that are induced during the disease. In particular, research has focused on the roles of the kynurenine pathway in modulating the transition between AP and AP-induced multi organ dysfunction syndrome (AP-MODS).

In AP-MODS, the most commonly affected extra-pancreatic organ is the lung. Histological analysis of experimental AP Kmo^{wt} mice identified alveolar wall thickening, inflammatory cell infiltration and interstitial oedema (Mole *et al*., 2016). Acute kidney injury (AKI) also occurs in AP-MODS, with histological TUNEL analysis identifying marked cellular apoptosis in Kmo^{wt} kidney tissue. To identify whether KMO has a specific role in the pathogenesis and severity of AP-MODS, the Mole group created a strain of mice that is homozygous for *Kmo* knockout-first *tm1α* allele (Kmo^{null}) that were unable to produce 3HK. The level of apoptosis seen in these mice was considerably lower and significant protection against acute lung and kidney injury was subsequently seen (Mole *et al*., 2016). This leads to the conclusion that KMO plays a key role in determining the progression of severe sterile inflammatory disease states into critical illness. (Mole *et al*., 2016). These findings were recapitulated using the novel KMO inhibitor GSK180 in an experimental rat model of AP. KMO inhibition can therefore protect against AP-MODS.

1.3 Pharmacokinetics and Pharmacodynamics

Drug discovery and development requires an understanding of how a drug is absorbed, distributed, metabolised and eliminated (ADME/PK) from body systems, as well as an understanding how a drug effects these systems physiologically (pharmacodynamics, PD). PK/PD studies enable scientists and clinicians to understand the mechanisms of drug action, as well as identifying how a drug distributes across body compartments. Drugs can therefore be designed to achieve an optimal potency and desired effect at doses, which are therapeutic yet minimalise unwanted toxic side effects (Tuntland *et al*., 2014). The creation of a theoretical model of a drug's action before development, based on preclinical and clinical data analysis, can aid simulation of multiple aspects of drug behaviour and forecast its success in trialing. This includes simulation of the efficacy of a drug in clinical scenarios, whilst also predicting the dose-response relationship (Miller *et al*., 2005). Successful modeling in early drug discovery can benefit numerous facets during development, not only by aiding selection of the compound with the greatest potential, but also by reducing costs of development, as well as animal use, and reducing development time (Tuntland *et al*., 2014).

Despite research into the PK of TRP and the renal excretion of KYN during the 1980's (Moller, 1981), there has been little work since then to further develop and define the precise peripheral PK of TRP and its metabolites along the kynurenine pathway, especially of KYNA and 3HK. As the kynurenine pathway has been implicated in multiple disease states, it is important to understand the PK of the downstream kynurenine pathway metabolites and what proportions of metabolites become substrate for their corresponding enzymes and the rates of activity of these kynurenine pathway enzymes. These studies would allow the further modelling and simulation of the kynurenine pathway following KMO inhibition, identifying how KMO inhibitors affect the status quo of KYN metabolism thus uncovering the potential upstream and downstream consequences of this inhibition.

The parameters used in the mathematics of PK studies are discussed below:

1.3.1 Elimination Constant

The elimination constant, k_{el}, describes the exponential process that represents the rate at which a fraction of drug is removed from the body over a period of time. The removal of a drug is a dynamic process; normally dependent on the concentration of the drug. As the drug concentration reduces, the rate of change decelerates exponentially (Roberts & Freshwater-Turner, 2007). k_{el} can be calculated using the equation in Table 1.3, it can also be identified using a semi-log plot of concentration of drug against time (Figure 1.8).

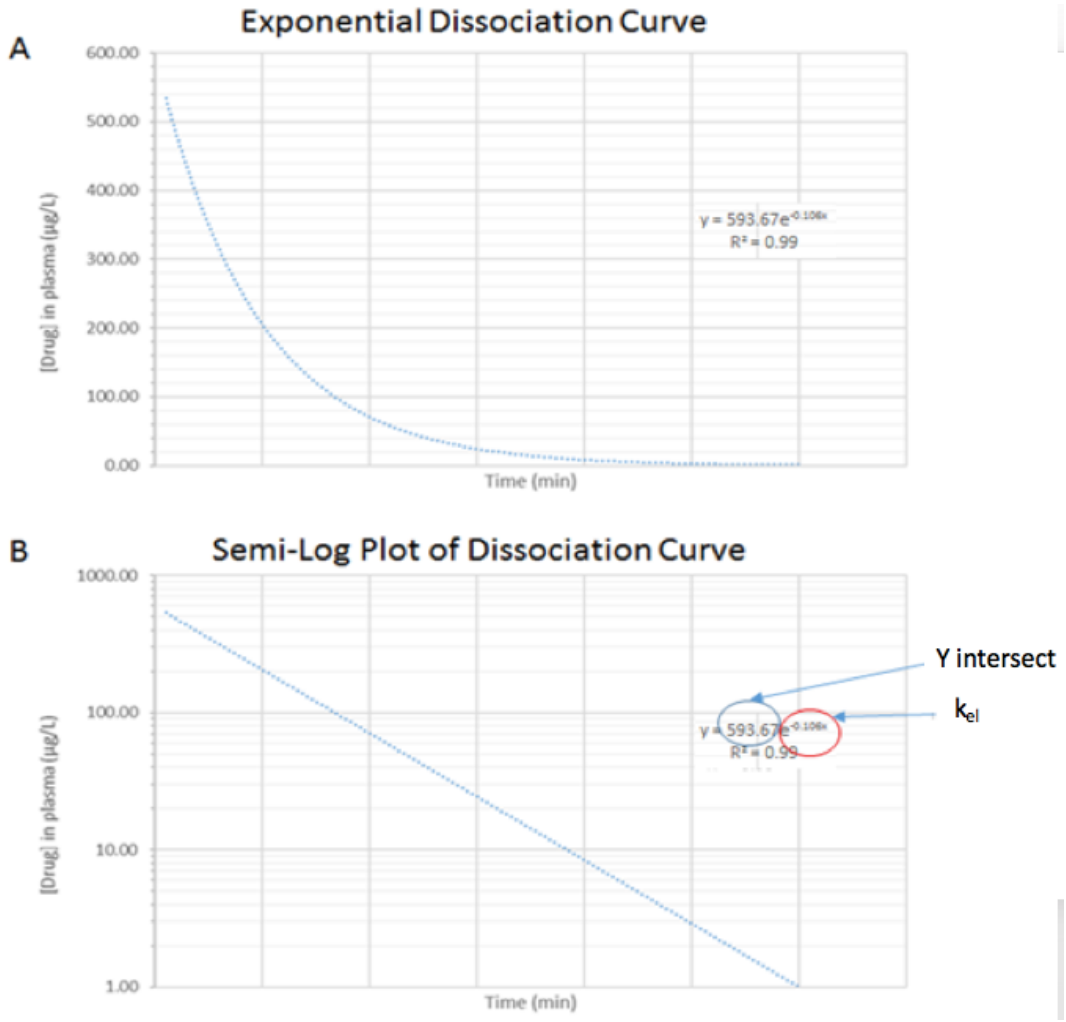

(Figure 1.8 – Example of an Exponential Curve. A) The concentration of drug in plasma shows an exponential decline in levels over time. B) This can be plotted on a semi-log plot to give the gradient of decline (y= intersect•e^{-kel}). This gradient can also be used to work out the initial concentration (C_i), where the trend-line crosses the y intersect (circled in blue). This can be used to calculate the drug's volume of distribution**)**

1.3.2 Volume of Distribution

The volume of distribution (V_d) represents the hypothetical volume of plasma that is required to contain the total amount of drug administered at the concentration that is observed in the plasma (C_p). It can be used to establish the target dose of drug needed to achieve optimal initial concentrations (Ci) in the blood. V_d is calculated using the equation in Table 1.2.

The value of the V_d for a drug represents the ability of the drug to readily be taken up by tissues. Values of V_d can appear to exceed that of normal body L/kg ratios. This is due to the ability of the drug to accumulate and concentrate in peripheral compartments such as fat and muscle, therefore reducing the circulating concentration. It is a theoretical volume and does not actually have to represent an anatomical compartment. The higher the value of V_d, the greater the drug's ability to distribute into tissues. Drugs with a low V_d are confined to the vascular compartment. This may occur for a variety of reasons: 1) due to the size of the drug and whether it can cross into cells; 2) whether the drug is highly polar or; 3) whether there is a high affinity for the drug to bind to plasma proteins such as albumin. There are a number of clinical implications arising from this. For example, only an unbound drug has the ability to exert its desired effects on the target. Therefore, binding to albumin reduces the drug potency and possibly the therapeutic efficacy.

1.3.3 Half-Life and Steady State.

The half-life ($t_{1/2}$) represents the time taken for C_p to halve. It is inversely related to k_{el} (Table 1.2), and therefore is governed by V_d and total clearance (CL_{tot}). $t_{1/2}$ is important clinically as it is used to determine the length of time it takes for a drug to accumulate to a therapeutic steady state level (four-five times $t_{1/2}$). The longer the $t_{1/2}$ of a drug, the longer it will take to achieve steady state, thus a loading dose may be required to reach a steady state more rapidly. It is also important for therapeutic drug monitoring, especially when using drugs with a very narrow therapeutic window where it is particularly important to minimalise drug adverse effects (Zhao & Jacqz-Aigrain, 2011).

1.3.4 Clearance

The collective elimination of a drug, over a unit of time, *via* hepatic metabolism (CL_{met}), renal excretion (CL_{ren}) and other routes of elimination (e.g. gaseous exchange and biliary excretion), (CL_{tot}). By generating an $AUC_{0\text{-}t}$ between the bolus dose (Q, time point 0) and the last measured time point (t), CL_{tot} can be calculated (Table 1.2). CL_{tot} is an important parameter in PK as it aids calculation of the target therapeutic dose and the length of the therapeutic window. Clinically, changes to renal function, such as chronic kidney disease, will affect CL_{tot} and therefore drugs have to be dosed accordingly (Munar & Singh, 2007). CL_{tot} can be used to calculate the rate of elimination (eq. 1) as well as k_{el}.

$$Rate\ of\ Drug\ Elimination = Concentration\ in\ Plasma\ (C_p)\ x\ CL_{tot} \quad \rightarrow$$

(Equation .1)

Table 1.2 - PK Parameters and Their Corresponding Equations

Parameter	**Symbol**	**Units**	**Equation**
Initial Concentration	C_i	µg/L	$C_i = \frac{D}{V_d}$
Half-life	$t_{1/2}$	min	$t_{1/2} = \frac{0.693 \cdot Vd}{CL_{tot}} = \frac{\ln 2}{k_{el}} = \frac{0.693}{k_{el}}$
Elimination Rate Constant	k_{el}	1/min	$k_{el} = \frac{CL_{tot}}{V_d}$
Clearance	CL_{tot}	ml/min	$CL_{tot} = k_{el} \cdot V_d$ or $CL_{tot} = \frac{Q}{AUC_{0-\infty}}$
Volume of Distribution	V_d	L/kg	$V_d = \frac{Total\ drug\ in\ body}{[drug]\ in\ plasma} = \frac{D}{C_i}$
Dose	D	µg/kg	
Steady State Enzymatic turnover	SS	(µg/L)/min	$SS = [analyte]_{endog} \cdot k_{el}$

1.3.5 The Partition Coefficient, Log*P*

The 1-octanol-water partitioning coefficient (*P*) represents the lipophilicity/hydrophobicity of a compound in solution at equilibrium. It defines the distribution of a compound between two immiscible phases, cytosol and lipid bilayer in cells. These two phases are represented by water and 1-octanol respectively, and therefore can be used to compare the ability of a compound to solubilise and distribute across biological membranes (Griffin *et al.,* 1999). Log*P* is measured by mixing a compound in a solution of water and 1-octanol, allowing the two phases to separate, then measuring and comparing the concentrations of the compound in each phase (Bowman & Sans, 1983). The difference between the two concentrations, *P*, can be assessed on a logarithmic scale (Log*P*, eq.2). Low Log *P* values represents a hydrophilic compound, whilst high Log*P* values are hydrophobic. We therefore can theorise the bioavailability of a drug and how successful it can be distributed amongst body compartments using Log*P*. Log*P* is particularly important in oral drug design as it aids ADME/PK modelling. Using Log*P* helps distinguish a drug's ability to be absorbed in the gastrointestinal tract (GIT), to cross hydrophobic cell membranes and distribute in aqueous cytosol. This aids the modeling of its distribution across body and cellular compartments (Harris & Logan, 2014). Log*P* is also crucial in determining a drug's lipophilic efficiency (LipE, eq.3), a critical parameter used to establish the quality of a drug in terms of potency (effectiveness of a drug to inhibit a specific biological function (IC_{50})) and toxicity (Eddershaw *et al.*, 2000). Changes in Log*P* after drug alterations can be used to establish whether the modification is beneficial, as a reduction in Log*P* represents a decline in a drug's toxicity (Hughes *et al.*, 2008). Lipophilic drugs transfer readily into cells due to their increased membrane fluidity and permeability, therefore augmenting their metabolism (Kalepu *et al.,* 2013). This enhancement in metabolism can lead to heightened action and thus increasing the prospect of drug toxicity. Therefore a drug with a high LipE and a low Log*P* can be deemed as a high quality clinical candidate (Freeman-Cook *et al.,* 2013).

$$\text{Log}P = \log\left(\frac{[Compound]1-octanol}{[Compound]\,water}\right) \quad \rightarrow \text{(Equation 2)}$$

$$\text{LipE} = -\log(IC_{50}) - \text{Log}P \quad \rightarrow \text{(Equation 3)}$$

The predicted Log*P* values for the kynurenine pathway analytes are all low, with QUIN being the most hydrophilic whilst KYNA is the most lipophilic. They are highlighted in Table 1.3.

Table 1.3 – Partition Coefficients of Endogenous Kynurenine Metabolites *(The Royal Society of Chemistry, 2016)*.

Solute	**Log*P***
TRP	1.04
KYN	1.09
KYNA	2.28
3HK	1.05
QUIN	-1.44
AA	1.21
3HAA	1.05

1.4 Summary of Introduction

The kynurenine pathway is an important metabolic pathway in the regulation of inflammation in multiple disease states. KMO is a fundamental gateway enzyme that converts KYN into the cytotoxic metabolite 3HK. Current research by the Mole group, in collaboration with GlaxoSmithKline Plc, has established the importance of the metabolites of the kynurenine pathway in the progression of AP into AP-MODS and the subsequent poor patient outcomes. Consequently, a novel, potent inhibitor of KMO, GSK180, has been developed which prevents the progression of AP to AP-MODS in rodents. KMO inhibition provides a novel approach to the therapeutic treatment strategies in systemic inflammation and thus could radically reduce mortality rates seen in patients with severe AP progressing to AP-MODS.

Section 2: Aims

AIM:

To investigate and determine the precise pharmacokinetics of the kynurenine pathway in the systemic circulation, with focus on the enzyme reaction rate of KMO.

OBJECTIVE:

To use stable isotope tracers, ($^{13}C_6$ or ^{2}H) TRP, KYN, KYNA and 3HK to develop a metabolic model of TRP metabolism *via* the kynurenine pathway, identifying the exact rates of formation and elimination of each metabolite of interest, and the percentage of KYN used as substrate by KMO, and to determine the rate of 3HK formation.

SECONDARY AIMS AND OBJECTIVES:

Because two of the tracers (D_5-KYNA and $^{13}C_6$-3HK) in preliminary studies could not be detected and quantified in rat plasma using the protein precipitation and mass spectrometry methods previously used by the Mole group, an additional aim was to develop and validate a precise, sensitive, accurate and reliable laboratory assay that encompasses:

- The extraction of all major kynurenine pathway metabolites from plasma.
- Measurement of all major kynurenine pathway metabolites *via* liquid chromatography tandem mass spectrometry (LC-MS/MS) under one assay.
    - With a Limit of Quantification (LOQ) of 50 µg/L, or lower, for all metabolites.
    - Improved detection of D_5-KYNA and $^{13}C_6$-3HK at low plasma levels.
    - Calibration curves achieving excellent linearity ($R^2 > 0.99$) and method validation in compliance with FDA guidelines.

Lastly, the aim was to formulate a pharmacokinetic model of the kynurenine pathway. To achieve this, the data obtained, using the newly developed LC-MS/MS assay, for the rat plasma that had been intravenously (IV) infused with tracer will be subjected to PK analysis software. The data from the software was then interpreted appropriately.

Section 3: General Laboratory Methods

This chapter describes the laboratory methods and apparatus that were used in the design and development of the experimental assay used in the analysis of plasma samples from rats that had been given a bolus IV injection of specific kynurenine pathway metabolite tracers.

3.1 Materials

3.1.1 Tracers

All tracers were purchased in powdered form and suspended in high performance liquid chromatography (HPLC) grade water to produce the concentrations stated in Table 3.1. The concentrations of D_5-TRP and $^{13}C_6$-KYN used were formulated by identifying the endogenous levels found in rats and estimating a concentration of tracer that would represent 10% of these levels. Higher concentrations of D_5-KYNA and $^{13}C_6$-3HK were required to achieve suitable peak areas for quantifiable detection on the LC-MS/MS, in keeping with FDA guidelines. Therefore, the concentrations identified in Table 3.1 are the lowest achievable concentrations that enabled the modelling of these tracers' PK whilst adhering to FDA requirements.

Table 3.1 - Structures of Stable Isotope Tracers**.** (Sigma Aldrich®)

Tracer	***Molecular weight (g.mol^{-1})***	***Empirical Formula***	***Structure***	***Concentration Used (µg/ml)***
L-tryptophan-(indole-d_5) (D_5-TRP)	209.26	$C_{11}D_5H_7N_2O_2$	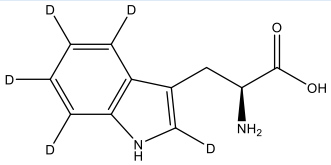	500
[$^{13}C_6$] – L-Kynurenine ($^{13}C_6$-KYN)	214.17	$C_4{}^{13}C_6H_{12}N_2O_3$	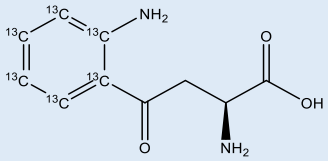	20
Kynurenic acid-3,5,6,7,8-d_5 (D_5-KYNA)	194.20	$C_{10}D_5H_2NO_3$	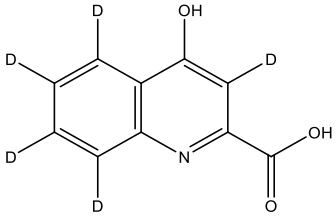	1
[U-Ring $^{13}C_6$] -3-Hydroxykynurenine ($^{13}C_6$-3HK)	230.17	$C_4{}^{13}C_6H_{12}N_2O_4$	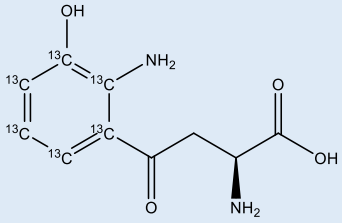	20

Table 3.1.2 - Reagents and Materials used for Sample Extraction and Liquid Chromatography tandem Mass Spectrometry

Item	Brand
Disposable Culture Tubes Borosilicate Glass (12x75 mm)	Fisherbrand, Loughborough
HiPerSolv grade Methanol (CH_3OH)	VWR Prolabo Chemicals, Leicestershire
HPLC grade Water (H_2O)	Fisher Scientific UK, Loughborough
Formic Acid Reagent Grade >95%	Sigma Aldrich®, Dorset
Phosphoric Acid Reagent Grade 85 wt. % in H_2O	Sigma Aldrich®, Dorset
Finnpipettes F2 kit 4	Thermo Scientific, Cupar
Pipette Tips volume range 10 µl -1 ml	Thermo Scientific, Cupar
Oasis® Hydrophilic Lipophilic Balanced (HLB) 96 well plate (10 mg Sorbent well, 30 µm Particle Size)	Waters Limited, Hertfordshire
Greiner Masterblock® 96-well collection plate	Sigma Aldrich®, Dorset
IST VacMaster™ 96-well vacuum manifold	Biotage®, Sweden
Driblock DB3 Sample Concentrator	Techne, Staffordshire
Needles (76 mm long)	Techne, Staffordshire
SPE Dry™ 96 Dual Sample Concentrator System Microplate Sample Evaporation System for 96-well plates	Biotage®, Sweden
PV-1 Vortex Mixer	Grant Instruments, Cambridgeshire
KS 260 Basic Shaker	IKA®, Germany
4% Phosphoric Acid (H_3PO_4) in HPLC Grade water	
0.1% Formic Acid (CH_2O_2) in HPLC Grade water	
0.1% Formic Acid (CH_2O_2) in HPLC Grade water	
80% Methanol (CH_3OH) in HPLC Grade H_2O	

3.2 Methods

3.2.1 Jugular Vein and Carotid Artery Cannulation in Rats Protocol

The studies of the pharmacokinetics and pharmacodynamics of kynurenine pathway metabolite tracers were performed in rats (male, *Sprague Dawley,* body weight 250-350g) obtained from Charles River Laboratories. Central vascular catheters, jugular vein and carotid artery, were placed under terminal anaesthesia (Isoflurane) (Mole *et al.,* 2008). Rats were then dosed with predetermined optimised concentrations of tracer (see Table 3.1) *via* IV infusion (0.1 ml / 100 g) through the jugular vein. Blood samples (500 µl) were collected *via* the carotid artery 1 minute before IV infusion, then at 1, 5, 10, 15, 30, 60, 120, 180 minute intervals for D_5-TRP and $^{13}C_6$-KYN. For D_5-KYNA and $^{13}C_6$-3HK blood was collected at 1, 3, 5, 8, 15, 30, 60 minute intervals due to their faster metabolism. Patency of the cannulae was maintained throughout the experiment by flushing with sterile saline (500 µl) after each sample was taken. The samples were then immediately aliquoted into ethylenediaminetetraacetic acid (EDTA) tubes, inverted and then subjected to centrifugation (3 mins, 5,000 RPM). The plasma supernatant was then aliquoted (100 µl) into three 1.25 ml eppendorfs and then frozen at -80^{o}C.

3.2.2 Sample Extraction

3.2.2.1 Stock Solutions and Standard Calibration Curve

Individual stock solutions of each endogenous compound and tracer were prepared by dissolving in HPLC grade water and stored in a freezer (-20°C) (Table 3.2).

Table 3.2 – Individual Stocks of Compounds

Individual Stocks	**L-KYN**	**TRP**	**KYNA**	**3HK**	**3HAA**	**XA**	**QUIN**	**AA**	**D_5-TRP**	**$^{13}C_6$-KYN**	**D_5-KYNA**	**$^{13}C_6$-3HK**
Concentration (mg/ml)	1	1	1	1	1	1	2	2	1	0.4	5	0.5

Mixed-analyte master stocks (25 µg/mL concentrations) were then created by mixing the individual compounds together (Table 3.3). These were then serially diluted with methanol to create reference standard solution stocks (Table 3.4). All solutions were stored in a freezer at approximately -20°C prior to use.

Table 3.3 – Master Stocks (25 µg/ml)

	Volume Of Analyte (µl)												
Mixed Analyte Stock	**L-KYN**	**TRP**	**KYNA**	**3HK**	**3HAA**	**XA**	**QUIN**	**AA**	**D_5-TRP**	**$^{13}C_6$-KYN**	**D_5-KYNA**	**$^{13}C_6$-3HK**	**CH_3OH**
All Analytes	175	175	175	175	175	175	87.5	87.5	175	437.5	35	350	4778
9 Analyte (D_5-TRP)	175	175	175	175	175	175	87.5	87.5	175	0	0	0	5600
9 Analyte ($^{13}C_6$-KYN)	175	175	175	175	175	175	87.5	87.5	0	437.5	0	0	5338
9 Analyte (D_5-KYNA)	175	175	175	175	175	175	87.5	87.5	0	0	35	0	5770
9 Analyte ($^{13}C_6$-3HK)	175	175	175	175	175	175	87.5	87.5	0	0	0	350	5425

Table 3.4 – Reference Standard Solutions Stocks.

Reference Standard Curve Stock Created (µg/ml)	**Standard Analyte Mix Stock used for dilution (µg/ml)**	**Volume of Standard Analyte Mix Stock Used (ml)**	**Volume of CH_3OH (ml)**
10	25 (Master Stock)	2.8	4.2
5	10	3.5	3.5
2	5	2.8	4.2
1	2	3.5	3.5
0.5	1	3.5	3.5
0.2	0.5	2.8	4.2
0.1	0.2	3.5	3.5
0.05	0.1	3.5	3.5
0.02	0.05	2.8	4.2
0.01	0.02	3.5	3.5

The standard calibration curve consisted of one replicate of ten non-zero standards (Tables 3.5 and 3.6). Each calibration curve was prepared afresh on the day of sample extraction. All calibration curves were prepared by spiking 1% bovine serum albumin (BSA) in phosphate buffer solution (PBS), acting as a plasma matrix surrogate. The preparation of the standard calibration curves followed the exact same method as described in section 3.2.2.2.

Table 3.5 – Base Template for Standard Calibration Curves that were Created Fresh each Experiment whilst Analysing Levels of Tracer in Rat Plasma.

Amount (ng)	**Internal Standard (50 ng)**	**Volume of Mixed Analyte Standard Mix**
Double Blank	0	0
0	10 µl x 5 µg/ml	0
0.1	10 µl x 5 µg/ml	**10** µl x 0.01 µg/ml
0.2	10 µl x 5 µg/ml	**10** µl x 0.02 µg/ml
0.5	10 µl x 5 µg/ml	**10** µl x 0.05 µg/ml
1	10 µl x 5 µg/ml	**10** µl x 0.1 µg/ml
2	10 µl x 5 µg/ml	**10** µl x 0.2 µg/ml
5	10 µl x 5 µg/ml	**10** µl x 0.5 µg/ml
10	10 µl x 5 µg/ml	**10** µl x 1 µg/ml
20	10 µl x 5 µg/ml	**10** µl x 2 µg/ml
50	10 µl x 5 µg/ml	**10** µl x 5 µg/ml
100	10 µl x 5 µg/ml	**10** µl x 10 µg/ml

The base template for the calibration curves was adjusted and amended, depending on the tracer used, to maximise the number of points on the curve that lay within the range of tracer levels seen in the rat plasma. The internal standards used depended on the tracer analysed, D_5-TRP was used when analysing $^{13}C_6$-KYN, $^{13}C_6$-3HK and D_5-KYNA whilst $^{13}C_6$-KYN was used when analysing D_5-TRP.

3.2.2.2 Rat Plasma Sample Extraction using Solid Phase Extraction

This method describes the optimised protocol that developed throughout the study (Section 3.3)

3.2.2.2.1 Preparation of Calibration Curve and Rat Plasma Before Administration to Waters Oasis® HLB 96-well plate.

Plasma concentration of tracers and endogenous levels of kynurenine pathway metabolites were assessed using ultra-high performance liquid chromatography (UHPLC)-MS/MS. Plasma samples to be analysed were removed from -80^{o}C freezer and thawed in ice. A borosilicate glass tube was labelled for every plasma sample and calibration curve point. Internal standard (50 ng) was then added to every tube along with the corresponding volume of standard analyte mix to the calibration curve tubes. These were then placed in a preheated Driblock (40^{o}C) and evaporated to dryness. 100 µl of 4% phosphoric acid was then added to every tube and vortexed for ten seconds. 100 µl of rat plasma or 1% BSA was added to the corresponding tubes and subject to ten seconds of vortex.

3.2.2.2.2 Preparation of Waters Oasis® HLB 96-well Plate and Extraction of Rat Plasma.

Methanol (500 µl) was added to extraction wells (Oasis® Hydrophilic Lipophilic Balanced (HLB) 96-well 10 mg sorbent well, 30 µg particle size) before subjection to vacuum (0.35 Bar) to dryness. To condition, HPLC grade water was then added to equilibrate wells and prime them for sample administration. Standards and internal-standard-enriched samples (200 µl) were added. After incubation (RT, 5 mins) the HLB plate was then subjected to vacuum (0.35 Bar) to dryness. Wells were then washed with water (500 µl) and then vacuumed. A Masterblock® 96-well collection plate was then placed inside the vacuum manifold, 80% methanol (200 µl) added to HLB plate and extracts collected under vacuum. The eluates in the collection plate were then evaporated to dryness under oxygen-free nitrogen (OFN, 30 L/min, 60^{o}C). Analytes were then resuspended in HPLC grade water (70 µl) before the plate was placed on a shaker (5 mins). Methanol was then added (30 µl) and the plate was shaken again (5 mins). Samples were then injected onto the HPLC-MS/MS system (10 µl).

3.2.3 Instrumentation

The UHPLC-MS/MS, for use in the analysis of the rat samples, was comprised of a Shimadzu Nexera MP UHPLC with an AB SCIEX QTRAP 6500+ triple quadrupole system mass spectrometer, operated by Analyst® software (SCIEX, Cheshire, UK). The column used for analysis was an ACE Excel UHPLC silica column comprised of a C18 bonded to pentafluorophenyl (PFP) phase (C18-PFP) (1.7 µm, 2.1 x 100 mm, Advanced Chromatography Technologies Ltd., Aberdeen, Scotland). The sample was injected (10 µl); column oven temperature was 40^{o}C. Two mobile phases were used 0.1% formic acid (Phase A) in water and 0.1% formic acid in methanol (Phase B) at a flow rate of 0.4 ml.min^{-1}, compounds were eluted using the gradient as highlighted in Table 3.6.

Table 3.6 - Composition of Phases Being Pumped into LC-MS/MS Throughout Run.

Time (min)	Composition (%) A	Composition (%) B
0.00	10	90
1.00	10	90
6.00	80	20
8.00	80	20
8.10	10	90
9.00	Stop	

Mass spectra were recorded using electrospray ionisation mass spectrometry (ESI) in both positive and negative multiple reaction monitoring (MRM) modes over a run time of nine minutes. The parent/product transitions (Q1→Q3, *m/z*) along with typical retention times for each analyte were optimised (See Section 4). Instrument control, data acquisition and integration were processed using Analyst® Software, Version 1.6.3 (SCIEX, Cheshire, UK). Data processing was performed using MultiQuant™ Software, Version 3.0.2 (SCIEX, Cheshire, UK). All peaks were analysed individually and only accepted if they satisfied the criteria described in the FDA guidelines (Food and Drug Administration, 2001).

3.3 Method Formulation and Validation

In order to develop an optimised, enhanced and precise method of kynurenine pathway metabolite analysis, multiple experiments were undertaken to assess the following:

3.3.1 Extraction Method

Three main approaches to protein extraction were identified: protein precipitation (PPT), supported liquid extraction (SLE) and solid phase extraction (SPE). Plasma was enriched with a four tracer mix (100 ng). The recovery and ion suppression of each tracer analyte were used to compare these approaches.

3.3.1.1 LC-MS/MS Method for Formulation

During the method formulation, a different LC-MS/MS method was used due to availability of systems. This LC-MS/MS system comprised of a Waters ACQUITY UPLC® with an AB SCIEX QTRAP 5500. Samples were analysed by LC-MS/MS in MRM mode, by injecting 10 µl onto an XSelect High Strength Silica (HSS) PFP column (3 x 100 mm; 2.5 µm). Once the extraction method had been optimised, the LC-MS/MS analysis was transferred to the Shimadzu Nexera MP front end with an AB SCIEX QTRAP 6500+, injecting 25 µl onto the same column. This column was then compared with a different UHPLC column, an ACE Excel UHPLC (C18-PFP) (1.7 µm, 2 x 100 mm) column to finalise the complete assay.

3.3.1.2 Protein Precipitation

Plasma was precipitated using a protein precipitation plate (Isolute® PPT+ 96-fixed well 1ml, Biotage, Sweden). Three solvents were tested; acetonitrile (300 µl), methanol (500 µl) or 1 M TCA (300 µl). Samples were prepared in triplicate for each solvent. Plasma (100 µl), was enriched ($^{13}C_6$-KYN, $^{13}C_6$-3HK, D_5-KYNA and D_5-TRP, 100 ng) in a glass vial and the sample then transferred to the solvent prepared PPT+ 96-well plate. The sample was left to stand in the wells (60 mins) and a vacuum was applied (3 mins, 0.35 Bar) to elute. The solvent was dried down under OFN (60°C, 30 L/min) and resuspended in methanol and water (100 µl, 50:50, *v/v*). Non-enriched plasma (100 µl), was also subjected to protein precipitation and subsequently post-spiked with $^{13}C_6$-KYN, $^{13}C_6$-3HK, D_5-KYNA and D_5-TRP mixture (100 ng) at the time of resuspension in methanol in water (50:50, *v/v*), by adding a standard mixture in methanol (10 µl, 1 µg/ml), along with further methanol (40 µl) and water (50 µl).

3.3.1.3 Supported Liquid Extraction

Plasma was extracted using an SLE+ plate (Isolute® SLE+ 400 µl 96-fixed well, Biotage, Sweden). Standard tracer mix (100 ng) was added to water or plasma (100 µl) in a borosilicate glass vial and diluted with water (1:1) before being transferred to the SLE+ plate. A solvent (methyl tert-butyl ether (MTBE), dichloromethane (DCM), hexane or diethylether, 1 ml), was added before being left to incubate (30 mins). The solution was then pulled through by vacuum and dried down under OFN (60°C, 30 L/min) before being resuspended in methanol and water (100 µl, 50:50, *v/v*).

3.3.1.4 Solid Phase Extraction

Individual Oasis® HLB cartridges (10 mg sorbent, 30 µm particle size, Waters, USA) were used to extract plasma (100 µl) enriched with tracer standard mixture (100 ng). Each cartridge was conditioned with methanol (500 µl), equilibrated with water or 4% phosphoric acid (500 µl), then the sample was loaded (100 µl) with a dilution solution (4% phosphoric acid or 5% ammonium hydroxide) (100-400 µl). The

samples then underwent a first wash with water (500 µl), a second wash with another solvent (500 µl of 4% phosphoric acid or 5% methanol) and eluted with methanol (2 x 250 µl). The eluent was dried down under OFN (60^{o}C, 30L/min) and resuspended in methanol in water (100 µl, 50:50, *v/v*).

Different volumes of solvent at the loading step were tested (100, 200, 300 and 400 µl).

3.3.1.5 Optimising Solid Phase Extraction Method

The best results were achieved using the Oasis® HLB cartridges. The following method optimisation experiments were undertaken using the recommended protocol (Oasis® HLB, Waters, USA) as a construct (Figure 3.1) upon which to develop the ideal extraction protocol that enables all analytes to be extracted and analysed with one assay. Each experiment was analysed by comparing analyte recovery and ion suppression.

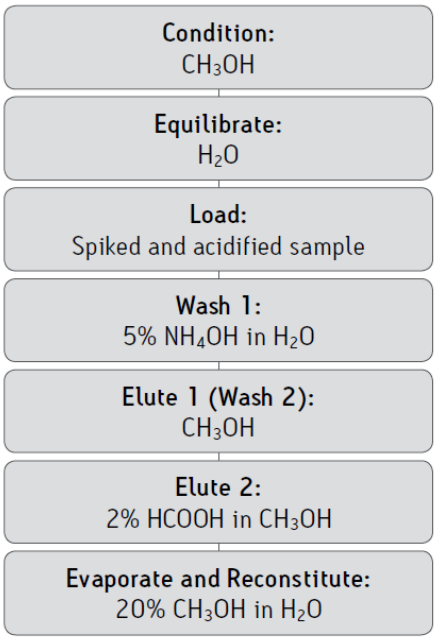

(**Figure 3.1 - Oasis® HLB Extraction Protocol** (Waters, USA))

Priming of Sample

Plasma samples were primed before administering onto columns using either an acid (4% phosphoric acid) or base (5% ammonium hydroxide) at a series of different dilutions (1:1, 1:2, 1:3, 1:4).

Equilibration of Column

Equilibration of columns was optimised by comparing the use of 4% phosphoric acid or HPLC grade water.

Wash 1 and 2

Washes were optimised by comparing the use of 5% methanol, water or 4% phosphoric acid. The number of post load washes were also compared.

Elution

The optimal elution solvent was assessed by comparing concentrations of methanol in water from 40% methanol to 100% in increments of 10%.

Resuspension

Premixed solutions of 50% and 70% methanol, along with individual additions of water and methanol were compared to identify the ideal resuspension conditions.

3.3.2 Chromatographic Conditions

To achieve optimal peaks, multiple chromatographic conditions were assessed, these were:

- LC-MS/MS apparatus
    - Two different LC-MS/MS systems were compared, a Shimadzu Nexera MP/ AB SCIEX QTRAP 6500+ triple quadrupole system and a Waters ACQUITY UPLC® / AB SCIEX QTRAP 5500 triple quadrupole system. The system that achieved superior peaks (peak shape and area) at low concentrations would then be used for analysis of rat plasma samples.
- Column
    - Two different columns were then compared on the superior system, an ACE Excel UHPLC (C18-PFP) (1.7 µm, 2.1 x 100 mm) and a Waters XSelect HSS PFP column (3 x 100 mm; 2.5 µm) to identify which column produced superior peaks for $^{13}C_6$-3HK and D_5-KYNA (peak shape and area).
- Flow rate
    - Different flow rates (400, 500, 600 µL/min) of mobile phase were then compared (peak shape and area).

3.3.3 Method Validation

For the method validation to be satisfactory, the data had to satisfy the following FDA criteria:

- The precision of the lowest acceptable standard on the calibration curve, the lowest limit of quantitation (LLOQ), around the mean value of a minimum of five out of 6 replicates must not exceed 20.0% relative standard deviation (RSD).
- The precision of all other standards on the calibration curve around the mean value of a minimum of five out of six replicates must not exceed ±15% RSD.
- The 1/x weighted linear regression correlation coefficient (R^2) of standard concentration versus instrument response should be at least 0.99 for every assay validation batch.
- A minimum of six standards on the calibration curve must fall within accuracy limits of ±20% at LLOQ and ±15% for all other standards. If there are insufficient numbers of standards that satisfy this criterium, the calibration curve should be re-evaluated using $1/x^2$ regression analysis.

3.3.3.1 Recovery and Ion Suppression

Replicates of four-tracer analyte mixes ($^{13}C_6$-KYN, $^{13}C_6$-3HK, D_5-KYNA and D_5-TRP, 100 ng) pre- or post-spiked in rat plasma (n=6) were compared to assess analyte recovery and ion suppression. Recovery was assessed by calculating the mean of the integrated peak areas of the extracted standards and displaying them as a percentage of the mean of the unextracted standards. Ion suppression was assessed by calculating the mean of peak areas of extracted samples and displaying them as a percentage of an unextracted methanol in water (30:70, *v/v*) sample.

3.3.3.2 Extraction Efficiency

The efficiency of the assay was measured by comparing the peak areas of seven kynurenine metabolite compounds (TRP, KYN, KYNA, 3HK, QUIN, AA, 3HAA), spiked in 1% BSA, in six standard curves across six separate days. Intra-day efficiency was also assessed by extracting and analysing six separate curves in the same day. Precision and accuracy were calculated using the mean and relative standard deviation for each concentration on the curve.

3.3.3.3 Optimisation of MS/MS Detector Parameters and Manual Tuning

The MRM scan mode parameters (Q1→Q3) were calibrated using Analyst® Software in conjunction with the Shimadzu Nexera MP/ AB SCIEX QTRAP 6500+ triple quadrupole system.

3.3.3.4 Dilution Linearity

Replicates (n=6) of extracted control rat plasma, were diluted ten-, twenty-, fifty- and a hundred- times in methanol in water (30:70, *v/v*) then analysed on the UHPLC-MS/MS system to assess dilution accuracy and linearity of endogenous analytes.

3.4 Pharmacokinetics Analysis of Data

PK analysis of the data was performed using PKSolver 2.0, an add-in program for Microsoft Excel (Zhang *et al.,* 2010). The entire data set for each tracer was originally inputted into Excel (time and concentration of tracer (µg/L)) and then transformed into a logarithmic scale to identify the first (distribution) and second (elimination) phases. The data points used for the elimination phase were then isolated and the gradient of the exponential line of best fit was identified ($y = k^{-x}$). The initial concentration for the elimination phase for each tracer was established using two methods, firstly using the value of 'k' and then inputting the data points in Log_{10} format into the 'INTERCEPT' function on Microsoft Excel. The C_i value was inputted into the PKSolver program (NCA IV Bolus formulation) along with the identified elimination phase data points to initiate PK analysis (Figure 3.2).

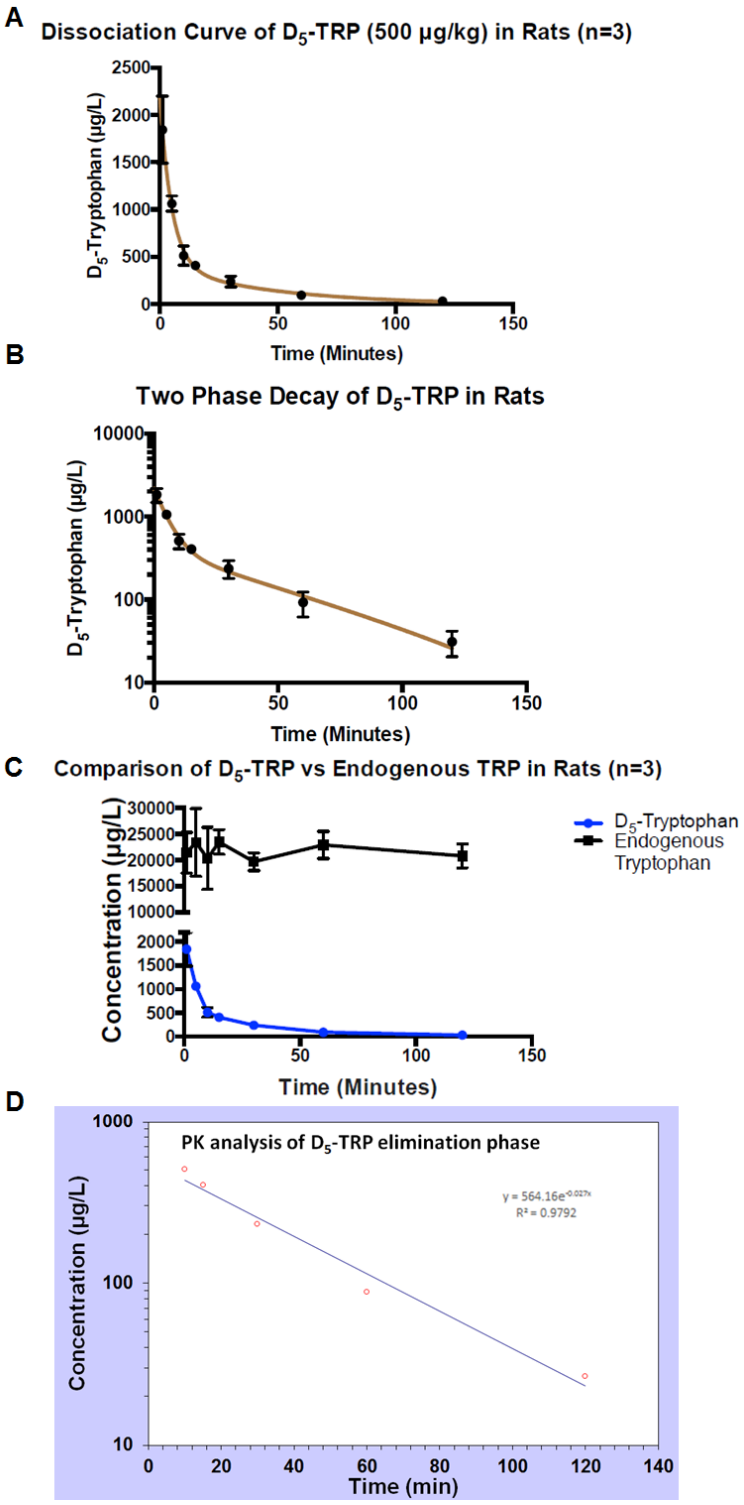

(**Figure 3.2 - Development of PK analysis of D5-TRP Tracer Data Sets.** A) Dissociation curve of D5-TRP. B) Logarithmic representation of D5-TRP dissociation C) Comparison of endogenous TRP with D5-TRP concentration levels. D) PKsolver analysis of elimination phase to identify the gradient of elimination.)

Section 4: Results

4.1 Mass Spectrometric Conditions of Analytes and Examination of Peaks.

The optimal LC-MS/MS conditions identified are detailed in Table 4.1.

Table 4.1 – Optimised LC-MS/MS method for analysis of kynurenine pathway analytes.

LC Settings

System – Shimadzu / QTRAP 6500+
Injection Volume: **10 µl**
Column: **ACE Excel UHPLC C18 PFP 1.7 µm 2.1 x 100 mm**
Column position**:**
Mobile Phase A: **H_2O / 0.1% CH_2O_2**
Mobile Phase B: **CH_3OH / 0.1% CH_2O_2**
Flow Rate: **400 µL/min**
Temperature: **Oven 40°C**

Time (mins)	*Flow (ml)*	*%A*	*%B*
Initial	0.4	10	90
1	0.4	10	90
6	0.4	80	20
8	0.4	80	20
8.1	0.4	10	90
9	stop		

MS settings

CURTAIN GAS	**40**
CAD	-2
IONSPRAY VOLTAGE	4500/ -4500
TEMPERATURE	600
GS1	60
GS2	40
SPRAY VOLTAGE	5500
TURBOSPRAY/APCI	Turbospray
ENTRANCE POTENTIAL	10 / -10

Injection manifold – bypass

Pressure range (Pump A/B/C 0-1300 bar)

All analytes were ionised in both positive and negative ESI conditions. The MRM qualifier transitions (Q1→Q3) were identified by tuning each individual analyte (see Figure 4.1). Most analytes were ionised effectively in positive polarity, QUIN was negatively ionised. The final MRM transitions used in the final LC-MS/MS method are highlighted in Table 4.2. Representative chromatograms for each analyte, including retention times, are displayed in Figures 4.2 and 4.3.

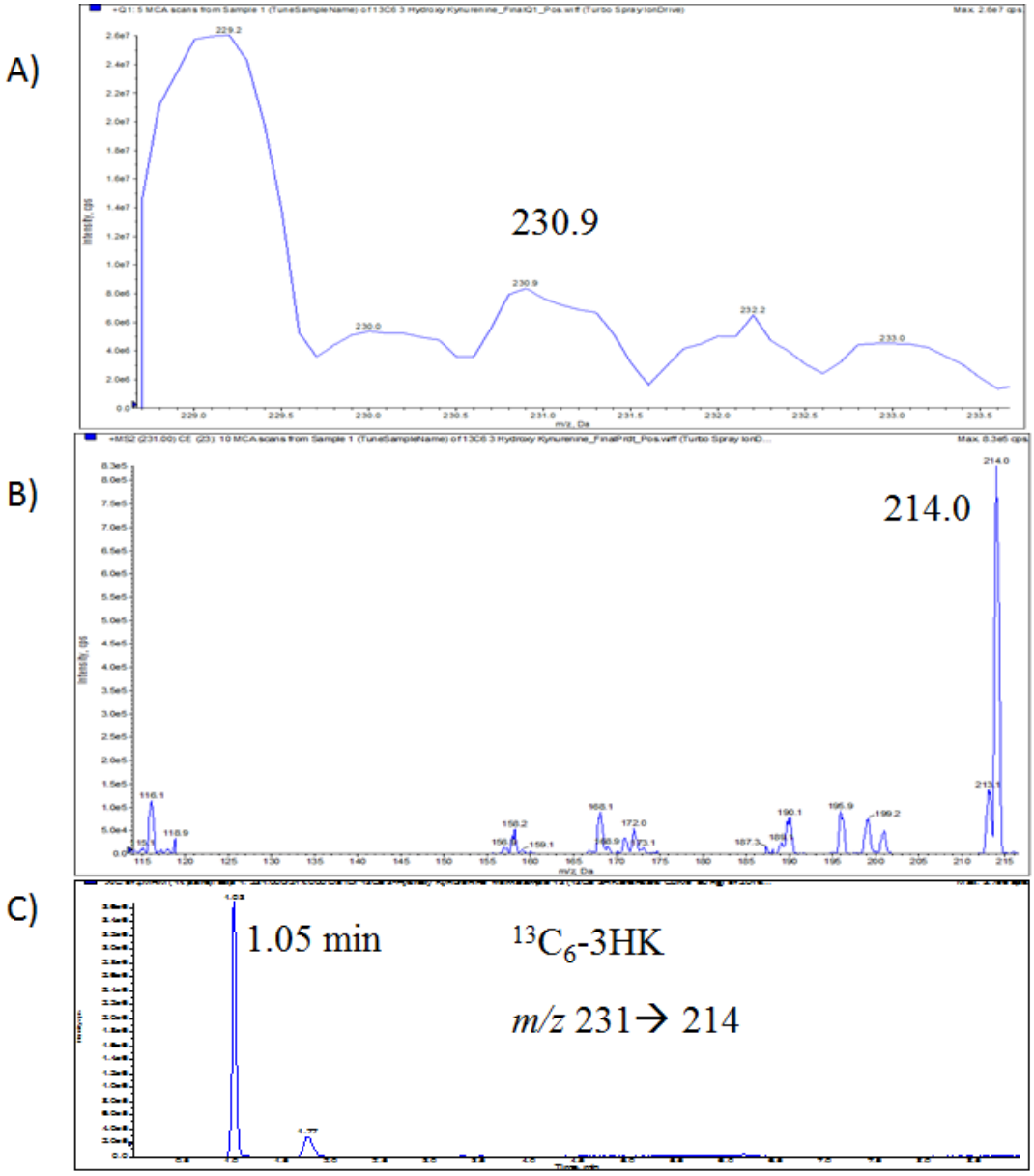

(**Figure 4.1 - Identifying Analyte Transitions –** A) Example of Q1 peaks in tuning using $^{13}C_6$-3HK. B) Final fragmented analyte peaks C) representative chromatogram of extracted $^{13}C_6$-3HK in 1% BSA (50 ng, m/z = mass to charge)

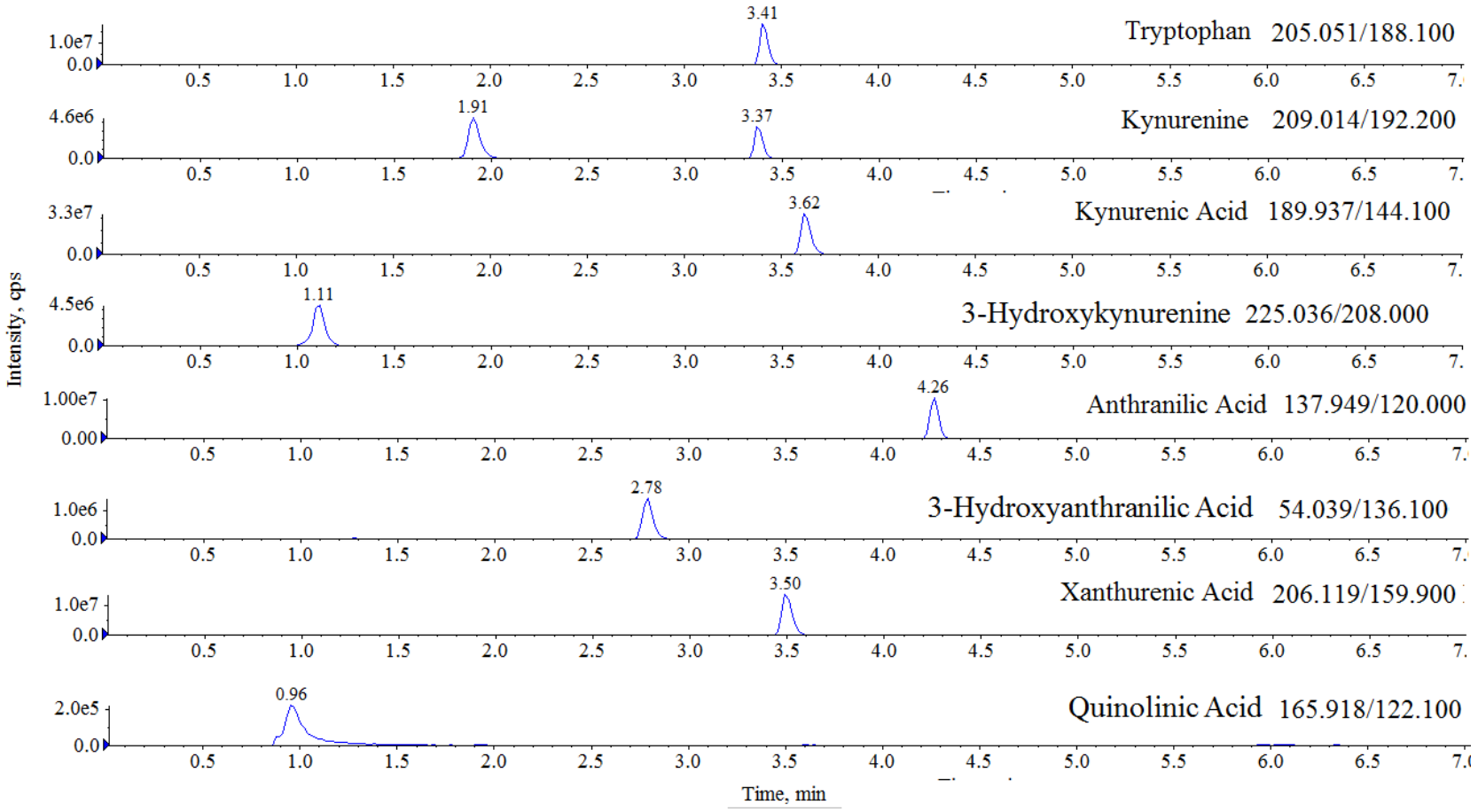

(**Figure 4.2 – Representative Chromatograms of Each Endogenous Analyte (100 ng).** Final quantifier transitions (m/z) are also displayed. Retention time of each analyte is displayed above corresponding peak. KYN chromatogram has a shadow peak from TRP (3.37 min), therefore this peak is not analysed in KYN measurement. Cps, counts per second; min, minutes)

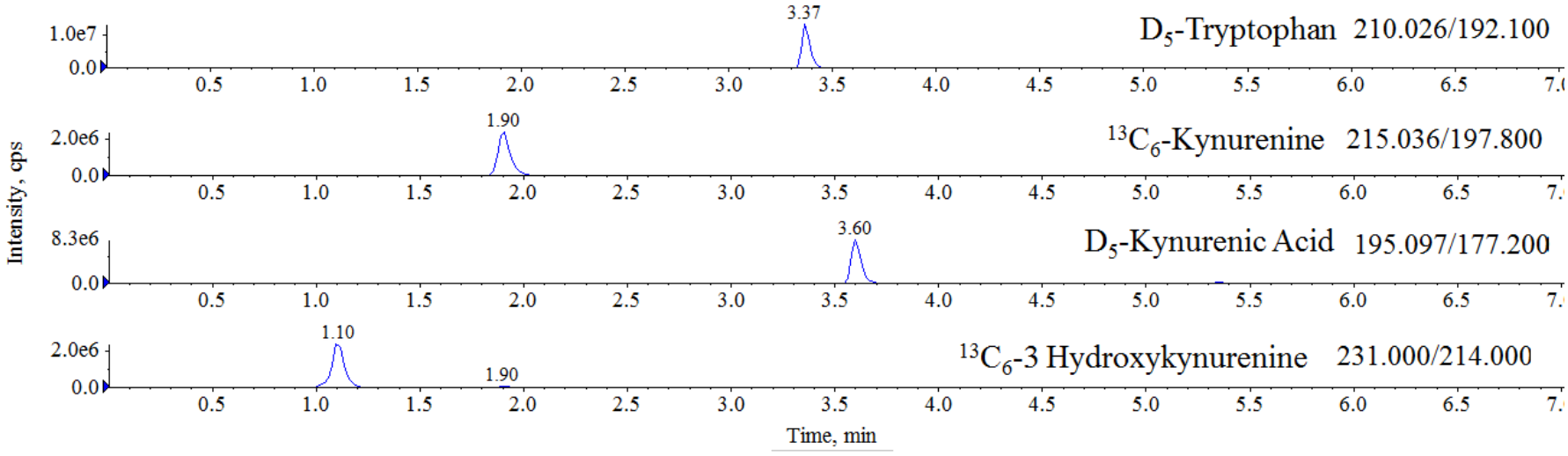

(**Figure 4.3 – Representative Chromatograms of Each Tracer (100 ng)**. Final quantifier transitions (m/z) are also displayed. Retention time of each analyte is displayed above corresponding peak. Cps, counts per second; min, minutes)

Table 4.2 – Parent/product molecular ion transitions (Q1→Q3, m/z) of all kynurenine pathway metabolites analysed using positive and negative ESI, along with their corresponding MRM mode settings (V, volts).

Compound	Parent Ion (Q1) (*m/z*)	Product Ion (Q3) (*m/z*)	Declustering Potential (V)	Collision Energy (V)	Collision Cell Exit Potential (V)
KYN	209.0	192.2	61	11	10
$^{13}C_6$-KYN	215.0	197.8	66	13	16
TRP	205.1	188.1	36	15	12
D_5-TRP	210.0	192.1	60	15	6
KYNA	189.9	144.1	46	23	10
D_5-KYNA	195.1	177.2	16	15	12
3HK	225.0	208.0	56	11	32
$^{13}C_6$-3HK	231.0	214.0	41	13	10
3HAA	154.0	136.1	56	13	12
AA	137.9	120.0	66	13	10
XA	204.1	159.9	46	25	22
negative QUIN	165.9	122.1	-5	-14	-21

4.2 UHPLC-MS/MS Method Optimisation

The initial step in the development of the UHPLC-MS/MS methods was to select the most efficient and effective method of kynurenine pathway metabolite extraction. Three different methods of extraction (SPE, PPT and SLE) were assessed and their recovery and ion suppression outcomes compared. The method of extraction that provided the best recovery of analyte from the plasma samples was the SPE method using Oasis® HLB cartridges (Table 4.3, Figure 4.4). There was a stark contrast between the SPE method and the PPT and SLE methods, the percentage recovery of all tracers was consistently higher using the Oasis® HLB cartridges.

Table 4.3 - Comparison of Extraction Methods using Tracer Analyte Recovery from Plasma. (Optimal result highlighted in bold; Recovery = peak area of tracer extracted/peak area of tracer unextracted)

Protein Precipitation	**D_5-TRP**	**$^{13}C_6$-KYN**	**D_5-KYNA**	**$^{13}C_6$-3HK**
MeCN	7.57%	7.34%	51.15%	2.57%
CH_3OH	6.44%	5.36%	51.39%	2.07%
TCA	3.22%	8.10%	74.98%	2.58%
Supported Liquid Extraction				
MTBE	1.44%	0.58%	0.01%	0.92%
DCM	0.98%	0.86%	0.01%	0.42%
Hexane	0.17%	0.81%	0.01%	0.26%
EtOEt	1.07%	0.96%	0.01%	0.57%
98:2 DCM/IPA	0.55%	0.41%	0.01%	0.43%
EtOAc	1.57%	1.27%	0.01%	0.80%
Solid Phase Extraction				
Acidified 1:1 HLB	**79.22%**	**28.82%**	92.50%	**6.75%**
Acidified 1:2 HLB	67.16%	23.18%	93.79%	5.53%
Acidified 1:3 HLB	39.74%	20.95%	95.92%	5.41%
Acidified 1:4 HLB	76.04%	13.91%	**97.97%**	3.25%
Base 1:1 HLB	16.43%	13.91%	3.70%	3.70%
Base 1:2 HLB	18.59%	14.12%	2.47%	2.47%
Base 1:3 HLB	22.10%	15.52%	2.15%	1.62%
Base 1:4 HLB	21.36%	14.24%	2.71%	1.78%

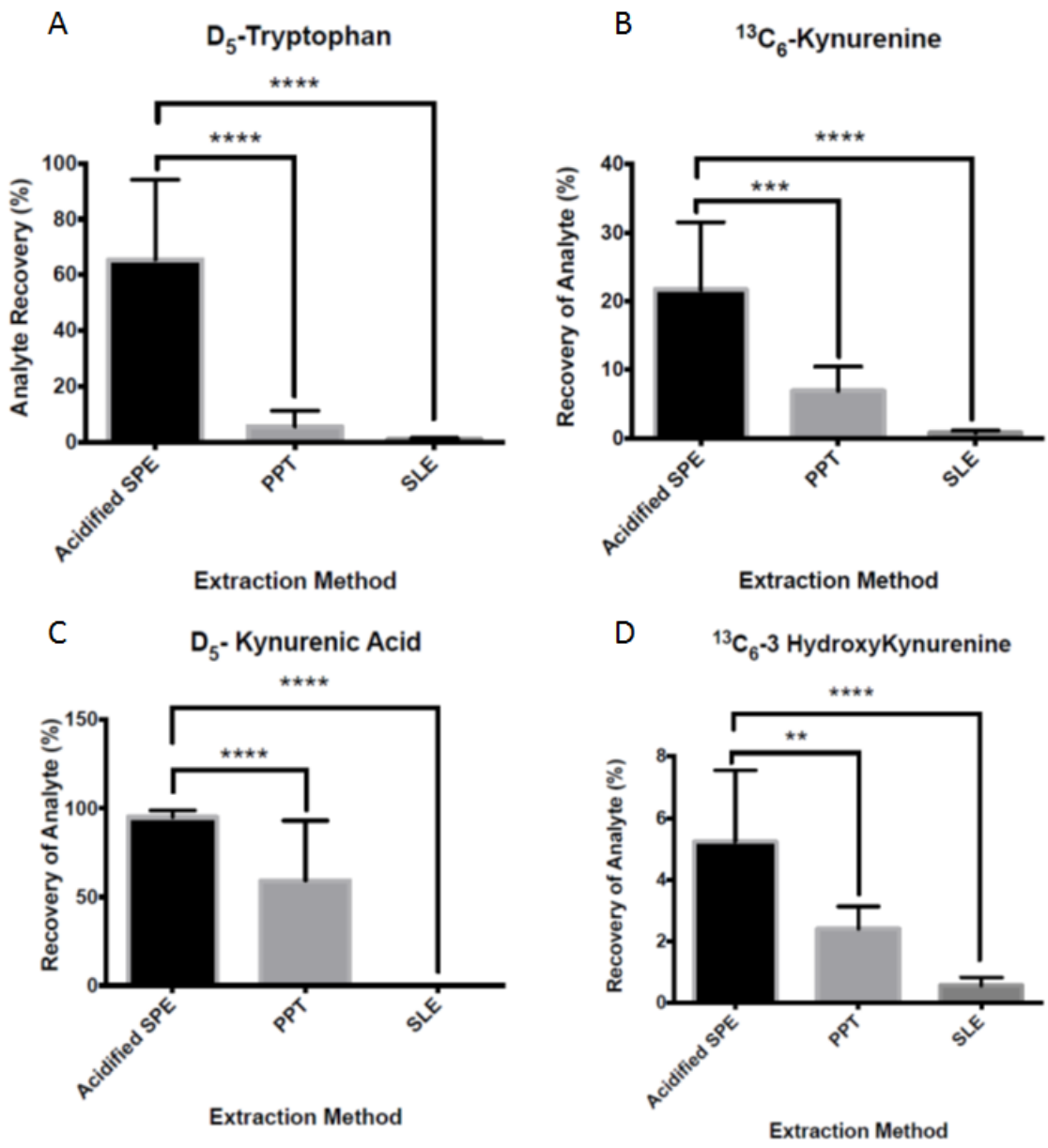

(**Figure 4.4 – Statistical Comparison of SPE against PPT and SLE Methods of Extraction.** The percentage recoveries, obtained by the acidified SPE method for each of the four tracers, were compared against the recoveries seen with samples extracted by PPT and SLE plates. The recoveries were significantly higher for every tracer. (Each tracer data set was subjected to a one-way ANOVA ($p < 0.0001$) with post hoc Tukey's multiple comparisons test (* = $p < 0.05$; ** = $p < 0.01$; *** = $p < 0.001$ **** = $p < 0.0001$)**)**

The next step was to optimise the Oasis® HLB extraction method, following the template provided by Waters but tweaking the steps to try and optimise recovery of $^{13}C_6$-3HK and D_5-KYNA. Acidifying the plasma in 4% phosphoric acid (1:1, *v/v*) provided the best recovery results (Table 4.3), with the exception of D_5-KYNA where a one in four dilution provided a 5.47% increase. The next steps in the cartridge preparation, equilibration and washing, were then further optimised (Table 4.4). By equilibrating and washing with HPLC grade water, analyte recovery was improved (D_5-TRP, +11.74%; $^{13}C_6$-KYN +78.87%; and $^{13}C_6$-3HK, +78.76%).

Table 4.4 - Comparison of Equilibration (1) and Wash (2) Steps using Recovery of Tracer Analytes.(Best result highlighted in bold)

Recovery	**D_5-TRP**	**$^{13}C_6$-KYN**	**D_5-KYNA**	**$^{13}C_6$-3HK**
1) Water **2) 5% CH_3OH**	82.32%	61.37%	64.91%	24.79%
1) 4% H_3PO_4 **2) 5% CH_3OH**	46.62%	41.19%	85.02%	18.47%
1) Water **2) Water**	**90.96%**	**107.15%**	134.15%	**85.51%**
1) 4% H_3PO_4 **2) Water**	82.35%	90.02%	**94.33%**	73.33%
1) 4% H_3PO_4 **2) 4% H_3PO_4**	0.84%	69.82%	107.89%	11.42%

The next step that was to assess the resuspension of analytes once dried down post-elution.

Table 4.5 - Comparison of Resuspension Elutions using Peak Areas of Tracers Spiked in Aqueous Solution. (%RSD = 100 x standard deviation/mean)

Peak Areas	**D_5-TRP**	**$^{13}C_6$-KYN**	**D_5-KYNA**	**$^{13}C_6$-3HK**
100 µl 50:50 (CH_3OH:H_2O)	34,383	2,935,667	21,233,333	651,433
100 µl 30:70 (CH_3OH:H_2O)	986,600	3,185,000	25,440,000	525,267
150 µl 50:50 (CH_3OH:H_2O)	619,005	2,284,500	18,745,000	370,000
200 µl 50:50 (CH_3OH:H_2O)	1,986,000	1,094,500	12,955,000	106,750
Relative Standard Deviation				
100 µl 50:50 (CH_3OH:H_2O)	80.35%	12.77%	11.35%	7.05%
100 µl 30:70 (CH_3OH:H_2O)	92.16%	4.29%	12.52%	2.37%
150 µl (50:50 CH_3OH:H_2O)	130.91%	3.06%	4.79%	7.99%
200 µl (50:50 CH_3OH:H_2O)	18.16%	7.04%	10.21%	8.15%

The 30:70 solution was better for the recovery of $^{13}C_6$-KYN and D_5-KYNA, however 50:50 was better for $^{13}C_6$-3HK and D_5-TRP at varying volumes. Due to the percentage relative standard deviation (%RSD) of D_5-TRP being far higher than any other analyte (Table 4.5), it was hypothesised that there may be an issue with the resuspension step of the method. Due to the differing solubility of analytes in aqueous environments, Log*P* (Table 1.3), it was questioned whether all the analyte was being retained in the vial rather than dissolved in the resuspension solution. The differences in Log*P* may affect the ability of an analyte to solubilise in the resuspension solution and thus different concentrations of methanol, along with adding methanol and water separately, were investigated to identify whether a certain percentage aided resuspension and recovery of the analytes. Previously, a pre-mix of methanol in water (50:50, *v/v*) solution was used for resuspension. Two different compositions (50:50 or 30:70, *v/v*) of the solution were compared. A premix was also compared against the individual addition of each component, followed by a vortex (3 s), to identify which process had the greatest impact on analyte recovery and reliability (%RSD) (Table 4.6).

Table 4.6 – Recovery (optimal highlighted in bold) and Relative Standard Deviations (optimal highlighted in bold) of Analytes in Different Resuspension Conditions (Av, Average)

100 ng aqueous extracted analyte mix (n=2)		**KYN**	**$^{13}C_6$-KYN**	**TRP**	**D_5-TRP**	**KYNA**	**D_5-KYNA**	**3HK**	**$^{13}C_6$-3HK**	**3HAA**	**XA**	**Av**
30:70 CH_3OH:H_2O	*Recovery(%)*	50	64	38	34	26	27	10	10	38	12	31
	%RSD	15	18	41	54	7	6	6	5	12	17	18
70 H_2O then 30 CH_3OH	*Recovery (%)*	100	125	89	84	46	49	19	18	58	21	**61**
	%RSD	3	3	2	4	13	17	16	14	0	12	8
30 CH_3OH then 70 H_2O	*Recovery (%)*	77	93	65	61	56	54	15	15	56	28	52
	%RSD	2	2	4	2	6	6	5	3	3	56	9
50:50 CH_3OH:H_2O	*Recovery (%)*	84	97	68	64	58	58	16	16	59	42	56
	%RSD	2	1	5	6	14	3	10	8	0	23	**7**
50 H_2O then 50 CH_3OH	*Recovery (%)*	80	97	65	62	62	60	17	17	55	34	55
	%RSD	8	9	9	12	1	7	1	0	12	37	10
50 CH_3OH then 50 H_2O	*Recovery (%)*	88	112	74	68	76	73	17	16	59	24	61
	%RSD	7	5	9	6	11	7	6	5	6	22	8

Extracted samples (*n*=2) for each resuspension phase were analysed and compared for peak areas and %RSD. The preferred resuspension step of the protocol involved the addition of water (70 µl, 3 s vortex), followed by methanol (30 µl, 3 s vortex) as this achieved the highest level of recovery (61%), and a good level of precision (8% RSD)

The last step to optimise was the elution step. To date all elutions were performed using methanol. However, as discussed, each analyte has a different Log*P* and thus using a more aqueous solvent may enhance the elution of hydrophilic analytes off the column. Different solution of methanol in water (40% methanol to 100% methanol in 10% increments) were used to elute the standard samples (100 ng analyte mixes) (Table 4.7). The largest peak area values for three of the tracers were produced with an 80% methanol elution solvent.

Table 4.7 – Results of the Elution Solvent Analysis. (Optimal result highlighted in bold; Ion Suppression = Peak Area of Tracer Extracted in Plasma/Peak Area of Tracer in Water)

Ion Suppression				
% Methanol	**D_5-TRP**	**$^{13}C_6$-KYN**	**D_5-KYNA**	**$^{13}C_6$-3HK**
40	64.48%	101.45%	26.63%	**31.46%**
50	70.89%	79.18%	64.37%	16.16%
60	81.24%	93.84%	78.90%	26.35%
70	81.69%	**95.49%**	83.02%	20.65%
80	**94.88%**	117.17%	**93.26%**	24.00%
90	65.51%	97.47%	83.31%	16.86%
100	14.28%	80.11%	79.74%	17.90%
Peak Areas				
40	8,603,500	5,239,500	15,505,000	**632,000**
50	9,459,000	4,089,000	37,475,000	324,700
60	10,840,000	4,846,500	45,930,000	529,350
70	10,900,000	4,931,500	48,330,000	414,800
80	**12,660,000**	**6,051,500**	**54,290,000**	482,200
90	8,740,500	5,034,000	48,500,000	338,650
100	1,905,000	4,137,500	46,420,000	359,650

Before rat plasma was analysed for tracer levels using this optimised method, the surrogate matrix for the standard curve was assessed. The average peak areas of each tracer (100 ng) were prepared in 4 different matrices (0.2%, 1%, 10% BSA and Human Plasma, Table 4.8) and compared. Overall, 1% BSA gave the most similar peak areas of analytes to plasma, therefore 1% BSA was adopted as the surrogate matrix for the preparation of the standard curves.

Table 4.8 – Comparison of Peak Areas in Surrogate Matrices (BSA) with Human Plasma (100 ng in BSA / 100 ng in Human Plasma)

Comparison with Human Plasma	**D_5-TRP**	**$^{13}C_6$-KYN**	**D_5-KYNA**	**$^{13}C_6$-3HK**
10% BSA	155%	136%	**113%**	180%
1% BSA	**123%**	**111%**	129%	137%
0.2% BSA	143%	120%	133%	**99%**

4.3 UHPLC-MS/MS Method Validation

4.3.1 Selectivity

Selectivity was evaluated to identify whether the tracers and analytes could be isolated and quantified in the presence of other compounds found in the rat plasma matrix. To address this, the average chromatographical retention times of the tracers and analytes in rat plasma were compared against the average retention times in 1% BSA (n=7 calibration curves) and are highlighted in Table 4.9.

Table 4.9 – Comparison of Retention Times of Tracers and Analytes in Rat Plasma and 1% BSA Established in the Chromatograms.

Analyte	***1% BSA Retention Time (mins)***	***Rat Plasma Retention Time (mins)***
TRP	3.41 ± 0.00	3.39 ± 0.78
KYN	1.91 ± 0.00	1.91 ± 0.44
KYNA	3.62 ± 0.00	3.63 ± 0.00
3HK	1.11 ± 0.00	1.10 ± 0.25
3HAA	2.78 ± 0.01	2.77 ± 0.02
AA	4.26 ± 0.00	4.26 ± 0.01
QUIN	0.96 ± 0.50	0.99 ± 0.02
XA	3.50 ± 0.01	3.51 ± 0.01
D_5-*TRP*	3.47 ± 0.02	3.42 ± 0.01
$^{13}C_6$-*KYN*	1.89 ± 0.01	1.91 ± 0.04
D_5-*KYNA*	3.67 ± 0.01	3.70 ± 0.01
$^{13}C_6$-*3HK*	1.06 ± 0.01	1.03 ± 0.06

4.3.2 Dilution Linearity

Due to saturation of the column while assessing endogenous plasma TRP levels, dilution linearity tests were performed to establish whether multiple dilution factors would produce the same, accurate and reliable results. The dilution linearity test was also used to assess the matrix suppression effect of rat plasma. The results prove there is a good dilution linearity for TRP (dilution factor 10 – 100, $R^2 = 0.9938$), therefore also identifying no severe matrix suppression effects (Figure 4.5). However, diluting samples by a factor of 100 produced a high relative standard deviation (32% RSD), therefore outside the optimal dilution range (1:10 to 1:50). Linearity analysis of all other analytes revealed there is no saturation of the column for these.

A

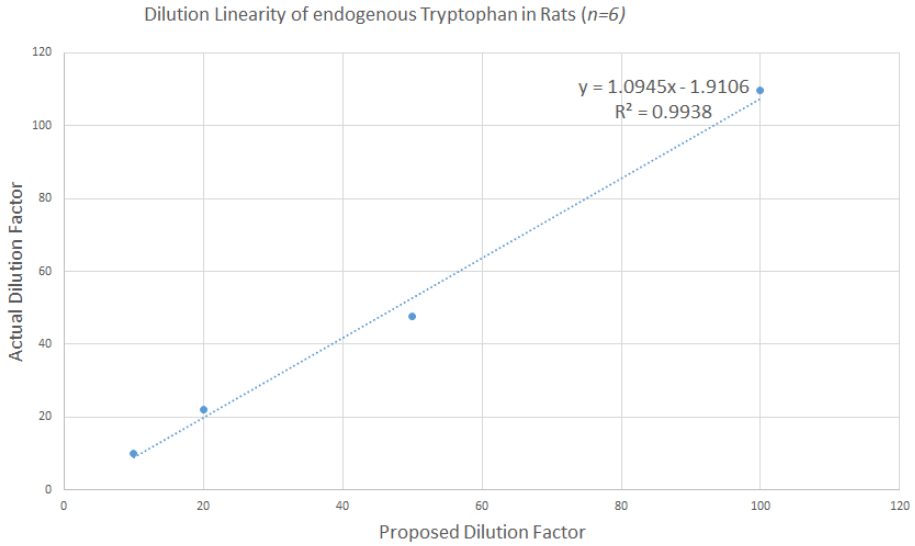

B

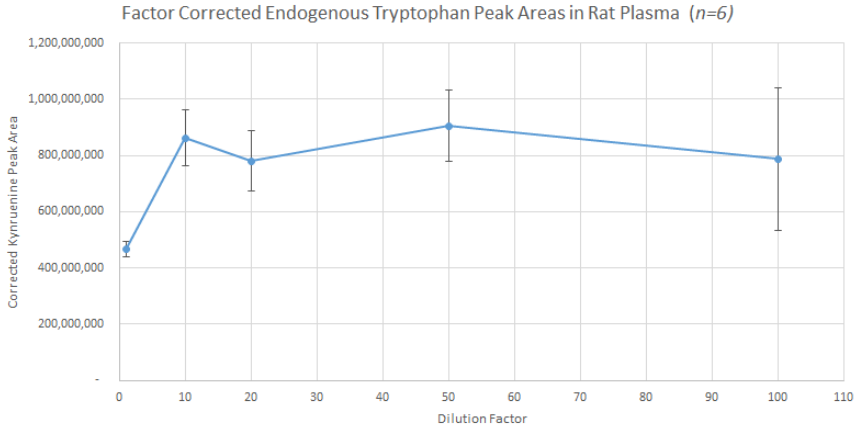

C

Dilution Factor Data (TRP)	1	10	20	50	100
Average Peak Area (n=6)	465,844,642	862,818,483	780,135,983	905,421,242	787,296,250
Standard Deviation	27,451,255	98,905,300	108,065,541	127,698,495	255,041,734
%RSD	6%	11%	14%	14%	32%

(Figure 4.5 – Linearity of TRP A) Actual dilution factor compared against proposed dilution factor gives good linearity (R^2=0.9938) B) Corrected peak areas identifies good level of similarity in reported results across each dilution and also reveals saturation of column at dilution factor 1. C) Analysis of variation of results for each dilution reveals high %RSD for dilution factor 100.**)**

4.3.3 Precision and Accuracy

In accordance with FDA guidelines, intra-day (six standard curves run on one day) and inter-day (six standard curves run on six different days) analysis of the standard curve precision and accuracy were performed and summarised in Table 4.10. At least five curves for each analyte were used in determining the method's abilities to produce accurate and precise data.

TABLE 4.10
Within- and Between-day analysis of compounds (n > 5).

	Within-Day					Between-Day				
	Conc^{n} (µg/L)	Mean (µg/L)	Accuracy (%)	Standard Deviation	RSD	Conc^{n} (µg/L)	Mean (µg/L)	Accuracy (%)	Standard Deviation	RSD
TRP	5	5.6	112	0.4	7	5	5.1	102	0.4	8
	50	53	106	5	9	50	53.2	106	7.7	14
	1000	1064	106	111	10	1000	1012.5	101	28.7	3
KYN	10	10	100	1.2	12	10	9.8	98	1.4	14
	100	95.2	95	7.4	8	100	104.4	104	8.3	8
	1000	1007	101	31.3	3	1000	997.6	100	30.4	3
KYNA	20	19.3	97	1.9	10	5	5	100	0.8	16
	100	99.2	99	8.5	9	100	88.5	88.5	13.6	15
	1000	1029	103	23.5	2	1000	997.4	100	42.6	4
3HK	10	10	100	0.8	8	10	10.9	109	2.6	24
	50	47.1	95	6.2	13	50	45.3	91	8.8	19
	200	195.5	98	11.1	6	200	195.7	98	13.7	7
3HAA	20	21	105	1.4	7	50	50.2	100	5.3	10
	500	499.5	100	37.3	7	500	548.8	110	75.2	14
	1000	1002	100	26	3	1000	1099.5	110	232	21
AA	5	4.9	98	0.9	18	10	9.8	98	0.8	8
	100	92.7	93	9.2	10	100	94.6	95	8.5	9
	1000	1024	102	143	14	1000	1013.4	101	47.4	5
QUIN	200	195	98	34.7	18	100	104.4	104	13.2	13
	500	475.8	95	59.4	12	500	456.7	91	38.7	8
	1000	1010.5	101	54.6	5	1000	941.3	94	231	25

Linearity of the curves used in the validation study are summarised in Table 4.11.

Table 4.11 - Summary of Calibration Curve Linearity (R^2) and Weighting.

Analyte	R^2 (Average)	Weighting
TRP	0.997481	$1/x^2$
KYN	0.998363	$1/x^2$
KYNA	0.993783	1/x
3HK	0.997892	$1/x^2$
3HAA	0.998616	1/x
AA	0.997144	$1/x^2$
QUIN	0.998255	1/x

4.3.4 Limit of Quantification

The analyte limits of quantitation, i.e. the lowest amount of analyte that produces a peak that is three times higher than background noise, are summarised in Table 4.12.

Table 4.12 – Limit of Quantification (LOQ) and Upper (ULOD) Limits of Detection of Kynurenine Pathway Analytes. The LOQ represents the lowest quantifiable peak in the standard curve used for analysis of that specific analyte. Representative linear curve weighting and linearity (R^2) are also displayed.

Analyte	***LOQ (µg/L) (n=3)***	***Signal to Noise Ratio at LOQ (n=3)***	***ULOD (µg/L)***
TRP	0.01	27.7	1000
KYN	0.03	3.7	1000
KYNA	0.01	12.5	1000
3HK	0.73	3.8	1000
D_5-TRP	1.00	12.5	2000
$^{13}C_6$-KYN	1.67	3.6	1000
D_5-KYNA	0.40	3.9	1000
$^{13}C_6$-3HK	20	5.6	1000
3HAA	0.01	11	1000
QUIN	50	7.6	1000
AA	0.04	4.4	1000
XA	0.02	4.7	1000

4.3.5 Comparison to Old Method

To confirm whether this new method was an upgrade to the old method, peak areas of the four main kynurenine pathway analytes, along with $^{13}C_6$-3HK and D_5-KYNA, from both methods were compared and the results are shown in Figure 4.6. Peak characteristics of old, intermediate and new methods were also compared and are displayed in Figure 4.7.

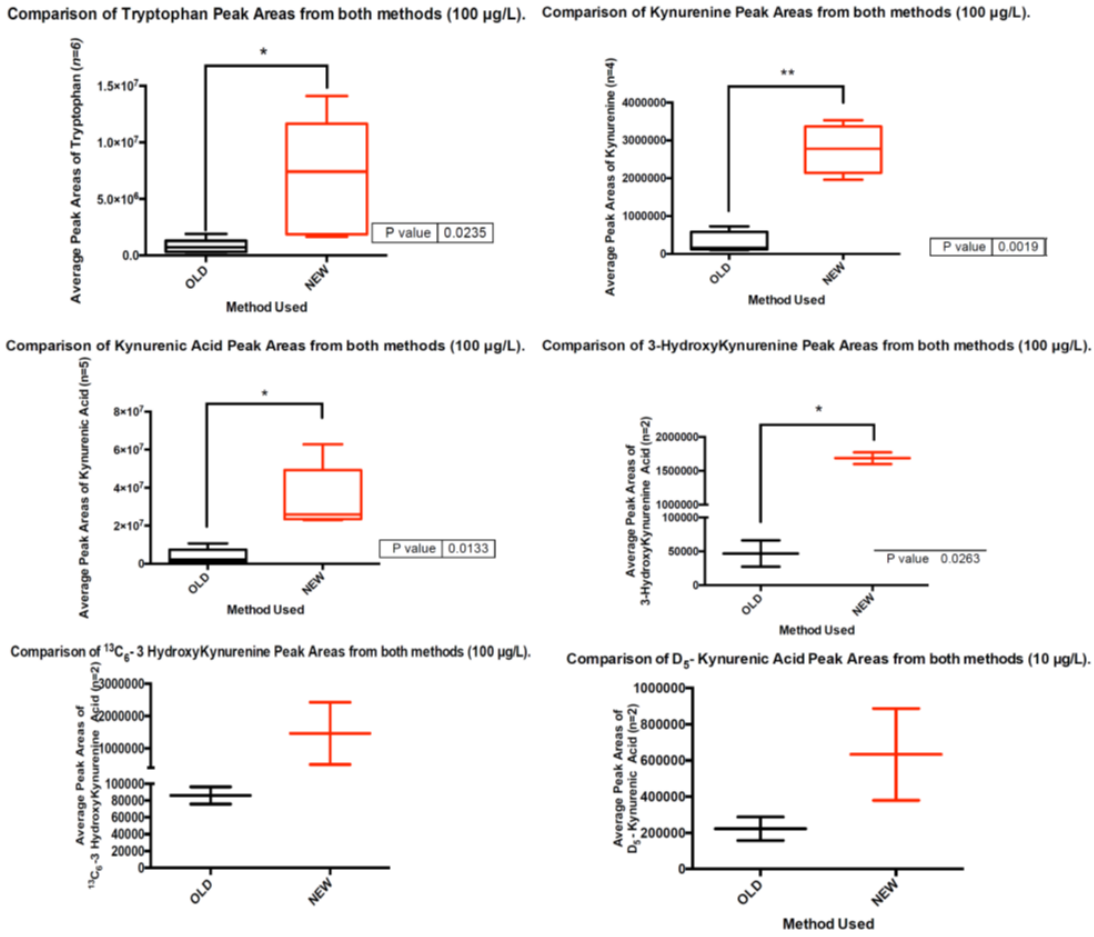

(Figure 4.6 – Statistical comparison between the oldest and final methods. These comparisons revealed a significant improvement in the sensitivity of the kynurenine pathway metabolites whilst visible improvement is seen in the sensitivity of $^{13}C_6$-3HK and D_5-KA (unpaired Student's t test * = $p < 0.05$; ** = $p < 0.01$)**)**

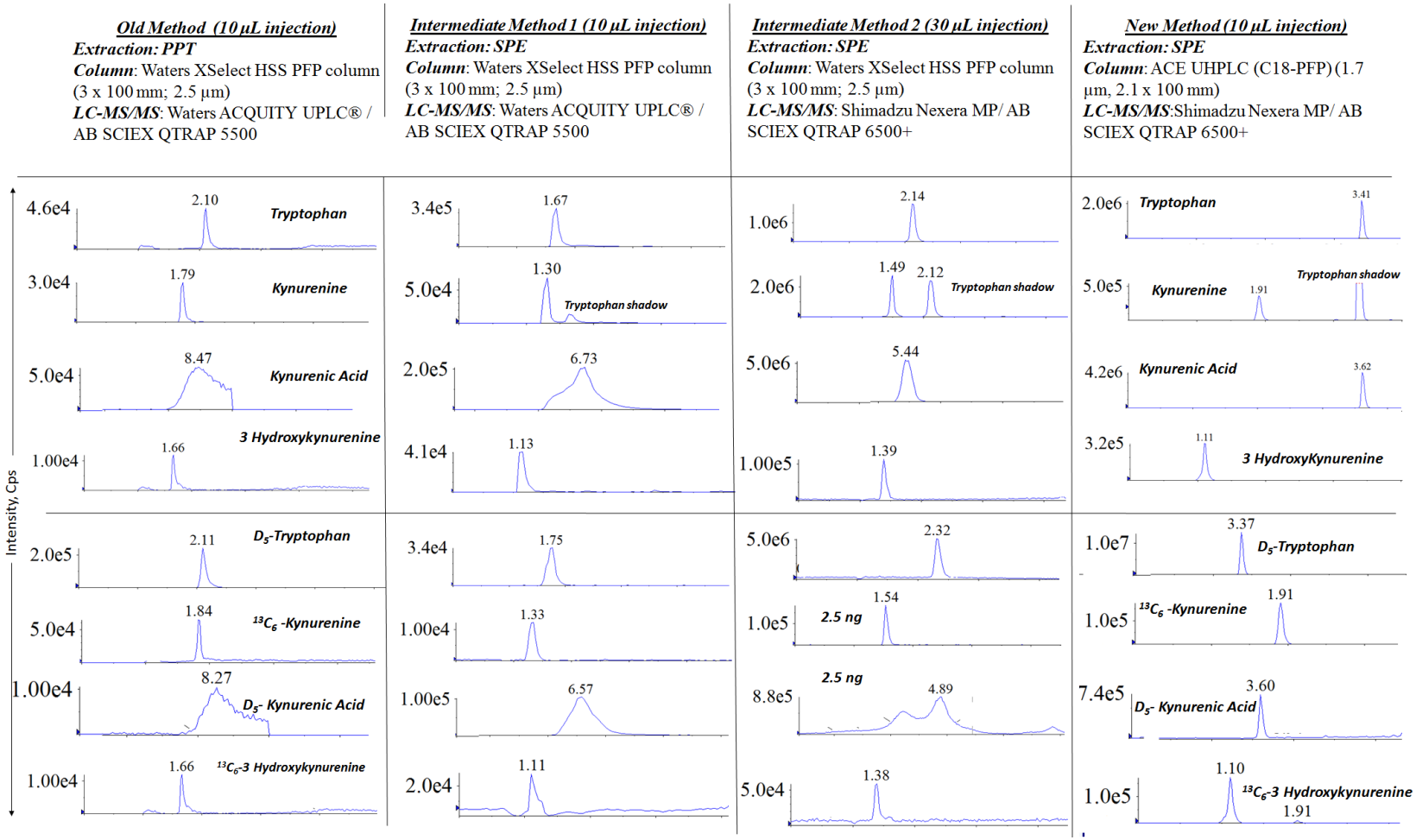

(Figure 4.7 – Comparison of Peaks Throughout Method Design. Systematic guide of peak morphology throughout method development. The new method has resulted in increased peak heights with generalised narrowing of the peaks in comparison to the original method. This is seen prominently with D_5-KYNA (Peak Heights – OLD = 9110, NEW = $1.6e^6$ cps; Peak Width – OLD >0.5 mins, NEW < 0.3 mins) and $^{13}C_6$-3HK (Peak Heights – OLD = 4000, NEW = $7.3e^4$ cps; Peaks represent 100 µg/L (10 ng) unless otherwise stated; cps = counts per second)

4.4 Method Application to Rat Tracer Studies

The standard curves, using peak area ratios (analyte area / internal standard area) used to analyse the rats dosed with each tracer are represented in Figure 4.8. Further details of each linear curve are highlighted in Table 4.13.

Table 4.13 – Data for Standard Curves Used in the Analysis of Tracer Concentrations in Rat Plasma

Tracer	**Data Points Used**	**Weighting**	**R^2 Value**	**Equation**
D_5-TRYP	6	$1/x^2$	0.99588	$y = 0.04236x + 0.01035$
$^{13}C_6$-KYN	6	$1/x^2$	0.99667	$y = 1.09324e^5x + 18133.453$
D_5-KYNA	7	1/x	0.99048	$y = 0.17080x + -0.01082$
$^{13}C_6$-3HK	5	1/x	0.99939	$y = 0.00456x + -0.01948$

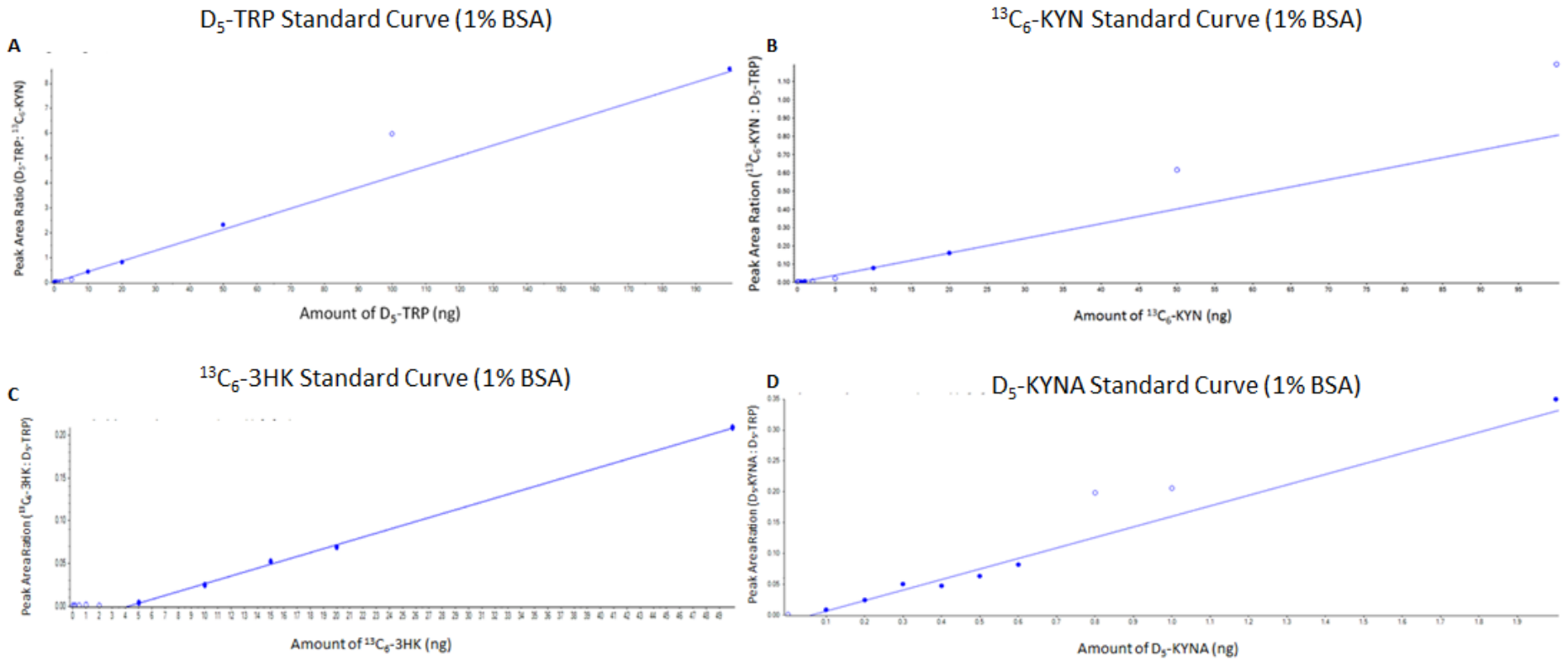

(Figure 4.8 – Standard Curves of Each Tracer Prepared in 1% BSA Used for Analysis. Data points accepted onto curve are represented with blue fill. Internal standard, $^{13}C_6$-KYN (50 ng)**)**

The mean averages and standard deviations of the plasma concentrations of each tracer are summarised in Table 4.14 whilst their corresponding dissociation curves, logarithmic scales and their levels compared to endogenous compounds are shown in Figure 4.9. The plasma concentrations were calculated by reading the corresponding peak area ratio value off the standard curve, the same standard curve was used for every rat in that tracer experiment. The values of each tracer at time point '0' were used as a value for background noise and were subtracted from all the following measured time point concentrations.

Table 4.14 – Average Concentration of Tracers Decreasing Over Time, with Standard Deviations. All data has been 'zeroed' by subtracting the value at time point 0 from all other temporal values.

	Average [D_5-TRP] (µg/L) (n=3)	***Average [$^{13}C_6$-KYN] (µg/L) (n=4)***
0	4.37 ± 0.85	1.4 ± 0.5
1	1837.57 ± 356.84	98.78 ± 30.20
5	1057.33 ± 80.46	35.78 ± 10.54
10	506.87 ± 103.47	18.70 ± 6.32
15	402.27 ± 41.75	16.35 ± 3.41
30	232.70 ± 55.89	7.75 ± 2.51
60	88.33 ± 30.15	5.25 ± 2.00
120	26.63 ± 11.03	-
	Average [D_5-KYNA] (µg/L) (n=3)	***Average [$^{13}C_6$-3HK] (µg/L) (n=3)***
0	1.40 ± 0.66	51.13 ± 3.63
1	21.30 ± 2.42	207.77 ± 48.47
3	12.20 ± 5.37	112.77 ± 27.33
5	7.37 ± 2.08	68.70 ± 34.20
8	6.03 ± 2.72	58.10 ± 3.55
15	2.87 ± 1.48	44.60 ± 7.37
30	3.23 ± 4.05	20.57 ± 1.76
60	0.40 ± 0	6.87 ± 3.40

The data show that each tracer has two distinct phases, the distribution phase (reflecting on the movement of the tracer around the body and surrounding tissues) and the elimination phase. Doses of both D_5-TRP and $^{13}C_6$-KYN were sufficiently low enough to represent an initial plasma concentration of 10% of endogenous compound levels. The lowest achievable doses of D5-KYNA and $^{13}C_6$-3HK corresponded with an initial plasma concentration that was 62% and 256% of their endogenous compound levels respectively.

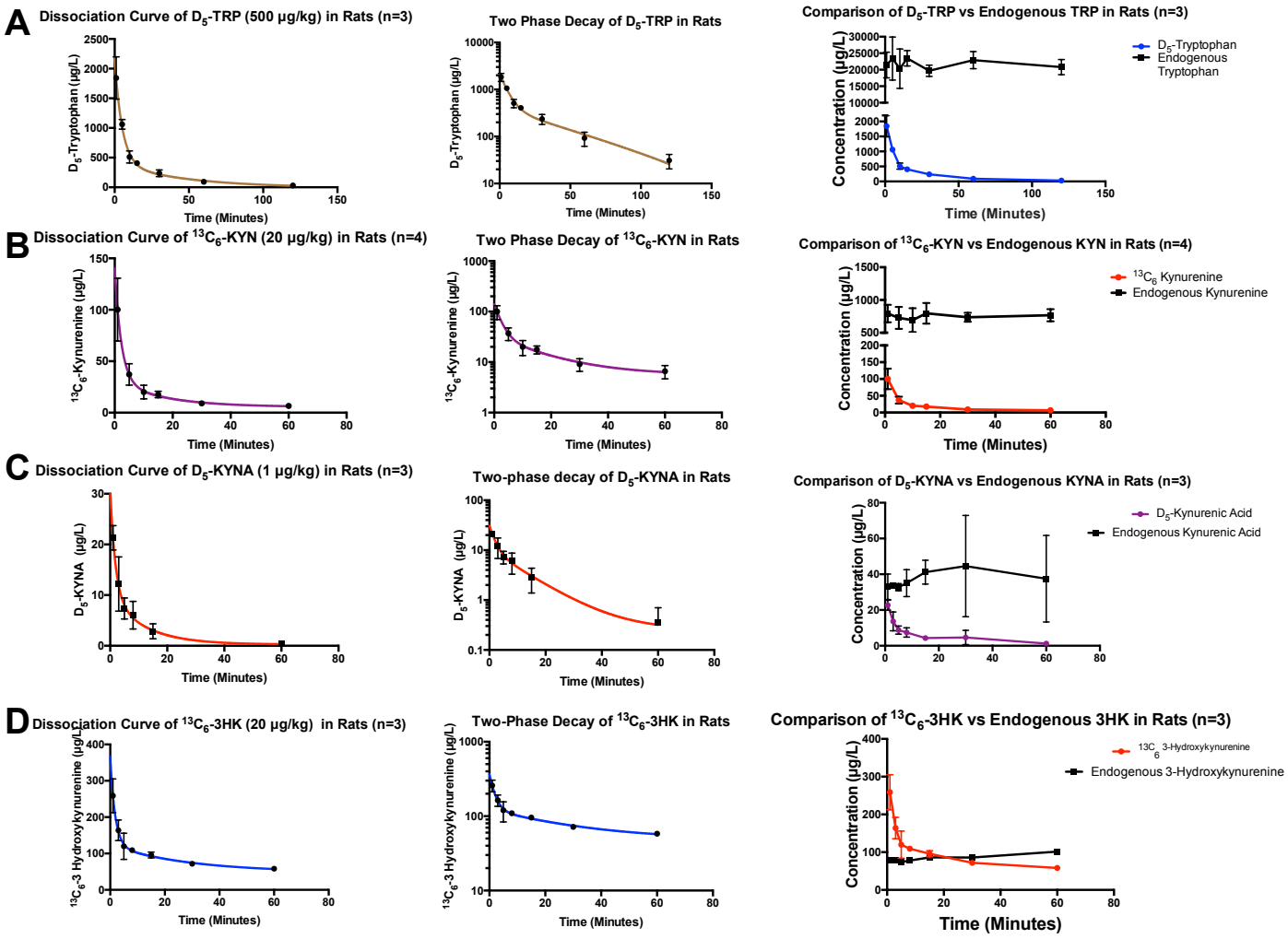

(**Figure 4.9 – Representation of Data from Table 4.12**, (means with s.d.). Each tracer has two identifiable phases in their decay, a distribution phase and an elimination phase. Doses of tracer are as close to 10% of endogenous as possible whilst staying in limits of detection. A) D_5-TRP. B) $^{13}C_6$-KYN. C) D_5-KYNA. D) $^{13}C_6$-3HK.)

4.4.1 Pharmacokinetics of Tracers

For the PK analysis, each rat was analysed individually using PK Solver, the data was then collated and summarised in Table 4.15. Average plasma concentrations of each tracer declined to undetectable levels, with the exception of D_5-TRP, within the experimental period. Assessment of each tracer's elimination phase revealed that $^{13}C_6$-KYN and D_5-KYNA have the longest and shortest half-lives respectively (D_5-TRP, 27.08; $^{13}C_6$-KYN, 29.12; D_5-KYNA, 12.14; $^{13}C_6$-3HK, 16.01 min) along with the highest V_d (D_5-TRP, 0.92; $^{13}C_6$-KYN, 0.96; D_5-KYNA, 0.12; $^{13}C_6$-3HK, 0.21 (µg/kg)/(µg/L)).

Table 4.15 – PK Parameter Analysis of Each Tracer.

PK Parameter	Units	D_5-TRP		$^{13}C_6$-KYN		D_5-KYNA		$^{13}C_6$-3HK	
		Range	Mean ± SD	Range	Mean ± SD	Range	Mean ± SD	Range	Mean ± SD
Weight	*g*	320-325	323.33 ± 2.89	310-340	318.75 ± 14.36			315-340	330 ± 13.23
Dose	*µg/kg*	500		20		1		20	
Half Life ($t_{1/2}$)	*min*	23.20-31.44	27.08 ± 4.14	18.914-36.99	29.12 ± 7.51	8.56-18.5	12.14 ± 5.52	12.76-21.05	16.01 ± 4.43
Elimination Constant (K_{el})	*L/min*	0.022-0.030	0.026 ± 0.004	0.019-0.037	0.025 ± 0.008	0.037-0.081	0.064 ± 0.023	0.033-0.054	0.045 ± 0.011
Initial Concentration (C_i)	*µg/L*	540.42-598.03	563.55 ± 30.44	13.95-29.28	22.27 ± 6.34	5.1-15.6	9.7 ± 5.4	70.03-123.99	92.47 ± 27.69
Volume of Distribution (V_d)	*(µg/kg)/(µg/L)*	0.78-1.09	0.92 ± 0.16	0.67-1.23	0.96 ± 0.25	0.06-0.20	0.12 ± 0.07	0.14-0.28	0.21 ± 0.07
Clearance (CL)	*(µg/L)/min*	0.020-0.027	0.024 ± 0.004	0.016-0.027	0.024 ± 0.005	0.0050-0.0075	0.007 ± 0.001	0.007-0.011	0.009 ± 0.002
Area Under Curve (AUC_{0-t})		18068-24658	20607 ± 3546	625-840	668 ± 145	118-139	131 ± 11	1747-2717	2072 ± 568
Total Endogenous Levels of compound	*µg/L*		19189.14		816.92		34.49		81.26
Formation/ Elimination Rate of compound	*(µg/L)/min*		498.28 (total TRP) 49.89 (estimated free TRP)		20.73		2.21		3.68

Section 5: Discussion and Conclusion

5.1 Discussion

The kynurenine pathway is the primary systemic route of TRP metabolism. It is a biological process that plays a fundamental role in health and in the pathology of multiple disease states. These range from neurological disorders, for instance Huntington's disease (Thevandavakkam *et al*. 2010) and Parkinson's disease (Okuda *et al*. 1998); to ageing, irritable bowel syndrome (Majewski *et al.,* 2016), systemic inflammation and multi organ dysfunction syndrome (Mole *et al*. 2016). Despite the importance of the kynurenine pathway in disease, the flux of the pathway has previously not been defined. This project therefore aimed to accurately define the rate of formation for TRP, KYN, KYNA and 3HK in health. The work presented in this dissertation details the exact pharmacokinetic parameters for each of the four metabolites studied. The enzymatic rates, in health, have been determined for KMO, KYNU and the collaborative rates of IDO and TDO. To make this possible, a new LC-MS/MS analytical method, combined with a new extraction method, has been developed, enabling analyte concentrations as low as 0.01 μg/L to be accurately quantified, signifying this assay as one of the most sensitive assays for kynurenine metabolite analysis currently available.

Prior to this body of work, the Mole group extracted kynurenine pathway analytes from plasma samples using a trichloroacetic acid (TCA) protein precipitation assay. This previous extraction analysis assay was optimised for the investigation of endogenous analytes in plasma and not for the tracers. Therefore it was not suitable for the analysis of D_5-KYNA and $^{13}C_6$-3HK tracers. Therefore a new assay was developed and optimised, from extraction to LC-MS/MS analysis, to address these issues. This culminated in a robust, reliable method used to analyse tracer-infused rat plasma.

The initial experiments to detect these tracers at low levels with the old assay, produced erratic, wide and low intensity peaks. This lead to erratic standard curves and subsequent unreliability in quantification. Two leading factors to these issues were the large margin for human error during sample preparation and the low sensitivity to these tracers. Therefore, it was difficult to obtain suitable recovery of D_5-KYNA and

$^{13}C_6$-3HK tracers as well as their endogenous counterparts at low concentrations and consequently difficulty in identifying quantifiable peaks in rat plasma suitable for the pharmacokinetic modelling of the kynurenine pathway.

Because of this, the assay was redeveloped starting from analyte extraction from samples. The most common method of extraction used in LC-MS/MS studies of kynurenine pathway metabolites is PPT (Huang *et al*., 2013; Liu *et al.,* 2011; Ohashi *et al*., 2013; Yamada *et al.,* 2008), whilst SPE has also been used (de Jong *et al*., 2009; Möller *et al.,* 2012). To identify the optimal method of extraction, three commonly used types of purposely made extraction cartridges/plates; PPT, SLE and SPE, were compared. Analyte recovery of the tracers from each method was used as a tool to compare and identify the superior extraction process. SPE produced superior analyte recovery compared to the other two methods (Table 4.3). With D_5-KYNA and $^{13}C_6$-3HK being the two hardest tracers to detect at low levels, the selection of the extraction method was driven by results for these two tracers. The impact of phospholipids co-eluting and being present in the final sample to be ionised in the LC-MS/MS can be a complication in analysis. Phospholipids contribute to the 'matrix effect' whereby the plasma matrix causes ion suppression leading to a decline in the sensitivity and precision of the LC-MS/MS (Ahmad *et al*., 2012). The Oasis® HLB cartridges limit the amount of phospholipids being eluted, thus cleaning the samples and reducing the ion suppression effects of the plasma matrix. The SLE plate also removes phospholipids from the sample. However, the analytes may not have adhered to the column and therefore could have been lost in the extraction process. These results led to the SPE method being chosen as the base template for further method design and optimisation. Multiple elements of the pre-determined Oasis® HLB extraction process were then addressed and optimised for kynurenine pathway compound analysis. These included the agents and volumes used in the acidification of the sample; conditioning, equilibration and washing of extraction cartridges or wells; eluting and resuspension of the samples. For example, during resuspension, adding 70 µL of water, vortexing, and then adding 30 µL of methanol before vortexing again improved recovery of all analytes (Table 4.6) when compared to using a premix or adding methanol first. Thus, this sequence of resuspension in sample preparation was adopted. The final method being highlighted in Figure 5.1.

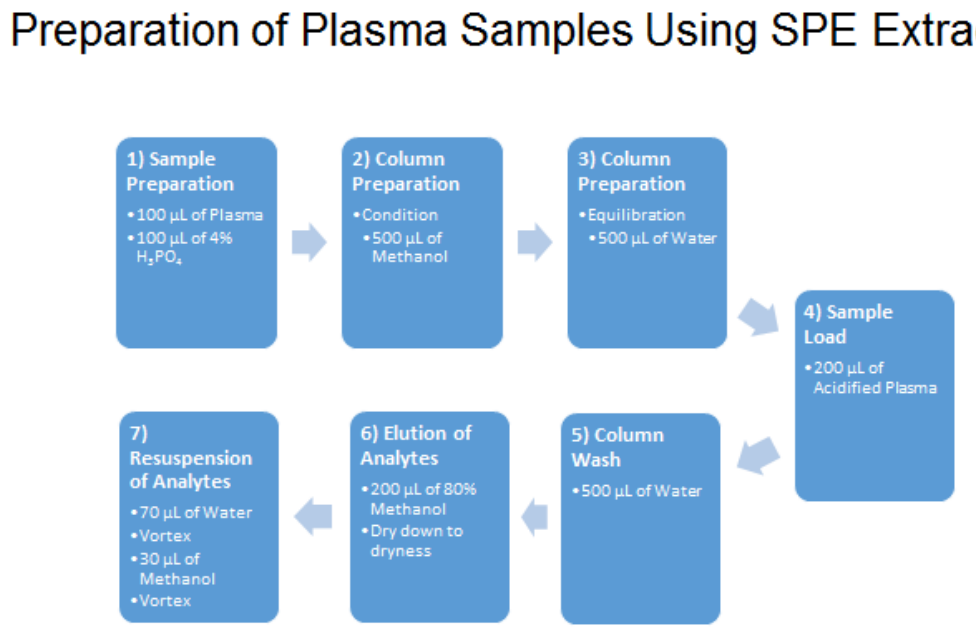

(Figure 5.1 – The Finalised Sample Extraction Method using Oasis® HLB 96-well plates.**)**

The old method and intermediate method 1 peaks seen in Figure 4.7 are examples of the marked difference the SPE extraction method had on the resolution and sensitivity of the analytes, with every analyte having enhanced peaks. The improvements seen in the peaks of KYNA, D_5-TRP and D_5-KYNA are particularly superior in comparison with the PPT extraction method.

Because tracer levels in rats were being analysed, the purpose of this work was to develop an optimised single-run assay that could analyse all kynurenine pathway analytes and tracers from one plasma sample. With the newly developed assay, this can be accomplished. Analysing the majority of endogenous tryptophan metabolites, in one run, has been achieved before (Fuertig *et al*., 2016b; Möller *et al*., 2012). Other groups have focused on a select group of analytes (Huang *et al*., 2013; Orsatti *et al*., 2015; Zhen *et al*., 2011) (Table 5.1).

To be confident that the developed assay was reliable and robust, the target set was to achieve symmetrical and sharp peaks that would be easily quantifiable. This would enable the accurate identification of the PK parameters of each analyte. As low as

possible LOQs were sought, to permit the use of low doses of tracer, that equate to 10% of endogenous levels, which would still be detected on the LC-MS/MS system. Doses equating to 10% of endogenous levels were chosen as the ideal target so as not to risk enzyme saturation and the potential of altering the flux of the kynurenine pathway (Uings, personal communication, 2016). To achieve this, the new assay would need to produce peaks of enhanced sensitivity and quality that could be quantified and used with confidence for PK analysis.

Because there was difficulty in detecting low plasma concentration levels of D_5-KYNA and $^{13}C_6$-3HK levels with the old method, the key peak characteristics that this project aimed to improve were height, an indicator of sensitivity to the analyte, and width, a marker of assay resolution and precision. An improved peak height, whilst reducing the noise, would improve the signal to noise ratio (S/N) and provide reliable and accurate peak areas for quantitation. Both sensitivity and resolution were improved by upgrading the LC-MS/MS system and applying a new UHPLC column respectively.

The LC-MS/MS was upgraded to a Shimadzu Nexera MP LC tandem AB SCIEX QTRAP 6500+ system. The new system had similar sensitivity and resolution for the majority of analytes, with the exception of $^{13}C_6$-3HK where there was a great improvement in peak heights and areas when compared with the intermediate method. Using this system, different columns, along with changing flow rates, were then compared to alter the resolution and identify the conditions that achieved peaks, in the biological samples, that were adequately separated, had excellent peak areas and were quantifiable, thereby producing reliable and accurate data that could then be utilised in PK analysis. Two columns were used. The ACE Excel UHPLC (C18-PFP, 1.7 µm, 2 x 100 mm) column provided larger and sharper peaks across all concentrations in comparison to the Waters XSelect HSS PFP column (3 x 100 mm; 2.5 µm) whilst also reducing run times from eleven minutes to nine minutes. By reducing the particle size of the column (2.5 µm to 1.7 µm), the theoretical number of plates inside the column is increased (Van Deemter Equation), enabling more analyte to adhere to the column before being eluted. Figure 4.7 demonstrates the impact the reduced particle size had

on the resolution of the tracer peaks. Although using the Waters column on the new system provided greater sensitivity, shown as greater peak heights, the resolution was inferior to the ACE column. The characteristics of the 3HK, KYNA and their respective peaks seen using the Waters column were too wide and difficult to quantify due to hesitancy on which area of the peak truly represented the analyte. Therefore, the ACE column was chosen despite its lower sensitivity, due to the crispness of the peaks and subsequently enhancing the reliability and precision of the assay. However, there was one limitation to the assay, the column was easily saturated at concentrations above 1,000 µg/L. This was an issue as endogenous levels of TRP are higher than the level of saturation, therefore a dilution analysis (1:10 – 1:100) was carried out to assess whether there was linearity across dilutions and therefore reliability in the data from diluted samples. Figure 4.5 highlights the results of the dilution experiment and shows that there is a good linearity across the dilutions with RSDs acceptable between 1:10 – 1:50 dilutions, therefore samples would be diluted fifty-fold when analysing endogenous TRP levels.

Conditions such as flow rates and compositions of mobile phase were altered for each column in an effort to achieve optimal conditions. The optimal flow rate for the ACE column was 0.4 ml/min and the varying compositions of mobile phase over time, along with all other conditions for the LC and MS components, are highlighted in Table 4.1. The analyte transitions were optimised using MRM scan mode parameters and the transitions that yielded the best peaks were incorporated into the MS method (See Figure 4.1 and Table 4.2). The highest sensitivity for TRP, KYN, KYNA, 3HK, AA, XA and 3HAA was seen using positive ionization whilst the highest sensitivity for QUIN was seen in negative ionization. These findings were mostly in agreement with those reported previously. However, in the literature there are differences in the ionization for QUIN and XA. Fuertig et al. report having better sensitivity if they are positively ionised (Fuertig *et al*., 2016a), whilst Möller *et al*. report they have better sensitivity if they are negatively ionised (Möller *et al*., 2012). Unfortunately, XA was unable to be separated entirely from TRP and therefore cannot be confidently quantified. Thus, future studies will need to optimise conditions further to be able to measure endogenous XA.

Once the assay had been finalised, the robustness, reliability and accuracy were investigated, according to the guidelines set out by the FDA. The method was subjected to a variety of different tests, described in Section 3. The intra- and inter-day studies of precision and accuracy revealed that the system was reliable, precise and produced accurate levels of each analyte (measured by %RSD) ranging from concentrations representing levels lower than seen in plasma, to high standard concentrations (within-day 2-18 %RSD; between-day 3-15 %RSD). The range of each analyte standard curve encompassed the natural range of endogenous analyte seen in rat plasma samples, with the exception of TRP, which needs to be diluted as previously described.

A secondary aim of this study was to lower the LOQs for each analyte. Experiments were performed, using low concentrations of analyte mixes (0.01 – 0.2 μg/L; *n*=3) to identify the sensitivity of the assay. The LOQs established in this assay compare favourably with those established by other groups (Table 5.2). Each analyte, with the exception of QUIN, has a lower LOQ, using the assay described, than any of the previous reports. The signal to noise ratios of TRP, KYNA and 3HAA also suggest that the assay may detect these analytes at even lower concentrations (Table 4.12). The assay differs from all the previously reported HPLC methods (Table 5.1) and represents the first use of UHPLC for the analysis of the kynurenine pathway. Fuertig et al. were able to produce the lowest LOQs from the literature previously reported. However, these were produced in aqueous solvent, thus there was no matrix to have an effect on the signal to noise ratio. This dissertation has provided LOQs that have been produced from samples where analyte has been spiked into a 1% bovine serum albumin and 4% phosphoric acid solvent. The work described in Section 4 (Table 4.8) has proved that this matrix environment is the best plasma surrogate matrix for the standard curves. Therefore, this assay may be one of the most sensitive assays for kynurenine metabolite analysis currently available.

Table 5.1 - Comparison of LC-MS/MS Methods (This project highlighted in bold)

Group	Extraction Method	Volume of Sample (µl)	Resuspension Volume (µl)	Injection Volume (µl)	Run Time (mins)	LC system	Column	Mass Spec	Flow Rate (mL/min)	R^2 >
De Jong et al. 2009	on-line SPE	250	300	50	8	HPLC	Atlantis dC18 (100 x 2.1 mm; 3µm)	Micromass Quattro Premier with Z Spray	0.05	0.99
Zhen et al. 2011	PPT	100	N/A	25	8	HPLC	BDS-Hypersil-C8 (150mm x 4.6 mm; 5 µm)	not reported	0.6	0.99
Moller et al. 2012	SPE	800	150	10	12	HPLC	Restek C18 Aqueous 100 x 2.1 mm	API 2000 Triple Quadrople (ESI, SIR)	0.2	0.95
Huang et al. 2013	PPT	100	N/A	5	4.5	HPLC	Synergi Polar RP (75 x 4.6 mm)	Micromass Quattro Ultima Triple Quadrople (ESI, SRM)	1	0.99
Orsatti et al. 2015	PPT	50	Not reported	10	4.3	HPLC	Atlantis dC18 (2.1 mm x 100 mm; 3 µm)	API-6500 Triple Quadrople (ESI, MRM)	0.5	0.99
Fuertig et al. 2016	PPT / Ultrafiltration	10	40-50	20	5.5	HPLC	GRACE VisionHT C18 (100 x 2.1 mm; 3 µm)	API-4000 Triple Quadrople	0.4	N/A
Murray et al. 2016	**SPE**	**100**	**100**	**10**	**9.1**	**UHPLC**	**ACE Excel C18-PFP (2.1 x 100 mm; 1.7 µm)**	**AB Sciex 6500+ Triple Quadrople (ESI, MRM)**	**0.4**	**0.99**

Table 5.2 - Comparison of Limits of Quantification (This project highlighted in bold)

		Limit of Quantification (µg/L)							
Group	**Matrix**	**TRP**	**KYN**	**KYNA**	**3HK**	**3HAA**	**AA**	**QUIN**	**XA**
De Jong et al. 2009	Pooled Plasma	22.48	10.41	N/A	5.16	N/A	N/A	N/A	N/A
Zhen et al. 2011	Plasma	811	88	N/A	0.98	N/A	N/A	N/A	N/A
Moller et al. 2012	Plasma	7.2	7.3	10.0	N/A	12.9	6.4	336.6	N/A
Huang et al. 2013	Water	1250	62.5	N/A	N/A	N/A	N/A	N/A	N/A
Orsatti et al. 2015	Water/acetonitrile (9/1) w 0.1% formic acid	N/A	9.8	0.49	0.098	N/A	0.49	N/A	N/A
Fuertig et al. 2016	Acidified mobile phase	0.51	0.10	0.07	0.17	0.15	N/A	0.42	0.05
Murray et al. 2016	**1% BSA**	**0.01**	**0.03**	**0.01**	**0.73**	**0.01**	**0.04**	**50**	**0.02**

Having solved the issues of producing symmetrical, quantifiable and reliable peaks for both $^{13}C_6$-3HK and D_5-KYNA (Figure 4.7), tracer-infused rat plasma samples were extracted and analysed using the method. The sensitivity of the method resulted in initial concentrations of D_5-TRP and $^{13}C_6$-KYN to be 10% of endogenous levels, whilst the initial concentrations of D_5-KYNA and $^{13}C_6$-3HK represented the lowest initial concentrations that provided us with quantifiable peaks throughout the duration of the experiment.

In the analysis, standard curves that were used were linear and had an excellent line of best fit ($R^2 > 0.99$). The data points included in these curves reflected the range of tracer levels seen in the samples (Figure 4.8). For D_5-TRP and $^{13}C_6$-KYN, the sensitivity of the system was sufficient to be able to infuse doses of tracer that were representative of 10% of endogenous levels, so not to disturb the flux of the pathway and risk saturating KMO and IDO respectively. For D_5-KYNA and $^{13}C_6$-3HK, this low level of detection could not be achieved, thus doses of tracer that were used represented the lowest dose that would achieve quantifiable levels of tracer throughout the experiment (D_5-KYNA, 62%; $^{13}C_6$-3HK, 256% of endogenous levels; Figure 4.9).

Because a sufficient number of peaks were able to be quantified throughout the duration of each experiment, the pharmacokinetic model of the kynurenine pathway was defined. The enzymatic turnover for KMO in health has now been described along with the half-life, volume of distribution and elimination constants for each metabolite of interest.

The data produced illustrates the two-phase decay of each tracer. The first phase representing each tracer being distributed into tissues rapidly. The second phase representing the elimination of the tracer from the plasma. Using this elimination phase, the PK parameters for each tracer (Table 4.15) were formulated. Thus, the PK of their corresponding kynurenine pathway compound was predicted. Each compound has a short half-life (D_5-TRP 27.08 ± 4.14; $^{13}C_6$-KYN 29.12 ± 7.51; D_5-KYNA 12.14 ± 5.52; $^{13}C_6$-3HK 16.01 ± 4.43; mins) highlighting the rapid flux of the pathway. Secondly, all tracers have a low V_d, with $^{13}C_6$-KYN having the highest (0.96 ± 0.25 (μg/kg)/(μg/L)) and D_5-KYNA having the lowest (0.12 ± 0.07 (μg/kg)/(μg/L)). These differences in the V_d may aid the understanding of the reasons as to why there are marked differences in the formation/elimination rates of each compound (Figure 5.2).

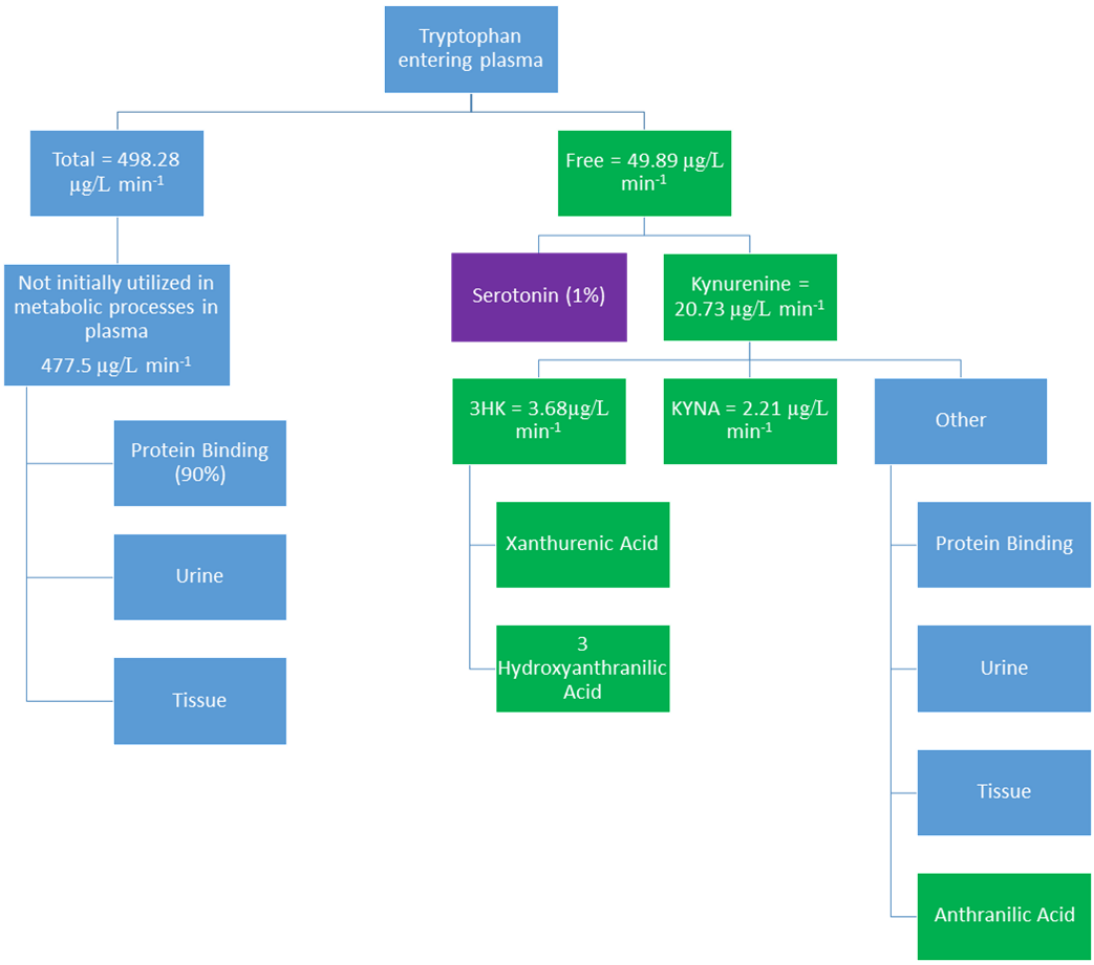

(Figure 5.2. The Predicted Flux of the Kynurenine Pathway. It is predicted that of the circa 500 µg/L min^{-1} of TRP that enters and is eliminated from the blood circulation system during basal metabolic conditions, only 4.1% of this (20.73 µg/L min^{-1}) is converted into KYN. Around 90% of the TRP will be bound to protein (circa 448.39 µg/L min^{-1}), leaving 29.1 µg/L min-1of free TRP to be eliminated *via* other mechanisms such as the production of serotonin, distribution into tissue and urinary excretion. 28% of the produced KYN is converted into either KA or 3HK, with the remaining 72% likely to be protein bound, metabolised into AA, distributed into tissues or excreted. Green boxes indicate progression down the kynurenine pathway. Values indicate the rate of formation/elimination of the compound. Blue boxes indicate other mechanisms of elimination. Purple box indicates serotonin pathway)

The relatively high V_d of TRP and KYN compared to 3HK and KYNA implies that the marked difference between formation/elimination rates across the metabolites could be due to high distribution of TRP and KYN into the surrounding tissues, or, be due to high levels binding to protein in the plasma, and therefore being absorbed into their corresponding reserve pool. It is known that 90% of TRP is protein bound in the plasma (Salter *et al.,* 1989). As the assay measured total plasma levels of TRP, 90% of the TRP detected would have been bound to protein, therefore the remaining 10% (49.83 μg/L min^{-1}) is the proportion of TRP that is subjected to metabolism and further tissue distribution. PK analysis identified that 42% of free TRP is converted into KYN. KYN has been implicated in the competitive dissociation of TRP from albumin in the blood (Cangiano *et al*., 1999), thus the disparity between the elimination of KYN and the formation of KYNA and 3HK is likely to be due to KYN becoming protein bound or being eliminated *via* urinary excretion, reported to be twenty-five μg per day in rats (Saito *et al*., 2000). Another reason for these disparities along the kynurenine pathway could be due to the V_d and the ability for tissue distribution. TRP and KYN have a higher V_d than KYNA and 3HK. Thus, a larger amount of TRP and KYN will be distributed into cells, most notably the liver and kidneys where they are then metabolised. Thus this exodus of TRP and KYN into the tissue contributes to the elimination of these compounds from the plasma. The low V_d of 3HK and KYNA highlights the fact that these compounds prefer a hydrophilic environment and thus stay in the blood. This is further indicated with the varying levels of clearance from the plasma for each metabolite, where clearance is comparably high for TRP and KYN (0.024 ± 0.004 and 0.024 ± 0.005 μg/L min^{-1} respectively) and low for KYNA and 3HK (0.007 ± 0.001 and 0.009 ± 0.002 μg/L min^{-1} respectively). Interestingly, the elimination constants for KYNA and 3HK (0.064 ± 0.023 and 0.045 ± 0.011 L/min respectively) were treble and double, respectively, the rates seen for TRP and KYN (0.026 ± 0.004 and 0.025 ± 0.008 L/min respectively). Thus, if KYNA and 3HK are being removed from the body at a higher rate than TRP and KYN, yet their formation/elimination rates in plasma are radically lower, then it must be the abilities of TRP and KYN to infiltrate tissue and bind to protein that is affecting these disparities.

This study successfully detailed the pharmacokinetics of four kynurenine pathway metabolites due to the development of a highly sensitive, reliable and robust LC-MS/MS assay. The strengths of this study include the method of tracer administration. The use of indwelling vascular cannulae guarantees an exact dose of tracer. Cannulae also allow for accurate and timely retrieval of plasma from the rats, maximising the precision of the data obtained.

The strengths of the LC-MS/MS assay include a low injection volume, therefore samples can be stored and analysed at a future date if needed. The low LOQs of the analytes culminated in an assay that can identify low levels of endogenous analytes with confidence. The low LOQs for D_5-TRP and $^{13}C_6$-KYN also facilitated the administration of these tracers at doses that equated to ten per cent of levels of their endogenous counterparts. The assay is robust and reliable, therefore the data obtained can be interpreted with confidence, culminating in a pharmacokinetic model that is precise. This pharmacokinetic model of the kynurenine pathway has defined the precise enzymatic rates of KMO and the enzymes upstream along with detailing the precise pharmacokinetic parameters for each analyte of interest.

There are aspects of this project that could be improved with further development. The relatively high LOQs of D_5-KYNA and $^{13}C_6$-3HK, in comparison to their endogenous counterparts, prevented the study from achieving a dose that was equal to ten per cent of endogenous KYNA or 3HK. These high doses mean that the flux of the kynurenine pathway may have been altered, therefore there is potential that the precision of the PK data may have been affected. The fate of each analyte has also not yet been accounted for, with tissue and urine still to be examined. The downstream kynurenine metabolites have also not yet been analysed, therefore the flux of the entire kynurenine pathway is still to be defined.

Finally, the large volume of plasma (100 µl) used for the initial SPE extraction accounts for up to 50% of the plasma retrieved for each time point. Therefore, the margins for error are low due to lack of plasma available if problems do occur.

To address these issues, there are multiple experiments that can be done in future studies. To identify the precise distribution, metabolism and excretion of each analyte, analysis of urine collected from the tracer studies should be carried out. This will identify the quantities of tracer and the endogenous compounds that are not metabolised in the kynurenine pathway and are excreted through the urine. Proportions of the formation/elimination rate attributed to urine excretion can then be formulated. Levels of these analytes should also be identified in the tissues. Data from this study highlight marked differences in the V_d of each metabolite and the fate of each metabolite has yet to be fully defined. There are significant differences in their formation/elimination rates at each stage of the pathway. The analysis of different tissues will also aid the anatomical definition of the kynurenine pathway, detailing the exact locations of metabolite accumulation.

The tracer experiments can also be used to identify the impact that KMO inhibition has on the flux through the pathway. Therefore these experiments could be repeated using a KMO inhibitor in rats, as well as using genetically altered KMO knockout mice, to identify the precise changes of metabolite levels upstream and downstream of KMO. These would identify the alterations in the pharmacokinetic model of the kynurenine pathway under conditions of absent KMO activity.

Finally, further work into the optimisation of the LC-MS/MS assay should be carried out to reduce plasma volumes needed and to increase the sensitivity to D_5-KYNA and $^{13}C_6$-3HK, enabling the study of their metabolism at doses <10% of their endogenous counterparts.

5.2 Conclusion

To conclude, the aim of this dissertation was to describe the flux of the kynurenine pathway, focusing on the enzyme reaction rate of KMO and the enzymes upstream. To identify these parameters, a new, single-run assay was developed for the identification and quantification of kynurenine pathway metabolites in rat plasma. This assay is capable of detecting and quantifying kynurenine pathway metabolites at concentrations as low as 0.01 μg/l, highlighting its excellent sensitivity.

The PK of four of these metabolites (TRP, KYN, KYNA and 3HK) have been assessed and described, highlighting the variation in distribution and subsequent abilities to distribute into surrounding tissue. Consequently, the enzymatic reaction rates, in the healthy physiological state, were formulated. KMO has a basal reaction rate of 3.68 μg/l min^{-1}, the combination of TDO and IDO generates KYN at 20.73 μg/l min^{-1} and KYNU yields KYNA at 2.21 μg/l min^{-1}. Further work investigating the alterations to these rates, using both KMO inhibitors and mouse models of KMO knockouts are required to understand the consequences of KMO blockade.

References

AHMAD, S., Kalra, H., Gupta, A., Raut, B., Hussain, A., & Rahman, M. A. (2012). HybridSPE: A novel technique to reduce phospholipid-based matrix effect in LC-ESI-MS Bioanalysis. *J Pharm Bioallied Sci, 4*(4), 267-275. doi:10.4103/0975-7406.103234

AKAIKE, A., Katsuki, H., Kume, T., & Maeda, T. (1999). Reactive oxygen species in NMDA receptor-mediated glutamate neurotoxicity. *Parkinsonism Relat Disord, 5*(4), 203-207.

ALBERATI-GIANI, D., Cesura, A. M., Broger, C., Warren, W. D., Röver, S., & Malherbe, P. (1997). Cloning and functional expression of human kynurenine 3-monooxygenase. *FEBS Letters, 410*(2–3), 407-412. doi:http://dx.doi.org/10.1016/S0014-5793(97)00627-3

AMARAL, M., Levy, C., Heyes, D. J., Lafite, P., Outeiro, T. F., Giorgini, F., Leys, D., Scrutton, N. S. (2013). Structural basis of kynurenine 3-monooxygenase inhibition. *Nature, 496*(7445), 382-385. doi:10.1038/nature12039

BARAN, H., Jellinger, K., & Deecke, L. (1999). Kynurenine metabolism in Alzheimer's disease. *J Neural Transm, 106*(2), 165-181.

BASSAMI, M., Ahmadizad, S., Doran, D., & MacLaren, D. P. (2007). Effects of exercise intensity and duration on fat metabolism in trained and untrained older males. *Eur J Appl Physiol, 101*(4), 525-532. doi:10.1007/s00421-007-0523-7

BECKINGHAM, I. J., & Bornman, P. C. (2001). ABC of diseases of liver, pancreas, and biliary system. Acute pancreatitis. *BMJ, 322*(7286), 595-598.

BECONI, M. G., Yates, D., Lyons, K., Matthews, K., Clifton, S., Mead, T., Prime, M., Winkler, D., O'Connell, C., Walter, D., Toldeo-Sherman, L., Munoz-Sanjuan, I., Dominguez, C. (2012). Metabolism and Pharmacokinetics of JM6 in Mice: JM6 Is Not a Prodrug for Ro-61-8048. *Drug Metabolism and Disposition, 40*(12), 2297-2306. doi:10.1124/dmd.112.046532

BEGGIATO, S., Tanganelli, S., Fuxe, K., Antonelli, T., Schwarcz, R., & Ferraro, L. (2014). Endogenous kynurenic acid regulates extracellular GABA levels in the rat prefrontal cortex. *Neuropharmacology, 82*, 11-18. doi:10.1016/j.neuropharm.2014.02.019

BOEGMAN, R. J., el-Defrawy, S. R., Jhamandas, K., Beninger, R. J., & Ludwin, S. K. (1985). Quinolinic acid neurotoxicity in the nucleus basalis antagonized by kynurenic acid. *Neurobiol Aging, 6*(4), 331-336.

BOWMAN, B. T., & Sans, W. W. (1983). Determination of octanol-water partitioning coefficients (KOW) of 61 organophosphorus and carbamate insecticides and their relationship to respective water solubility (S) values. *Journal of Environmental Science and Health, Part B, 18*(6), 667-683. doi:10.1080/03601238309372398

BRETON, J., Avanzi, N., Magagnin, S., Covini, N., Magistrelli, G., Cozzi, L., & Isacchi, A. (2000). Functional characterization and mechanism of action of recombinant human kynurenine 3-hydroxylase. *Eur J Biochem, 267*(4), 1092-1099.

CAMPBELl, B. M., Charych, E., Lee, A. W., & Möller, T. (2014). Kynurenines in CNS disease: regulation by inflammatory cytokines. *Front Neurosci, 8*, 12. doi:10.3389/fnins.2014.00012

CANGIANO, C., Cardelli, P., Peverini, P., Giglio, R. M., Laviano, A., Fava, A., & Rossi Fanelli, F. (1999). Effect of kynurenine on tryptophan-albumin binding in human plasma. *Adv Exp Med Biol, 467*, 279-282.

CHEN, Y., & Guillemin, G. J. (2009). Kynurenine pathway metabolites in humans: disease and healthy States. *Int J Tryptophan Res, 2*, 1-19.

CHIARUGI, A., Cozzi, A., Ballerini, C., Massacesi, L., & Moroni, F. (2001). Kynurenine 3-mono-oxygenase activity and neurotoxic kynurenine metabolites increase in the spinal cord of rats with experimental allergic encephalomyelitis. *Neuroscience, 102*(3), 687-695. doi:http://dx.doi.org/10.1016/S0306-4522(00)00504-2

CHRISTEN, S., Peterhans, E., & Stocker, R. (1990). Antioxidant activities of some tryptophan metabolites: possible implication for inflammatory diseases. *Proc Natl Acad Sci U S A, 87*(7), 2506-2510.

COLIN-GONZALEZ, A. L., Maldonado, P. D., & Santamaria, A. (2013). 3-Hydroxykynurenine: an intriguing molecule exerting dual actions in the central nervous system. *Neurotoxicology, 34*, 189-204. doi:10.1016/j.neuro.2012.11.007

CONRAD, M. L., Moser, A. C., & Hage, D. S. (2009). Evaluation of indole-based probes for high-throughput screening of drug binding to human serum albumin: Analysis by high-performance affinity chromatography. *J Sep Sci, 32*(8), 1145-1155. doi:10.1002/jssc.200800567

COYLE, C. H., & Kader, K. N. (2007). Mechanisms of H2O2-induced oxidative stress in endothelial cells exposed to physiologic shear stress. *ASAIO J, 53*(1), 17-22. doi:10.1097/01.mat.0000247157.84350.e8

CROZIER-REABE, K. R., Phillips, R. S., & Moran, G. R. (2008). Kynurenine 3-Monooxygenase from Pseudomonas fluorescens: Substrate-like Inhibitors both Stimulate Flavin Reduction and Stabilize the Flavin−Peroxo Intermediate yet Result in the Production of Hydrogen Peroxide. *Biochemistry, 47*(47), 12420-12433. doi:10.1021/bi8010434

CROZIER, K. R., & Moran, G. R. (2007). Heterologous expression and purification of kynurenine-3-monooxygenase from Pseudomonas fluorescens strain 17400. *Protein Expr Purif, 51*(2), 324-333. doi:http://dx.doi.org/10.1016/j.pep.2006.07.024

DE JONG, W. H., Smit, R., Bakker, S. J., de Vries, E. G., & Kema, I. P. (2009). Plasma tryptophan, kynurenine and 3-hydroxykynurenine measurement using automated on-line solid-phase extraction HPLC-tandem mass spectrometry. *J Chromatogr B Analyt Technol Biomed Life Sci, 877*(7), 603-609. doi:10.1016/j.jchromb.2009.01.015

DONG-RUYL, L., Sawada, M., & Nakano, K. (1998). Tryptophan and its metabolite, kynurenine, stimulate expression of nerve growth factor in cultured mouse astroglial cells. *Neurosci Lett, 244*(1), 17-20.

DUNN, A. J., & Welch, J. (1991). Stress- and endotoxin-induced increases in brain tryptophan and serotonin metabolism depend on sympathetic nervous system activity. *J Neurochem, 57*(5), 1615-1622.

EDDERSHAW, P. J., Beresford, A. P., & Bayliss, M. K. (2000). ADME/PK as part of a rational approach to drug discovery. *Drug Discov Today, 5*(9), 409-414. doi:http://dx.doi.org/10.1016/S1359-6446(00)01540-3

ELLIS, M. P., French, J. J., & Charnley, R. M. (2009). Acute pancreatitis and the influence of socioeconomic deprivation. *Br J Surg, 96*(1), 74-80. doi:10.1002/bjs.6414

ERICKSON, J. B., Flanagan, E. M., Russo, S., & Reinhard Jr, J. F. (1992). A radiometric assay for kynurenine 3-hydroxylase based on the release of 3H2O during hydroxylation of l-[3,5-3H]kynurenine. *Anal Biochem, 205*(2), 257-262. doi:http://dx.doi.org/10.1016/0003-2697(92)90432-7

FERNSTROM, J. D., & Fernstrom, M. H. (2006). Exercise, serum free tryptophan, and central fatigue. *J Nutr, 136*(2), 553S-559S.

FOOD AND DRUG ADMINISTRATION, F. (2001). *Guidance for Industry: Bioanalytical Method Validation*.

FOSTER, A. C., Miller, L. P., Oldendorf, W. H., & Schwarcz, R. (1984). Studies on the disposition of quinolinic acid after intracerebral or systemic administration in the rat. *Exp Neurol, 84*(2), 428-440.

FOSTER, A. C., Okuno, E., Brougher, D. S., & Schwarcz, R. (1986). A radioenzymatic assay for quinolinic acid. *Anal Biochem, 158*(1), 98-103.

FOSTER, A. C., Vezzani, A., French, E. D., & Schwarcz, R. (1984). Kynurenic acid blocks neurotoxicity and seizures induced in rats by the related brain metabolite quinolinic acid. *Neurosci Lett, 48*(3), 273-278.

FOSTER, A. C., Whetsell, W. O., Jr., Bird, E. D., & Schwarcz, R. (1985). Quinolinic acid phosphoribosyltransferase in human and rat brain: activity in Huntington's disease and in quinolinate-lesioned rat striatum. *Brain Res, 336*(2), 207-214.

FOSTER, A. C., White, R. J., & Schwarcz, R. (1986). Synthesis of quinolinic acid by 3-hydroxyanthranilic acid oxygenase in rat brain tissue in vitro. *J Neurochem, 47*(1), 23-30.

FREEMAN-COOK, K. D., Hoffman, R. L., & Johnson, T. W. (2013). Lipophilic efficiency: the most important efficiency metric in medicinal chemistry. *Future Medicinal Chemistry, 5*(2), 113-115. doi:10.4155/fmc.12.208

FRUMENTO, G., Rotondo, R., Tonetti, M., Damonte, G., Benatti, U., & Ferrara, G. B. (2002). Tryptophan-derived catabolites are responsible for inhibition of T and natural killer cell proliferation induced by indoleamine 2,3-dioxygenase. *J Exp Med, 196*(4), 459-468.

FUERTIG, R., Ceci, A., Camus, S. M., Bezard, E., Luippold, A. H., & Hengerer, B. (2016a). LC-MS/MS-based quantification of kynurenine metabolites, tryptophan, monoamines and neopterin in plasma, cerebrospinal fluid and brain. *Bioanalysis, 8*(18), 1903-1917. doi:10.4155/bio-2016-0111

GOLDACRE, M. J., & Roberts, S. E. (2004). Hospital admission for acute pancreatitis in an English population, 1963-98: database study of incidence and mortality. *BMJ, 328*(7454), 1466-1469. doi:10.1136/bmj.328.7454.1466

GOLDSTEIN, L. E., Leopold, M. C., Huang, X., Atwood, C. S., Saunders, A. J., Hartshorn, M., Lim J. T., Faget, K.Y., Muffat, J. A., Scarpa, R. C., Chylack, L. T. Jr., Bowden, E. F., Tanzi, R. E., Bush, A. I. (2000). 3-Hydroxykynurenine and 3-Hydroxyanthranilic Acid Generate Hydrogen Peroxide and Promote α-Crystallin Cross-Linking by Metal Ion Reduction†. *Biochemistry, 39*(24), 7266-7275. doi:10.1021/bi992997s

GOOSZEN, H. G., Besselink, M. G., van Santvoort, H. C., & Bollen, T. L. (2013). Surgical treatment of acute pancreatitis. *Langenbecks Arch Surg, 398*(6), 799-806. doi:10.1007/s00423-013-1100-7

GOSHIMA, N., Wadano, A., & Miura, K. (1986). 3-hydroxykynurenine as O2−· scavenger in the blowfly, Aldrichina grahami. *Biochemical and Biophysical Research Communications, 139*(2), 666-672. doi:http://dx.doi.org/10.1016/S0006-291X(86)80042-0

GRIFFIN, S., Wyllie, S. G., & Markham, J. (1999). Determination of octanol–water partition coefficient for terpenoids using reversed-phase high-performance liquid chromatography. *Journal of Chromatography A, 864*(2), 221-228. doi:http://dx.doi.org/10.1016/S0021-9673(99)01009-2

GUIDETTI, P., Bates, G. P., Graham, R. K., Hayden, M. R., Leavitt, B. R., MacDonald, M. E., Slow, E. J., Wheeler, V. C., Woodman, B., Schwarcz, R. (2006). Elevated brain 3-hydroxykynurenine and quinolinate levels in Huntington disease mice. *Neurobiology of Disease, 23*(1), 190-197. doi:http://dx.doi.org/10.1016/j.nbd.2006.02.011

GUIDETTI, P., & Schwarcz, R. (1999). 3-Hydroxykynurenine potentiates quinolinate but not NMDA toxicity in the rat striatum. *European Journal of Neuroscience, 11*(11), 3857-3863. doi:10.1046/j.1460-9568.1999.00806.x

GUILLEMIN, G. J. (2012). Quinolinic acid, the inescapable neurotoxin. *FEBS J, 279*(8), 1356-1365. doi:10.1111/j.1742-4658.2012.08485.x

GUILLEMIN, G. J., Kerr, S. J., Smythe, G. A., Smith, D. G., Kapoor, V., Armati, P. J., Croitoru, J., Brew, B. J. (2001). Kynurenine pathway metabolism in human astrocytes: a paradox for neuronal protection. *J Neurochem, 78*(4), 842-853.

GUILLEMIN, G. J., Smith, D. G., Smythe, G. A., Armati, P. J., & Brew, B. J. (2003). Expression of the kynurenine pathway enzymes in human microglia and macrophages. *Adv Exp Med Biol, 527*, 105-112.

HARRIS, M. F., & Logan, J. L. (2014). Determination of log Kow Values for Four Drugs. *Journal of Chemical Education, 91*(6), 915-918. doi:10.1021/ed400655b

HARTAI, Z., Juhasz, A., Rimanoczy, A., Janaky, T., Donko, T., Dux, L., Penke, B., Toth, G. K., Janka, Z., Kalman, J. (2007). Decreased serum and red blood cell kynurenic acid levels in Alzheimer's disease. *Neurochem Int, 50*(2), 308-313. doi:10.1016/j.neuint.2006.08.012

HUANG, Y., Louie, A., Yang, Q., Massenkoff, N., Xu, C., Hunt, P. W., & Gee, W. (2013). A simple LC-MS/MS method for determination of kynurenine and tryptophan concentrations in human plasma from HIV-infected patients. *Bioanalysis, 5*(11), 1397-1407. doi:10.4155/bio.13.74

HUGHES, J. D., Blagg, J., Price, D. A., Bailey, S., DeCrescenzo, G. A., Devraj, R. V., Ellsworth, E., Fobian, Y. M., Gibbs, M. E., Gilles, R.W., Greene, N., Huang, E., Krieger-Burke, T., Loesel, J., Wager, T., Whiteley, L., Zhang, Y. (2008). Physiochemical drug properties associated with in vivo toxicological outcomes. *Bioorganic & Medicinal Chemistry Letters, 18*(17), 4872-4875. doi:http://dx.doi.org/10.1016/j.bmcl.2008.07.071

HUTTER, R., Niederberger, P., & DeMoss, J. A. (1986). Tryptophan biosynthetic genes in eukaryotic microorganisms. *Annu Rev Microbiol, 40*, 55-77. doi:10.1146/annurev.mi.40.100186.000415

KALEPU, S., Manthina, M., & Padavala, V. (2013). Oral lipid-based drug delivery systems – an overview. *Acta Pharmaceutica Sinica B, 3*(6), 361-372. doi:http://dx.doi.org/10.1016/j.apsb.2013.10.001

KALGUTKAR, A. S., Crews, B. C., Saleh, S., Prudhomme, D., & Marnett, L. J. (2005). Indolyl esters and amides related to indomethacin are selective COX-2 inhibitors. *Bioorg Med Chem, 13*(24), 6810-6822. doi:10.1016/j.bmc.2005.07.073

KARPE, F., Dickmann, J. R., & Frayn, K. N. (2011). Fatty acids, obesity, and insulin resistance: time for a reevaluation. *Diabetes, 60*(10), 2441-2449. doi:10.2337/db11-0425

KESZTHELYI, D., Troost, F. J., & Masclee, A. A. (2009). Understanding the role of tryptophan and serotonin metabolism in gastrointestinal function. *Neurogastroenterol Motil, 21*(12), 1239-1249. doi:10.1111/j.1365-2982.2009.01370.x

KOCH-WESER, J., & Sellers, E. M. (1976). Binding of drugs to serum albumin (first of two parts). *N Engl J Med, 294*(6), 311-316. doi:10.1056/NEJM197602052940605

KOHLER, C., Okuno, E., Flood, P. R., & Schwarcz, R. (1987). Quinolinic acid phosphoribosyltransferase: preferential glial localization in the rat brain visualized by immunocytochemistry. *Proc Natl Acad Sci U S A, 84*(10), 3491-3495.

LAFON-CAZAL, M., Culcasi, M., Gaven, F., Pietri, S., & Bockaert, J. (1993). Nitric oxide, superoxide and peroxynitrite: putative mediators of NMDA-induced cell death in cerebellar granule cells. *Neuropharmacology, 32*(11), 1259-1266.

LAPIN, I. P. (1976). Depressor effect of kynurenine and its metabolites in rats. *Life Sci, 19*(10), 1479-1483.

LAUBE, M., Tondera, C., Sharma, S. K., Bechmann, N., Pietzsch, F.-J., Pigorsch, A., Kockerling, M., Wuest, F., Pietzsch, J., Kniess, T. (2014). 2,3-Diaryl-substituted indole based COX-2 inhibitors as leads for imaging tracer development. *RSC Advances, 4*(73), 38726-38742. doi:10.1039/C4RA05650G

LEIPNITZ, G., Schumacher, C., Dalcin, K. B., Scussiato, K., Solano, A., Funchal, C., Dutra-Filho, C. S., Wyse, A. T., Wannmacher, C. M., Latini, A., Wajner, M. (2007). In vitro evidence for an antioxidant role of 3-hydroxykynurenine and 3-hydroxyanthranilic acid in the brain. *Neurochem Int, 50*(1), 83-94. doi:10.1016/j.neuint.2006.04.017

LEWITT, P. A., Li, J., Lu, M., Beach, T. G., Adler, C. H., Guo, L., & Arizona Parkinson's Disease, C. (2013). 3-hydroxykynurenine and other Parkinson's disease biomarkers discovered by metabolomic analysis. *Mov Disord, 28*(12), 1653-1660. doi:10.1002/mds.25555

LIN, S. J., & Guarente, L. (2003). Nicotinamide adenine dinucleotide, a metabolic regulator of transcription, longevity and disease. *Curr Opin Cell Biol, 15*(2), 241-246.

LIU, L., Chen, Y., Zhang, Y., Wang, F., & Chen, Z. (2011). Determination of tryptophan and kynurenine in human plasma by liquid chromatography–electrochemical detection with multi-wall carbon nanotube-modified glassy carbon electrode. *Biomedical Chromatography, 25*(8), 938-942. doi:10.1002/bmc.1550

LUGO-HUITRON, R., Ugalde Muniz, P., Pineda, B., Pedraza-Chaverri, J., Rios, C., & Perez-de la Cruz, V. (2013). Quinolinic acid: an endogenous neurotoxin with multiple targets. *Oxid Med Cell Longev, 2013*, 104024. doi:10.1155/2013/104024

MAJEWSKI, M., Kozlowska, A., Thoene, M., Lepiarczyk, E., & Grzegorzewski, W. J. (2016). Overview of the role of vitamins and minerals on the kynurenine pathway in health and disease. *J Physiol Pharmacol, 67*(1), 3-19.

MANDI, Y., & Vecsei, L. (2012). The kynurenine system and immunoregulation. *J Neural Transm, 119*(2), 197-209. doi:10.1007/s00702-011-0681-y

MCKAY, C. J., Evans, S., Sinclair, M., Carter, C. R., & Imrie, C. W. (1999). High early mortality rate from acute pancreatitis in Scotland, 1984-1995. *Br J Surg, 86*(10), 1302-1305. doi:10.1046/j.1365-2168.1999.01246.x

MCMENAMY, R. H. (1965). Binding of indole analogues to human serum albumin. Effects of fatty acids. *J Biol Chem, 240*(11), 4235-4243.

MILLER, R., Ewy, W., Corrigan, B. W., Ouellet, D., Hermann, D., Kowalski, K. G., Lockwood, P., Koup, J. R., Donevan, S., El-Kattan, A., Li, C. S., Werth, J. L., Feltner, D. E., Lalonde, R. L. (2005). How modeling and simulation have enhanced decision making in new drug development. *J Pharmacokinet Pharmacodyn, 32*(2), 185-197. doi:10.1007/s10928-005-0074-7

MOLE, D. J., McFerran, N. V., Collett, G., O'Neill, C., Diamond, T., Garden, O. J., Kylanpaa, L., Repo, H., Deitch, E. A. (2008). Kynurenine Catabolites Of Tryptophan Carried In Mesenteric Lymph Contribute To Pancreatitis-Associated Organ Failure In Rats And Humans. *Pancreas, 35*(4), 417. doi:10.1097/01.mpa.0000297749.12057.3b

MOLE, D. J., McFerran, N. V., & Diamond, T. (2008). Differential preservation of lipopolysaccharide-induced chemokine/cytokine expression during experimental pancreatitis-associated organ failure in rats shows a regulatory expressed phenotype. *Pancreatology: Official Journal Of The International Association Of Pancreatology (IAP) 8*(4-5), 478-487. doi:10.1159/000151775

MOLE, D. J., Webster, S. P., Uings, I., Zheng, X., Binnie, M., Wilson, K., Hutchinson, J. P., Mirguet, O., Walker, A., Beaufils, B., Ancellin, N., Trottet, L., Beneton, V., Mowat, C. G., Wilkinson, M., Rowland, P., Haslam, C., McBride, A., Homers, N. Z., Baily, J. E., Sharp, M G., Garden, O. J., Hughes, J., Howie, S. E., Holmes, D. S., Liddle, J., Iredale, J. P. (2016). Kynurenine-3-monooxygenase inhibition prevents multiple organ failure in rodent models of acute pancreatitis. *Nat Med, 22*(2), 202-209. doi:10.1038/nm.4020

MÖLLER, M., Du Preez, J. L., & Harvey, B. H. (2012). Development and validation of a single analytical method for the determination of tryptophan, and its kynurenine metabolites in rat plasma. *Journal of Chromatography B, 898*, 121-129. doi:http://dx.doi.org/10.1016/j.jchromb.2012.04.030

MOLLER, S. E. (1981). Pharmacokinetics of tryptophan, renal handling of kynurenine and the effect of nicotinamide on its appearance in plasma and urine following L-tryptophan loading of healthy subjects. *Eur J Clin Pharmacol, 21*(2), 137-142.

MORONI, F., Cozzi, A., Sili, M., & Mannaioni, G. (2012). Kynurenic acid: a metabolite with multiple actions and multiple targets in brain and periphery. *J Neural Transm, 119*(2), 133-139. doi:10.1007/s00702-011-0763-x

MULLER, W. E., & Wollert, U. (1975). Benzodiazepines: specific competitors for the binding of L-tryptophan to human serum albumin. *Naunyn Schmiedebergs Arch Pharmacol, 288*(1), 17-27.

MUNAR, M. Y., & Singh, H. (2007). Drug dosing adjustments in patients with chronic kidney disease. *Am Fam Physician, 75*(10), 1487-1496.

NAJJAR, S., Pearlman, D. M., Alper, K., Najjar, A., & Devinsky, O. (2013). Neuroinflammation and psychiatric illness. *J Neuroinflammation, 10*, 43. doi:10.1186/1742-2094-10-43

OGAWA, T., Matson, W. R., Beal, M. F., Myers, R. H., Bird, E. D., Milbury, P., & Saso, S. (1992). Kynurenine pathway abnormalities in Parkinson's disease. *Neurology, 42*(9), 1702-1706.

OHASHI, H., Iizuka, H., Yoshihara, S., Otani, H., Kume, M., Sadamoto, K., Ichiba, H., Fukushima, T. (2013). Determination of L-tryptophan and L-kynurenine in Human Serum by using LC-MS after Derivatization with (R)-DBD-PyNCS. *International Journal of Tryptophan Research, 6*(3773-IJTR-Determination-of-L-tryptophan-and-L-kynurenine-in-Human-Serum-by-using.pdf), 9-14. doi:10.4137/IJTR.S11459

OKAMOTO, H., Yamamoto, S., Nozaki, M., & Hayaishi, O. (1967). On the submitochondrial localization of l-kynurenine-3-hydroxylase. *Biochem Biophys Res Commun, 26*(3), 309-314.

OKUDA, S., Nishiyama, N., Saito, H., & Katsuki, H. (1998). 3-Hydroxykynurenine, an endogenous oxidative stress generator, causes neuronal cell death with apoptotic features and region selectivity. *J Neurochem, 70*(1), 299-307.

ORSATTI, L., Speziale, R., Orsale, M. V., Caretti, F., Veneziano, M., Zini, M., . . . Dominguez, C. (2015). A single-run liquid chromatography mass spectrometry method to quantify neuroactive kynurenine pathway metabolites in rat plasma. *Journal of Pharmaceutical and Biomedical Analysis, 107*, 426-431. doi:http://dx.doi.org/10.1016/j.jpba.2015.01.030

PHILLIP, V., Steiner, J. M., & Algul, H. (2014). Early phase of acute pancreatitis: Assessment and management. *World J Gastrointest Pathophysiol, 5*(3), 158-168. doi:10.4291/wjgp.v5.i3.158

REINHART, P. H., & Kelly, J. W. (2011). Treating the periphery to ameliorate neurodegenerative diseases. *Cell, 145*(6), 813-814. doi:10.1016/j.cell.2011.05.031

RIOS, C., & Santamaria, A. (1991). Quinolinic acid is a potent lipid peroxidant in rat brain homogenates. *Neurochemical Research, 16*(10), 1139-1143. doi:10.1007/BF00966592

ROBERTS, F., & Freshwater-Turner, D. (2007). Pharmacokinetics and anaesthesia. *Continuing Education in Anaesthesia, Critical Care & Pain, 7*(1), 25-29. doi:10.1093/bjaceaccp/mkl058

RÖVER, S., Cesura, A. M., Huguenin, P., Kettler, R., & Szente, A. (1997). Synthesis and Biochemical Evaluation of N-(4-Phenylthiazol-2-yl)benzenesulfonamides as High-Affinity Inhibitors of Kynurenine 3-Hydroxylase. *Journal of Medicinal Chemistry, 40*(26), 4378-4385. doi:10.1021/jm970467t

RUDDICK, J. P., Evans, A. K., Nutt, D. J., Lightman, S. L., Rook, G. A., & Lowry, C. A. (2006). Tryptophan metabolism in the central nervous system: medical implications. *Expert Rev Mol Med, 8*(20), 1-27. doi:10.1017/S1462399406000068

SAITO, K., Fujigaki, S., Heyes, M. P., Shibata, K., Takemura, M., Fujii, H., . . . Seishima, M. (2000). Mechanism of increases in L-kynurenine and quinolinic acid in renal insufficiency. *Am J Physiol Renal Physiol, 279*(3), F565-572.

SALTER, M., Knowles, R. G., & Pogson, C. I. (1989). How does displacement of albumin-bound tryptophan cause sustained increases in the free tryptophan

concentration in plasma and 5-hydroxytryptamine synthesis in brain? *Biochemical Journal, 262*(1), 365-368.

SANTAMARIA, A., Galvan-Arzate, S., Lisy, V., Ali, S. F., Duhart, H. M., Osorio-Rico, L., Rios, C St'astny, F. (2001). Quinolinic acid induces oxidative stress in rat brain synaptosomes. *Neuroreport, 12*(4), 871-874.

SCHWARCZ, R., Bruno, J. P., Muchowski, P. J., & Wu, H.-Q. (2012). Kynurenines in the mammalian brain: when physiology meets pathology. *Nat Rev Neurosci, 13*(7), 465-477.

SCHWARCZ, R., Whetsell, W. O., Jr., & Mangano, R. M. (1983). Quinolinic acid: an endogenous metabolite that produces axon-sparing lesions in rat brain. *Science, 219*(4582), 316-318.

SMITH, J. R., Jamie, J. F., & Guillemin, G. J. (2016). Kynurenine-3-monooxygenase: a review of structure, mechanism, and inhibitors. *Drug Discov Today, 21*(2), 315-324. doi:10.1016/j.drudis.2015.11.001

SPANO, P. F., Szyszka, K., Galli, C. L., & Ricci, A. (1974). Effect of clofibrate on free and total tryptophan in serum and brain tryptophan metabolism. *Pharmacol Res Commun, 6*(2), 163-173.

STONE, T. W. (2000). Inhibitors of the kynurenine pathway. *Eur J Med Chem, 35*(2), 179-186.

STONE, T. W., & Darlington, L. G. (2002). Endogenous kynurenines as targets for drug discovery and development. *Nat Rev Drug Discov, 1*(8), 609-620. doi:10.1038/nrd870

STOY, N., Mackay, G. M., Forrest, C. M., Christofides, J., Egerton, M., Stone, T. W., & Darlington, L. G. (2005). Tryptophan metabolism and oxidative stress in patients with Huntington's disease. *J Neurochem, 93*(3), 611-623. doi:10.1111/j.1471-4159.2005.03070.x

SZALARDY, L., Zadori, D., Toldi, J., Fulop, F., Klivenyi, P., & Vecsei, L. (2012). Manipulating kynurenic acid levels in the brain - on the edge between neuroprotection and cognitive dysfunction. *Curr Top Med Chem, 12*(16), 1797-1806.

TATTER, S. B., Galpern, W. R., Hoogeveen, A. T., & Isacson, O. (1995). Effects of striatal excitotoxicity on huntingtin-like immunoreactivity. *Neuroreport, 6*(8), 1125-1129.

THE ROYAL SOCIETY OF CHEMISTRY, R. (2016). http://www.chemspider.com/.

THEVANDAVAKKAM, M. A., Schwarcz, R., Muchowski, P. J., & Giorgini, F. (2010). Targeting kynurenine 3-monooxygenase (KMO): implications for therapy in Huntington's disease. *CNS Neurol Disord Drug Targets, 9*(6), 791-800.

TUNTLAND, T., Ethell, B., Kosaka, T., Blasco, F., Zang, R. X., Jain, M., Gould, T., Hoffmaster, K. (2014). Implementation of pharmacokinetic and pharmacodynamic strategies in early research phases of drug discovery and development at Novartis Institute of Biomedical Research. *Front Pharmacol, 5*, 174. doi:10.3389/fphar.2014.00174

UEMURA, T., & Hirai, K. (1998). L-Kynurenine 3-Monooxygenase from Mitochondrial Outer Membrane of Pig Liver: Purification, Some Properties, and Monoclonal Antibodies Directed to the Enzyme. *Journal of Biochemistry, 123*(2), 253-262.

UYTTENHOVE, C., Pilotte, L., Theate, I., Stroobant, V., Colau, D., Parmentier, N., Boon, T., Van den Eynde, B. J. (2003). Evidence for a tumoral immune resistance mechanism based on tryptophan degradation by indoleamine 2,3-dioxygenase. *Nat Med, 9*(10), 1269-1274. doi:10.1038/nm934

VARMA, S. D., & Hegde, K. R. (2010). Kynurenine-induced photo oxidative damage to lens in vitro: protective effect of caffeine. *Mol Cell Biochem, 340*(1-2), 49-54. doi:10.1007/s11010-010-0399-4

VAZQUEZ, S., Aquilina, J. A., Jamie, J. F., Sheil, M. M., & Truscott, R. J. W. (2002). Novel Protein Modification by Kynurenine in Human Lenses. *Journal of Biological Chemistry, 277*(7), 4867-4873. doi:10.1074/jbc.M107529200

VECSEI, L., Szalardy, L., Fulop, F., & Toldi, J. (2013). Kynurenines in the CNS: recent advances and new questions. *Nat Rev Drug Discov, 12*(1), 64-82. doi:10.1038/nrd3793

WANG, J., Simonavicius, N., Wu, X., Swaminath, G., Reagan, J., Tian, H., & Ling, L. (2006). Kynurenic Acid as a Ligand for Orphan G Protein-coupled Receptor GPR35. *Journal of Biological Chemistry, 281*(31), 22021-22028. doi:10.1074/jbc.M603503200

WASSEF, A., Baker, J., & Kochan, L. D. (2003). GABA and schizophrenia: a review of basic science and clinical studies. *J Clin Psychopharmacol, 23*(6), 601-640. doi:10.1097/01.jcp.0000095349.32154.a5

WENNSTROM, M., Nielsen, H. M., Orhan, F., Londos, E., Minthon, L., & Erhardt, S. (2014). Kynurenic Acid levels in cerebrospinal fluid from patients with Alzheimer's disease or dementia with lewy bodies. *Int J Tryptophan Res, 7*, 1-7. doi:10.4137/IJTR.S13958

WHO/FAO/UNU, J. E. C. (2007). Protein and amino acid requirements in human nutrition. *World Health Organ Tech Rep Ser*(935), 1-265, back cover.

WILKINSON, M. (2013). *Structural Dynamics and Ligand Binding in Kynurenine-3-monooxygenase.* (PhD), University of Edinburgh.

WILSON, K., Mole, D. J., Binnie, M., Homer, N. Z., Zheng, X., Yard, B. A., Iredale, J. P., Auer, M., Webster, S. P. (2014). Bacterial expression of human kynurenine 3-monooxygenase: solubility, activity, purification. *Protein Expr Purif, 95*, 96-103. doi:10.1016/j.pep.2013.11.015

WONODI, I., McMahon, R. P., Krishna, N., Mitchell, B. D., Liu, J., Glassman, M., Hong, L. E., Gold, J. M. (2014). Influence of kynurenine 3-monooxygenase (KMO) gene polymorphism on cognitive function in schizophrenia. *Schizophrenia Research, 160*(1–3), 80-87. doi:http://dx.doi.org/10.1016/j.schres.2014.10.026

XIE, G., Keyhani, N. O., Bonner, C. A., & Jensen, R. A. (2003). Ancient origin of the tryptophan operon and the dynamics of evolutionary change. *Microbiol Mol Biol Rev, 67*(3), 303-342, table of contents.

YAMADA, K., Miyazaki, T., Shibata, T., Hara, N., & Tsuchiya, M. (2008). Simultaneous measurement of tryptophan and related compounds by liquid chromatography/electrospray ionization tandem mass spectrometry. *Journal of Chromatography B, 867*(1), 57-61. doi:http://dx.doi.org/10.1016/j.jchromb.2008.03.010

YAMAMOTO, H., Shindo, I., Egawa, B., & Horiguchi, K. (1994). Kynurenic acid is decreased in cerebrospinal fluid of patients with infantile spasms. *Pediatr Neurol, 10*(1), 9-12.

YAMAMURA, H. I., Reisine, T. D., & Beaumont, K. (1980). Huntington's disease: Alterations in GABA and benzodiazepine receptors in the human brain. *Brain Research Bulletin, 5, Supplement 2*, 773-775. doi:http://dx.doi.org/10.1016/0361-9230(80)90128-8

YAMASAKI, K., Chuang, V. T., Maruyama, T., & Otagiri, M. (2013). Albumin-drug interaction and its clinical implication. *Biochim Biophys Acta, 1830*(12), 5435-5443. doi:10.1016/j.bbagen.2013.05.005

YANOFSKY, C. (2007). RNA-based regulation of genes of tryptophan synthesis and degradation, in bacteria. *RNA, 13*(8), 1141-1154. doi:10.1261/rna.620507

ZHANG, Y., Huo, M., Zhou, J., & Xie, S. (2010). PKSolver: An add-in program for pharmacokinetic and pharmacodynamic data analysis in Microsoft Excel. *Computer Methods and Programs in Biomedicine, 99*(3), 306-314. doi:http://dx.doi.org/10.1016/j.cmpb.2010.01.007

ZHAO, W., & Jacqz-Aigrain, E. (2011). Principles of therapeutic drug monitoring. *Handb Exp Pharmacol, 205*, 77-90. doi:10.1007/978-3-642-20195-0_3

ZHEN, Q., Xu, B., Ma, L., Tian, G., Tang, X., & Ding, M. (2011). Simultaneous determination of tryptophan, kynurenine and 5-hydroxytryptamine by HPLC: Application in uremic patients undergoing hemodialysis. *Clin Biochem, 44*(2-3), 226-230. doi:10.1016/j.clinbiochem.2010.10.011

ZWILLING, D., Huang, S. Y., Sathyasaikumar, K. V., Notarangelo, F. M., Guidetti, P., Wu, H. Q., . . . Muchowski, P. J. (2011). Kynurenine 3-monooxygenase inhibition in blood ameliorates neurodegeneration. *Cell, 145*(6), 863-874. doi:10.1016/j.cell.2011.05.020